DELIVERING SCHIZOPHRENIA-ASSOCIATED MICRORNA137 TO THE PREFRONTAL CORTEX BY LIPID NANOPARTICLES

By

Michelle C. Palumbo

A DISSERTATION

Presented to the Department of Behavioral Neuroscience

and the Oregon Health & Science University

School of Medicine

in partial fulfillment of

the requirements for the degree of

Doctor of Philosophy

October 2023

School of Medicine

Oregon Health & Science University

TABLE OF CONTENTS

LIST OF FIGURES

LIST OF TABLES

LIST OF ABBREVIATIONS

ApoE – apolipoprotein E

ANOVA – analysis of variance

BBB – blood-brain barrier

CNS – central nervous system

CNV – copy number variant

DLS – dynamic light scattering

EE – encapsulation efficiency

EV – extracellular vesicle

FLuc – firefly luciferase

GABA – y-aminobutyric acid

GFAP – glial fibrillary acidic protein

GPCR – G protein-coupled receptor

GWAS – genome-wide association study

Iba1 – ionized calcium binding adaptor molecule 1

IVIS – *in vivo* imaging system

LNP – lipid nanoparticle

µl – microliter

µM – micromolar

miRNA – microRNA

miR137- microRNA137

mRNA – messenger RNA

mV – millivolts

N2A – Neuro2A cells

nm – nanometer

nM – nanomolar

NMDA – N-methyl-D-aspartate

NeuN – neuronal nuclear protein

PDI – polydispersity index

PEG – polyethylene glycol

PFC – prefrontal cortex

PBS – phosphate buffered saline

RCV – rare coding variant

RT-qPCR – reverse transcription quantitative polymerase chain reaction

SCZ – schizophrenia

SEM – standard error of the mean

SORT – selective organ targeting

sno202 – small nucleolar RNA 202

SNP – single nucleotide polymorphism

TEM – transmission electron microscopy

ZP – zeta potential

ACKNOWLEDGEMENTS

There are numerous people who I need to acknowledge for their contribution to this dissertation and my time at Oregon Health & Science University. First, I have had incredible scientific and personal support from my mentor, Dr. Aaron Janowsky. Thank you for teaching me the best principles of scientific rigor while keeping in mind the most important rule was to have fun. I am grateful to have an advisor that truly wants to see people succeed. The madness will always be in the methods. Thank you to my co-mentor, Dr. Atheir Abbas, who constantly had thoughtful insights into the best practices to model psychiatric disorders in rodents. Thank you for keeping morale high with copious amounts of candy. My dissertation advisory committee helped me to think critically and perform the best experiments possible for the questions I intended to answer. Thank you, Dr. Dan Marks for supporting my work and always providing me with excellent knowledge and resources. Thank you, Dr. Rajesh Miranda who brought so much insight and guidance, when I needed it most.

I would like to acknowledge the people who helped train me on various techniques throughout the years. Many thanks to Dr. Gaurav Sahay and Dr. Milan Gautam for helping to guide my project and teach me about lipid nanoparticles. This work could not have been possible without you both. Thank you to Tanya Korzun who brought me into the incredible world of nanomedicine and taught me how to use the IVIS. A huge thank you to Dr. Alex Sonnenborn who taught me stereotaxic surgeries, skeptically reviewed data with me, and has the most genuine willingness to help other people. Thank you to the OHSU proteomics core for sharing your knowledge of proteomic and biological data analysis.

Of course, I need to thank the members of the Janowsky lab. Bill Schutzer provided me with grant writing support, endless resources so I could perform my experiments, and a lifetime of terrible jokes. To my officemate, grad student-mate, and friend, Juli Huey, I can't thank you enough for your incredible humor and awesome morale. Grad school and traveling to conferences would not have been the same without you. A huge shoutout to Kat Wolfrum who supported me in multiple thoughtful ways throughout the years. We shared snacks, garden supplies, and she has the most detailed editing skills. Thank you to Xiao Shi who graciously and patiently taught me tedious techniques including western blotting, qPCR, and cell culture. She was incredibly knowledgeable and helpful to me in my years of graduate school. To all the past and current members of the Janowsky lab: Nick Minor, Amy Eshleman, Laura Kozell, Tracy Swanson, Jennifer Schmachtenberg, Shelley Bloom, John Reed, Sheila Benware, and Alyssa Riviera, thank you for your endless support.

The support from fellow past and present graduate students is unparalleled. They shared the good, the bad, and the ugliest of times. Samantha Rios and Randall Olson supported me after experiments failed, writer's block ensued, or when balancing graduate school and life became extremely taxing. Thank you for spending too much time with me at Suki's, playing sports, hiking, and doing crafts. They are more than just colleagues; they are lifelong friends and I couldn't have done this without them. To my incoming cohort of S's: Sophia Weber, Sophie Lambert, and Sylvie Bindas, the first year of graduate school and the global pandemic would have been unbearable without you all. Thank you to John Mootz who guided me through the final years of graduate school and helped me decide what direction to go next. And finally, thank you to my peer

mentor, Noah Milman, for keeping the spirit of valuable science alive with oxytocin and prairie voles.

I must thank the wonderful scientific women that brought me into the research world. Dr. Sara Freeman and Dr. Rebecca Lawrence from Dr. Karen Bales' lab are strong, intelligent, and incredible mentors to have by your side through undergraduate and post-bachelorette research. Thank you for your contribution to my scientific passions.

Finally, I would not be in the position I am today without the unconditional love and support from my family and friends. I'm beyond grateful for my partner, Tyler Taverniti. He pushed me to follow the challenging - yet immeasurably rewarding - path of scientific discovery. I cherish and value his support throughout this grueling process. Thank you to my mother, Dr. Gayle Palumbo, who has taught me to always stand up for what I believe in. Thank you to my father, Maurice Palumbo, who supported my interest in science from a very early age and reminded me that every scientific question can be answered by understanding physics. I have the sincerest gratitude for my brother, Massimo Palumbo, who asked thoughtful questions throughout graduate school and always wanted to stay updated on my progress. Thank you for reminding me why I love what I do.

This work was supported by funding from the NIDA ADA 12013, FDA CDER-20-I-0546, DEA D-15-OD-002, Department of Veterans Affairs 1IK6BX005754, an ARCS Foundation Scholarship, an N.L. Tartar Trust Fellowship, an Ashworth-Thomason Award, and an OHSU Graduate Scholar Research Award.

ABSTRACT

Schizophrenia (SCZ) is a complex neuropsychiatric disorder thought to arise from an interplay of environmental and genetic risk factors. The presentation of disease symptomology is heterogenous due to the polygenicity of the disorder. The standard antipsychotic drug treatments lack target specificity, have severe side effects, and do not alleviate the most disabling negative and cognitive symptoms. This may be due to a lack of understanding SCZ pathophysiology. Genome-wide association studies (GWAS) identified candidate alleles, largely involved in regulating synaptic function, which confer increased risk for SCZ. The host gene *MIR137*, contains the primary transcript of microRNA137 (miR137), is strongly implicated in SCZ risk and is associated with more severe psychiatric symptoms. MiR137 regulates tens to hundreds of target transcripts involved in neurodevelopment and synaptic function. Since SCZ is a neurodevelopmental disorder characterized by synaptic dysfunction, miR137 represents an interesting target to modulate protein expression in the prefrontal cortex (PFC), one of the most impacted brain regions. Thus, to improve treatments for people with SCZ, this dissertation investigated the ability of nanoparticles to deliver nucleic acid cargo to the PFC to alter synaptic protein expression.

Chapter 1 discusses the genetic heritability of SCZ, the dopamine and glutamate hypotheses of SCZ, and the hallmark pathologies that characterize the disorder. The biological function of microRNAs and the relationship of miR137 to SCZ will be discussed. Finally, an overview will be given of the three nanoparticle delivery systems that are compared in the following studies.

In Chapter 2, extracellular vesicles (EVs), polymeric nanoparticle, and lipid nanoparticle (LNP) formulations were compared as nucleic acid delivery vehicles in cell cultures. Particle size, heterogeneity, charge, toxicity, and encapsulation efficiency were measured to characterize the nanoparticle types. To analyze the function of nanoparticles *in vitro* the uptake, endocytosis, and nucleic acid cargo release was assessed. Based on the investigated determinants, LNPs were the most effective transportation vector and were used for further *in vivo* studies.

In Chapter 3, the pharmacokinetics, biodistribution, and cell type targeting of nucleic acids delivered by LNPs was determined after injection into the mouse PFC. LNPs injected into the PFC maintained expression for 24h, remained localized to the PFC injection site, and preferentially expressed cargo in neurons over microglia or astrocytes. Additionally, the toxicity of LNPs was measured to determine the immunogenicity *in vivo*. Single or multiple injections of LNPs did not affect animal survival, body weight, or tissue integrity. The effect of miR137 loaded LNPs was examined by target synaptic protein inhibition *in vitro* and *in vivo*. In cell culture experiments, miR137 inhibited synaptic protein expression, some of which were previously validated and some of which were novel targets. In the mouse PFC, miR137 inhibited a network of glutamatergic synaptic proteins, some of which are GWAS risk genes for SCZ. The LNPs themselves activated an immune response through cytokine and complement cascade enrichment.

Chapter 4 presents a general overview of the findings in this dissertation, including a summary of findings, potential clinical implications, limitations, and future directions for neuro-nanomedicine.

Together, these experiments support the potential of LNPs as nucleic acid delivery vehicles to the brain. The results of this research will inform future studies on non-viral gene therapies for psychiatric and other neurological disorders.

Chapter 1: Introduction

Schizophrenia

Schizophrenia (SCZ) is a complex neuropsychiatric disorder affecting nearly 1% of the global population (K. R. Patel et al., 2014a). This serious mental illness is associated with significant health, social, and economic concerns. SCZ is one of the top 15 leading causes of disability (GBD 2016 Disease and Injury Incidence and Prevalence Collaborators, 2017). Individuals with SCZ are more likely to die prematurely, have co-morbid diseases, and commit suicide (Olfson et al., 2015). On a global and economic scale, the direct costs associated with SCZ include health care, institutionalization, and medication (Chong et al., 2016). The indirect costs include loss of productivity and employment, social services, and criminal justice needs (Kadakia et al., 2022).

Individuals with SCZ demonstrate widespread heterogeneity of symptoms which makes SCZ one of the least understood neuropsychiatric disorders. Symptoms of SCZ are typically characterized as positive, negative, or cognitive. Positive symptoms manifest as psychotic symptoms including hallucinations, delusions, or disorganization of speech and/or behavior. Negative symptoms include loss of motivation, anhedonia, social withdrawal, or a loss of affect. Cognitive symptoms disrupt mental processing such as learning, working memory, and attention. The spectrum of patient symptomology correlates with diverse individual variation in SCZ presentation. As such, clinical studies of SCZ require large and diverse sample sizes.

However, SCZ is characterized by hallmark changes in brain structure and function, specifically in the prefrontal and medial temporal lobes (McCutcheon, Reis Marques, et al., 2020). The prefrontal and temporal brain regions cooperate in the

function of several behaviors including working and declarative memory, executive function, cognitive flexibility, behavioral inhibition, and attention (Barbas & Zikopoulos, 2007). Resting-state functional connectivity in medial prefrontal and temporal brain networks are linked to cognitive empathy and negative symptoms of SCZ (Abram et al., 2017). Furthermore, structural changes to the temporal lobe include reduction in gray matter volume (Shenton et al., 1992) which is correlated to more severe memory performance, hallucinations, and thought disorders (Kaur et al., 2020).

Within the frontal lobe, SCZ pathology is especially notable in the prefrontal cortex (PFC). Alterations in the PFC are evident across spatial and temporal resolutions in SCZ. For example, pyramidal neurons in the PFC of SCZ patients have smaller soma volumes, shorter dendritic branches, and fewer dendritic spines (Smucny et al., 2022). On a network level, synaptic inhibition of PFC GABAergic neurons synchronize oscillations to connecting brain regions (Gonzalez-Burgos & Lewis, 2008). The PFC is densely interconnected to critical brain regions including the hippocampus, thalamus, striatum, and cerebellum (Anastasiades & Carter, 2021). Thus, macrocircuit-level alterations of the PFC influence cognition and goal-directed behavior (N. P. Friedman & Robbins, 2022); which are hallmarks of SCZ. Thus, the PFC presents an attractive target to modulate gene and protein expression associated with symptoms of SCZ.

Genetic heritability for schizophrenia

The etiology of SCZ is multifactorial and thought to arise from an interplay of genetic and environmental factors. Several environmental factors such as abnormal fetal development, birthing complications, maternal immune activation, winter births,

and being born in an urban environment, increase the risk of developing SCZ (Stilo & Murray, 2019). However, the genetic risk factors play a fundamental role in SCZ pathology with ~80% heritability and a 46% concordance rate in monozygotic twins (Sullivan et al., 2019; Wahbeh & Avramopoulos, 2021). This significant genetic component led researchers to search for risk genes that increase the susceptibility of developing SCZ.

Genome and exome sequences with large population sizes indicate that each genome is extremely diverse (Mills et al., 2011). Approximately 85% of disease-related genetic variations are found in the coding region, suggesting exome sequencing will identify disease-susceptible genes (Singh et al., 2022). Much of the individual variation in SCZ risk is genetic and includes thousands of common alleles with small effect sizes, a few rare copy number variants (CNVs) with large effect sizes, and rare coding variants (RCVs) (Smeland et al., 2020). However, rare CNVs and RCVs have an estimated heritability around 2% (Weiner et al., 2023). Given the heterogeneity of SCZ, limiting genetic studies to exome sequencing might not give a comprehensive view of the genetic basis for disease risk.

Genome-wide association studies (GWAS) are used to scan the genome for common genetic variants which might confer an increased risk for SCZ. However, an “evolutionary paradox” exists whereby the effect size of risk alleles is inversely related to population frequencies. Much of the genetic heritability of SCZ risk genes are common alleles. Evidence suggests risk alleles are maintained at high frequencies due to strong purifying selection of loci at mutation hotspots as opposed to positive or balancing selection (Owen et al., 2023). Single nucleotide polymorphisms (SNPs) are the largest

GWAS contributors to allele heritability, estimated at 25% (Trubetskoy et al., 2022). SNPs that occur in the DNA between genes can act as biological regulators of nearby genes. SNPs within a gene or in a regulatory region of the gene serve a more direct role in the gene's function (Shastry, 2009). SNPs associated with SCZ risk include those linked to genes involved in dopaminergic, serotonergic, and glutamatergic neurotransmission (Ripke et al., 2014). Some of these genes include the dopamine D2 receptor *DRD2* and the glutamatergic NMDA and AMPA receptors *GRIN2A* and *GRIA1,* respectively (Trubetskoy et al., 2022). Many of the associated genes encode proteins that are critical for neurodevelopment, synaptic transmission, and the immune system. However, designing therapies to combat the wide-spread genetic and biological perturbations from SCZ neuropathology remains a challenge.

Dopamine and glutamate hypotheses

Antipsychotic drugs are the most common pharmacological treatment for patients with SCZ (K. R. Patel et al., 2014b). Many of the molecular target G protein-coupled receptors (GPCRs) for antipsychotic drugs are also GWAS candidate genes (Ripke et al., 2011). However, these medications have severe limitations. Antipsychotic medications bind to several GPCRs simultaneously, and this interaction is thought to be both beneficial and detrimental (Kinon & Lieberman, 1996). To start, only about half of patients with SCZ find symptom relief from these treatments (Andrade, 2016). Secondly, antipsychotics mainly ameliorate positive symptoms, and negative and cognitive symptoms are left untreated (Chokhawala & Stevens, 2023). Lastly, the promiscuous affinity of antipsychotics to multiple GPCRs – including the dopaminergic, serotonergic,

muscarinic, histamine, and noradrenergic receptors – can cause severe neurologic, motor and metabolic side effects (Stępnicki et al., 2018). It is common for SCZ patients to nonadhere to antipsychotic treatment due to the severity of side effects such as weight-gain, hyperlipidemia, glucose intolerance, type 2 diabetes, and metabolic syndromes (Siafis et al., 2018). However, in complex disorders such as SCZ, multi-target drugs were found to be more effective than single target pharmacotherapies (Roth et al., 2004; Wong et al., 2010). Unfortunately, since the genesis of antipsychotics in the 1950's, effective treatment options for SCZ have not substantially improved. However, in the last decade, a larger emphasis has been placed on investigating the genetic basis of SCZ to design personalized therapies for individualized medicine.

The dopamine hypothesis postulates that SCZ results from pathologic alterations in dopaminergic mesolimbic and mesocortical circuits (McCutcheon, Krystal, et al., 2020). First, the mesolimbic pathway is hyperactive in SCZ (McCutcheon et al., 2019). Patients with SCZ show increased presynaptic dopamine synthesis, and the amount of dopamine release is correlated with more severe psychotic symptoms (Grace, 2016). Second, the therapeutic effect of antipsychotic drugs depends on their ability to block dopamine receptors and thereby alleviate psychosis (Maric et al., 2016). The negative symptoms of SCZ are thought to be caused by mesocortical hypofunction and potentially worsened by dopamine D2 receptor antagonists (Stępnicki et al., 2018). Third, stimulants such as amphetamine and L-DOPA induce primary symptoms of SCZ (Carey et al., 1995). However, in the pathophysiology of SCZ, striatal dopaminergic hyperactivity could be secondary to alterations in the glutamatergic system (Kokkinou et al., 2021). Furthermore, the cognitive and negative symptoms of SCZ are unlikely to be

a consequence of dopamine dysfunction alone and emerging research has turned to additional neurotransmitter systems such as glutamate circuitry.

The dopamine hypothesis is complemented by the glutamate hypothesis in the pathophysiology of SCZ. Glutamate is the major excitatory neurotransmitter in the brain and the glutamatergic N-methyl-D-aspartate (NMDA) and α-amino-3-hydroxy-5-methyl-4-isoxazolepropionic acid (AMPA) receptors are widespread throughout the brain. NMDA receptor antagonists have psychotomimetic properties - and are indistinguishable from SCZ psychosis - supporting the glutamate hypothesis (Coyle et al., 2020; Moghaddam & Javitt, 2012). The glutamate hypothesis proposes that hypofunction of NMDA receptors on inhibitory GABAergic interneurons predominates, resulting in a net increase in excitation in pyramidal neurons (Kantrowitz & Javitt, 2012). The decrease in NMDA neurotransmission initiates a cascade of events including decreased excitatory postsynaptic currents, decreased interneuron output, reduced GABA release, and a disinhibition of postsynaptic excitatory neurons (Mei et al., 2018). This results in excessive glutamate release and increased activation of non-NMDA glutamate receptors. The dysfunction of glutamatergic neurotransmission in cortical pyramidal neurons results in aberrant synaptic function (Abbas et al., 2018). Moreover, poor antipsychotic response is associated with higher levels of glutamate metabolites (Egerton et al., 2021). However, current treatment options do not directly regulate glutamate; thus, emerging therapeutics for SCZ might focus on the direct regulation of glutamatergic synaptic transmission.

Synaptic disruptions

Synapses are the foundational interstitial spaces in which electrical and chemical signals are transferred from pre-synaptic to post-synaptic cells. Synaptic strength is dynamic and dependent on neuronal activity. This synaptic plasticity is essential for learning and memory. Importantly, synaptic perturbations are a characteristic of SCZ and include disruptions in synaptogenesis, synaptic pruning, and synaptic protein quantity or function (OBI-NAGATA et al., 2019). One idea suggests that anatomical disruptions in cellular spines, dendrites, and outgrowths impede synaptic connectivity between neurons in SCZ (Glausier & Lewis, 2013). Moreover, GWAS studies identified hundreds of candidate genes which code for synaptic proteins involved in voltage-gated calcium channels and postsynaptic density networks (Fromer et al., 2014; D.-M. Yin et al., 2012). These synaptic proteins are critical for proper long-term potentiation (LTP) and long-term depression (LTD) during synaptic plasticity. Therefore, disruption of synaptic structure and composition of key proteins impairs glutamatergic, GABAergic, dopaminergic, and cholinergic signaling necessary for neurotransmission (Brachya et al., 2006). Thus, further research is needed on the synaptic pathology of SCZ and potential treatment options to reverse synaptic dysfunction.

Inflammation in schizophrenia

In association with the glutamate hypothesis, one theory suggests aberrant neuronal glutamate release leads to microglial activation through the complement cascade, implicating the immune system in SCZ neuropathology (Parellada & Gassó, 2021). The central nervous system (CNS) immune system includes the cells that

maintain homeostasis in the brain – astrocytes and microglia. The neuroimmune system regulates innate and adaptive immune cells to prevent infection and communicate with the peripheral immune system. Astrocytes interact with pre- and post-synaptic neurons and regulate neurotransmitter release, maintenance, clearance, and signaling (Y. S. Kim et al., 2020). Microglia are primary immune cells that regulate brain development, maintain synaptic neurotransmission and plasticity, modulate circuit-level networks, and serve as injury repair cells (Cowan & Petri, 2018).

Attempts were made to study the association between the neuroimmune system and SCZ through post-mortem brain tissue, positron emission tomography ligands to image microglial activation, and testing anti-inflammatory therapeutics (Birnbaum & Weinberger, 2020). However, most of this work remains inconclusive given the limitations in technologies, small sample size, and difficulty controlling for heterogeneity in patient treatments. However, the largest piece of evidence linking the immune system to SCZ etiology arises from GWAS studies. Multiple GWAS studies repeatedly indicated the major histocompatibility locus to be significantly associated with SCZ risk (Sekar et al., 2016; Trubetskoy et al., 2022). This region encodes for the complement component C4 which is linked to excessive synaptic pruning in SCZ (Woo et al., 2020; Yilmaz et al., 2021). Furthermore, gene enrichment analyses suggest genes elevated in immune pathways including B-lymphocytes, TGF-ß signaling, and T- and B-cell activation (Network and Pathway Analysis Subgroup of Psychiatric Genomics Consortium, 2015). Given the mixed evidence for implicating the immune system in SCZ, it is important to understand whether the association is primary or secondary to the disease pathology.

MicroRNAs

The regulation of genetic information is a highly complex biological process. About 1.5% of the human genome accounts for protein-coding sequences and 98.5% of the genome consists of non-protein-coding sequences (Liao et al., 2023). Non-protein-coding sequences can code for long non-coding RNAs and short RNA species such as short interfering RNAs (siRNA), small nucleolar RNAs (snoRNAs), and microRNAs (miRNAs). MiRNAs are 19 to 25 nucleotide, single-stranded, noncoding RNAs that modulate developmental processes and cellular function. MiRNAs target specific sets of messenger RNAs (mRNAs) and are key transcriptional silencers of gene expression (Gulyaeva & Kushlinskiy, 2016). Importantly, miRNAs bind to target transcripts in the cytoplasm, which reduces the need to transport miRNAs across the nuclear barrier to function (Catalanotto et al., 2016). MiRNAs interact with target transcripts based on their complementary “seed sequence” which is six to eight nucleotides long (B. P. Lewis et al., 2005). There are several seed match types which differ by the number of base pair gaps and matching sequences that align miRNAs to mRNA transcripts. Generally, the bound mRNA will be degraded or translationally repressed, ultimately decreasing the expression of the target protein (Selbach et al., 2008).

Due to the short, and therefore less selective, miRNA seed sequence, an individual miRNA sequence can regulate tens to hundreds of gene targets simultaneously. Estimates of up to 80% of human genes are regulated by miRNAs, making miRNAs powerful regulators of interacting genetic networks (Selbach et al., 2008). Numerous recent studies quantified changes in miRNA expression profiles in biological and disease states including cancer, allergies, and neurological disorders (Ho

et al., 2022). A growing number of reports suggest utility of miRNAs for medical intervention, as modulators of drug resistance, or biomarkers of pathological conditions (Hanna et al., 2019). Thus, miRNAs have pleiotropic potential for RNA-based therapies.

MicroRNA137 and synaptic function

MicroRNA137 (miR137) is enriched in the nervous system and has a critical role in neuronal development and neurogenesis (Mahmoudi & Cairns, 2017). MiR137 levels increase 100-fold during embryonic neurodevelopment in brain regions important for cognitive function including the midbrain and the forebrain (J. Yin et al., 2014). MiR137 is located in the synapto-dendritic compartment of cortical, amygdala, hippocampal, cerebellar, and brain stem regions, where it targets a number of synaptic and developmental mRNAs (Willemsen et al., 2011).

Overexpression of miR137 *in vitro* disrupts synaptic transmission including LTP, paired pulse facilitation, and excitatory/inhibitory balance (Y. Cheng et al., 2018; Siegert et al., 2015). Overexpressing miR137 in embryonic neuronal stem cells reduced proliferation (Sun et al., 2011). Overexpressing miR137 in hippocampal neurons reduced synaptogenesis and dendritic spine formation, depressed synaptic transmission and spontaneous action potential release, reduced synaptic active zone length, and decreased the total number of docking synaptic vesicles (He et al., 2018). Overexpression of miR137 *in vivo* impaired sensory gaiting in the prepulse inhibition test, disrupted social behavior in the social novelty test, and worsened cognition in the novel objection recognition test (Arakawa et al., 2019).

Genetic deletion of miR137 in the germline of mice results in postnatal lethality (Crowley et al., 2015); while miR137 heterozygous mice have disrupted synaptic and dendritic growth, repetitive behavior, and impaired learning and social behavior (Y. Cheng et al., 2018). Additionally, inhibiting miR137 with a complementary sponge sequence decreased the number of AMPA-silent synapses and potentiated synaptic transmission (Olde Loohuis et al., 2015). Reduction of miR137 in neuroendocrine cells downregulated gene sets involved in neuronal transmission and synaptogenesis (Strazisar et al., 2015). Thus, it remains undetermined if decreased or elevated miR137 expression is needed to maintain proper synaptic functioning.

MicroRNA137 and schizophrenia

SCZ risk genes contain significantly more predicted miRNA-binding sites than protein-coding genes (Hauberg et al., 2016). Additionally, SCZ genomes are more likely to contain rare CNVs that over-lap with miRNA-encoding genes (Warnica et al., 2015). Additional non-coding RNAs, such as circularRNAs, act as miRNA sponges and exacerbate posttranscriptional gene silencing in SCZ (Mahmoudi et al., 2019).

Multiple GWAS studies replicated a significant link between the *MIR137* locus and increased risk for SCZ (Duan et al., 2014; Ripke et al., 2011, 2013, 2014). This association centers around the intron of the *MIR137* host gene and includes SNPs such as rs1625579, rs11998588, rs2660304, and rs2802535 (Siegert et al., 2015). SCZ patients homozygous for the T allele variants at *MIR137* are linked to SCZ clinical endophenotypes including earlier age of psychosis onset, more severe negative symptoms, worse attention and processing speed (Cummings et al., 2013; Kuswanto et

al., 2015; Lett et al., 2013), and alterations in brain structure and activity (Mahmoudi et al., 2020; van Erp et al., 2014). Genetic variation in *MIR137* is also associated with dorsolateral PFC hyper-activation (van Erp et al., 2014) and prefrontal-hippocampal functional connectivity (B. Liu et al., 2014; Ritchie et al., 2015).

The clinical literature is mixed if miR137 overexpression or inhibition is associated with SCZ risk. Some studies report lower (Duan et al., 2014; Guella et al., 2013), while others report no change (Santarelli et al., 2020) in miR137 expression in the dorsolateral PFC of postmortem brain tissue from SCZ patients. Alternatively, miR137 was increased in peripheral blood in first episode SCZ patients (Khadimallah et al., 2022; S. Liu et al., 2017; Wu et al., 2016). However, expressing *MIR137* variants in neuron-like SH-SY5Y cells reduces miR137 levels (Strazisar et al., 2015), while SNPs in *MIR137* in converted human-derived neurons increase miR137 expression (Siegert et al., 2015). However, miR137 levels may be altered in patients with advanced stages of SCZ due to chronic disease states or pharmacological manipulation such as antipsychotic or other prescription drugs. Thus, measuring the levels of miR137 might be limited in complex human populations. Overall, there could a narrow window of optimal miR137 levels that increase SCZ risk.

Disease-associated SNPs in *MIR137* may help to explain dysfunction in synaptic and neural circuit performance that drives the disease phenotype. Reductions in synapse number or function impair network level processing resulting in the core symptoms of SCZ. Since miR137 is enriched during neurodevelopment and is present in pluripotent stem cells, the two-hit model of SCZ vulnerability suggests miR137 arises during development and environmental contributions increase disease risk. This

“Delayed Mechanism” of disrupted miR137 levels during postnatal development could play a role in the onset of SCZ. For example, miR137 post-transcriptionally regulates dopamine signaling through the dopamine transporter (Jia et al., 2016), which could increase SCZ vulnerability during adolescence. Furthermore, there is substantial overlap of synaptic genes identified in GWAS studies and those that are regulated by miR137 (Loohuis et al., 2017; Sakamoto & Crowley, 2018; J. Yin et al., 2014). For example, miR137 regulates downstream proteins in the pathways of SCZ susceptibility genes neuregulin 1 (NRG1) and brain-derived neurotrophic factor (BDNF) (Thomas et al., 2017). Hence, changes in miR137 levels in critical brain regions known to be dysregulated in SCZ could be an important mechanism in the pathophysiology of the disorder.

In addition to SCZ, the *MIR137* disease-associated locus is included in 1p21.3 microdeletions that gives rise to intellectual disability and autism spectrum disorder (ASD), and these microdeletions are associated with decreased levels of miR137 (Willemsen et al., 2011). In addition to SCZ, the *MIR137* locus overlaps with CNVs in ASD and bipolar disorder patients (Pinto et al., 2014). Together, these findings suggest miR137 contributes to the pathogenesis of neuropsychiatric disorders.

Hemizygous microdeletions in the 22q11.2 region increase SCZ risk about 25-fold (Bassett & Chow, 2008). The 22q11.2 region includes CNVs in the *DGCR8* gene which impair miRNA microprocessor machinery, leading to widespread downregulation of miRNAs (Thomas & Zakharenko, 2021). However, contrasting reports suggest the miRNA biogenesis genes *DGCR8, DROSHA, and DICER1* are increased in SCZ patients but not in 22q11.2 mutations (Rey et al., 2020). It is possible that miR137 may

contribute to SCZ pathophysiology in multiple mechanisms including direct, delayed, and progressive regulation. Therefore, it's worth investigating if miR137 dysregulation is a factor in brain disorders associated with synaptic dysfunction.

Nanoparticles

Nanomedicine is an emerging field that combines technological advances from interdisciplinary fields to design novel therapeutics for previously unmet clinical needs. At the core of nanotherapeutics are nanoparticles: ultrafine particles that range from 1-100 nanometers (nm) in diameter (Khan et al., 2019). Nanoparticles encapsulate cargos for delivery to, or release from, specific tissues and organs. This cargo could include drugs, small molecules, or biomarkers of disease. The three major classifications of nanoparticles can be described as endogenous, synthetic, or a hybrid. Within each of these classifications, further parameters define nanoparticles based on their characteristics such as size, shape, structure, composition, charge, and chemical interactions. In addition to encapsulating therapeutic molecules, the surface of nanoparticles is a critical factor when determining targeting and uptake into specific cell types.

Synthetic nanoparticles have been widely used for clinical drug delivery since the 1990s. In the last few decades, increasing interest in nanomedicine has included research on liposomes, DNA-drug complexes, antibody-drug conjugates, polymer-drug conjugates, polymer nanocapsules, gold nanoparticles, and silver nanoparticles (Astruc, 2015). The most common FDA-approved nanoparticle platforms include polymeric (29%), liposomal (22%), and lipid-based (21%) nanoparticles (Namiot et al., 2023).

Today, the use of nanoparticles ranges from bioimaging markers, early detection screening, drug delivery, and investigations on potential therapeutic use. There is widespread interest in nanomedicine in multidisciplinary fields ranging from bioengineering, cancer biology, vaccinology, and neuroscience. However, the clinical utility of nanoparticles as therapeutic carriers must consider the cost-effectiveness, scale-up manufacturing, batch consistencies, storage capabilities, and time efficiencies of production (Witwer & Wolfram, 2021).

Extracellular vesicles

Extracellular vesicles (EVs) are endogenous nanoparticles released by all cells during intracellular communication (Tetta et al., 2013). The lipid membrane composition of EVs ensures the transportation stability of the vesicle and protection of internal cargo. The size of EVs (30-1,000 nm) allows for the passive diffusion of vesicles across the blood-brain barrier (BBB) to function in the CNS (Saint-Pol et al., 2020). EVs can signal over long ranges and are detectable in biofluids such as urine, cerebrospinal fluid, and plasma (Doyle & Wang, 2019). The substantial circulation of EVs in all tissues and biofluids makes these nanoparticles and their cargo important biomarkers of biological and pathological processes. EV cargo includes proteins, lipids, mRNA, and miRNA (Margolis & Sadovsky, 2019). Once EVs reach their target acceptor cells, the vesicles are endocytosed and release their functional cargo content (McKelvey et al., 2015).

As endogenous nano-delivery vectors, EVs possess properties that reduce immunogenic responses which might be beneficial in a therapeutic setting. However, the advancement of nano-scale technology has just begun to understand the internal

and external properties of EVs as transport carriers. Thus, as a biomolecule delivery system, caution must be taken when isolating and characterizing EVs due to their biologically heterogenous nature.

Polymeric nanoparticles

Polymeric nanoparticles are organic nanoparticles that are believed to be more biocompatible than other nanoparticle formulations. Their assembly depends on 1) electrostatic interactions (positively charged polymers and negatively charged nucleic acids), 2) hydrophobic interactions between polymer chains, and 3) van der Waals forces between polymer, solvent, and nucleic acids (Zielińska et al., 2020). Polymeric nanoparticles are typically composed of a single polymerized backbone monomer that serves multiple functions. The polymeric hydrophobic core increases drug solubility, and the hydrophilic membrane increases the nanoparticle circulation time.

Polymeric nanoparticles have versatile properties as drug delivery platforms due to their tunable size (10-1000 nm), ability for surface modifications, and high circulation time (W. Zhang et al., 2021). However, the use of polymeric nanoparticles has been limited due to toxicity issues (from the cationic polymer), and low biodegradability such that the encapsulated cargo is unable to be released when the polymeric structure does not break down (Raman et al., 2020). Nevertheless, the number of clinical trials using polymeric nanoparticles continues to climb each year (Namiot et al., 2023).

Lipid nanoparticles

Lipid nanoparticles (LNPs) are the most widely used non-viral delivery vectors for gene therapies. When encapsulating negatively charged nucleic acids in the LNP core, through rapid mixing during microfluidics, LNPs self-assemble by hydrophobic and electrostatic interactions with positively charged lipids.

LNPs are composed of many lipid-based components each with their own function and purpose (J. Kim et al., 2021). Cationic lipids are positively charged at or below physiological pH and interact ionically with negatively charged nucleic acids, forming a lipid complex. However, the permanent positive charge of cationic lipids rendered these formulations cytotoxic *in vivo* (*Granot & Peer, 2017*). Hence, ionizable lipids were generated as pH dependent lipids. Ionizable lipids are neutral at physiological pH but become positively charged at acidic pH. The acid dissociation constant (pK_a) of the ionizable lipid headgroup influences critical physiochemical properties such as surface charge, stability, potency and toxicity (P. Patel et al., 2021). In addition to cationic or ionizable lipids, LNPs typically include structural lipids (such as phospholipids or cholesterols) and polyethylene glycol (PEG) lipids which provide particle stability, increase circulation time and are more biocompatible.

Once released in the body, LNPs are trafficked and intracellularly endocytosed via low-density lipoprotein receptors (LDLRs) in an apolipoprotein E (ApoE)-dependent manner (Akinc et al., 2010; Rungta et al., 2013). The majority of LDLRs line epithelial hepatocytes (Dilliard et al., 2021). Thus, delivering LNPs to neurons without off-target expression in the liver has remained a challenge. The majority of brain-derived ApoE is synthesized by astrocytes (H. Wang & Eckel, 2014). However, astrocytes and neurons

cooperate in the regulation and metabolism of lipoproteins and both contain LDLRs (Li et al., 2021; Pfrieger & Ungerer, 2011).

Dissertation Goals

The overarching goal of the work described in this dissertation is to deliver nucleic acids to the brain via nanoparticles, with a focus on miR137 and the regulation of its target proteins. I hypothesized that overexpressing miR137 would decrease the expression of synaptic proteins related to SCZ risk genes. Using neuroblastoma cell cultures, I characterized EVs, polymeric nanoparticles, and LNPs as miR137 delivery vectors (Chapter 2). To test the structure of nanoparticles, I measured particle size, shape, heterogeneity, charge, and encapsulation efficiency. To test the function of nanoparticles, I measured the uptake, toxicity, and release of miRNA cargo *in vitro*. These studies confirmed that LNPs were the most effective delivery vectors *in vitro*, and I continued further work with *in vivo* mouse models. I next investigated the pharmacokinetics, biodistribution, toxicity, and cell type targeting of LNPs in the mouse PFC (Chapter 3). Finally, I used quantitative proteomics to understand the effect of miR137 loaded LNPs on protein expression in the mouse PFC (Chapter 4). Using gene ontology and biological pathway databases, I determined the subcellular location and function of enriched proteins following miR137 or blank LNP treatment. The dissertation concludes with a general discussion (Chapter 5) of the larger implications of LNPs as nucleic acid delivery vehicles as neuroscience tools to modulate gene and protein expression in the brain.

Chapter 2: Nanoparticle formulation and characterization

This chapter contains data that are unpublished.

Introduction

Recent advancements in nanotechnology utilize nano-sized particles to improve disease diagnosis, image tissues with precision scale, and specify treatment to targeted regions (Mitchell et al., 2021). Interest in nanoparticle research has spread to fields such as immunology, cancer biology, and to a lesser extent, neuroscience. However, despite increasing interest, deciding which nanomaterial to use for specific applications remains a challenge.

Extracellular vesicles (EVs) are endogenous nanoparticles released from every cell type in the body and carry proteins, lipids, and nucleic acids. Synthetic nanoparticles, such as polymeric or lipid nanoparticles (LNPs), offer the ability to encapsulate any cargo of choice, but may be more immunogenic than EVs (Mohamed et al., 2019). Polymers are comprised of organic monomers, while LNPs are composed of cholesterol, polyethylene glycol (PEG), cationic, and ionizable lipids. The differences in nanoparticle composition can affect biophysiological properties such as particle size, charge, heterogeneity, encapsulation efficiency, and release properties. In the following experiments, we chose to compare and characterize EVs, polymeric nanoparticles, and LNPs as nucleic acid delivery vehicles.

We overexpressed microRNA137 (miR137) in a mouse neuroblastoma Neuro2A (N2A) cell line and isolated released EVs by size exclusion chromatography. We

detected EV markers in eluted EV fractions and found an incorporation of miR137 in N2A EVs. However, the protocol for EV isolation and overexpression in a biological cell line rendered this nanoparticle type too heterogenous, inconsistent, and low throughput for *in vivo* applications. Next, we characterized the size, heterogeneity, and charge of miR137-loaded polymeric nanoparticles and visualized the cellular uptake in N2A cells. Due to toxicity and inconsistent cargo release, we determined polymeric nanoparticles were not effective delivery vectors. Finally, using miR137-loaded LNPs we characterized the nanoparticle size, heterogeneity, charge, encapsulation efficiency and visualized intracellular endocytosis and miR137 cargo release. LNPs displayed minimal cytotoxicity, homogenous batch results, and effective cargo release, establishing LNPs as the most effective delivery vector. These studies support the use of LNPs as nucleic acid carriers in neuroblastoma cell culture systems.

Materials and Methods

Materials

Mmu-miR137-3p mimic (Assay ID MC10513) and miR mimic negative control #1 (4464058) were purchased from Thermo Fisher Scientific (Waltham, MA). Generation 4 poly(propyleneimine) dendrimer (PPIG4) was obtained from SyMO-Chem (SyMO-Chem; Eindhoven, Netherlands). α-Maleimide-ω-N-hydroxysuccinimide ester poly(ethylene glycol) (MAL-PEG-NHS 5 kDa) was acquired from NOF Corporation (NOF Corporation; White Plains, NY). Ionizable lipid Dlin-MC3-DMA (MC3) was purchased from BioFine International Inc, (BC, Canada). Cationic lipid 1,2-dioleoyl-3-trimethylammoniumpropane (DOTAP; chloride salt) and 2-distearoyl-sn-glycero-3-

phosphocholine (18:0 PC, DSPC) were acquired from Avanti Polar Lipids (Alabaster, AL). Cholesterol and 1,2-dimyristoyl-rac-glycero-3-methoxypolyethylene glycol-2000 (DMG-PEG2k) were purchased from Sigma Aldrich (St Louis, MO).

Nanoparticle Formulation and Characterization

Synthesis of polymeric particles was adapted from previously published protocols (Schumann et al., 2018). Preparation of the nanoplatform was initiated by mixing 10 mg/uL of cyanine7.5 (Thermo Fisher Scientific; Waltham, MA) in 1 mL of Milli-Q water with the PPI G4 dendrimer at a nitrogen to phosphate (N/P) ratio of 0.5 and vortexing the reaction mixture for 30 min at room temperature. 10 mM of mmu-miR137-3p (MC10513, Thermo Fisher Scientific; Waltham, MA) was incorporated into the nanoplatform by mixing into the solution for 30 min at room temperature. The final concentrations of miRNA and PPI G4 dendrimer in the solution were 50 μM and 131.25 μM, respectively. Afterward, MAL-PEG-NHS was added to the reaction mixture (5 mg/mL) and the solution was vortexed during 1 h at room temperature. The prepared nanoparticles were purified by dialysis. Polymeric nanoparticle solutions were stored at 4 °C until used.

Synthesis of LNPs were formulated via microfluidic mixing of one-part ethanol phase (containing the lipids) and three parts aqueous phase (containing the nucleic acid cargo). The ethanol phase contains the MC3:DOTAP:DSPC:Cholesterol:DMG-PEG2k at a molar ratio of 25:50:5:19:1.0 and a mass percentage of 24.8:53.9:6.1:11.3:3.9, respectively (Kinsey et al., 2022; Mousli et al., 2022; X. Yu et al., 2023). The N/P ratio of

lipid to nucleic acid was 5.67. The aqueous phase consists of the nucleic acid cargo in 50 mM citrate buffer at pH 4. Following microfluidic mixing in the NanoAssmblr™ Benchtop (Precision NanoSystem; Product code: NIT0055, BC, Canada) at a 1:3 (ethanol to aqueous) flow ratio, the LNPs were subjected to dialysis for 4 hours at room temperature with PBS (pH 7.2) using a 10 KDa Slide-A-Lyzer (Thermo Fisher Scientific; Waltham, MA) dialysis bag before being transferred to fresh PBS solution overnight at 4 °C. LNPs were then concentrated using pre-washed Amicon Ultra-15 100k MWCO (EMD Millipore) centrifugal filter tubes (Burlington, MA). The nanoparticles were stored at 4°C until used. The LNPs were characterized for hydrodynamic radius and polydispersity index (PDI) using dynamic light scattering (DLS) (Zetasizer Nano ZSP (Malvern Instruments; Malvern, UK). Nucleic acid encapsulation efficiency was determined using a modified Quant-iT RiboGreen RNA kit (Life Technologies; Carlsbad, CA).

Cell Culture

Neuro2A cells were grown in Dulbecco's modified Eagle's medium (DMEM) containing 10% FetalClone serum (Thermo Fisher Scientific; Waltham, MA) and maintained in a humidified incubator with 10% CO_2. Two days before the treatment, cells were plated in 12-well plates with 1×10^6 cells/well. For EV experiments, cells were treated with a final concentration of 200nM of miR137-3p (MiR Mimic MirVana, 4464067, Invitrogen, Waltham, MA), anti-miR137-3p (MiR Inhibititor MirVana, 4464085, Invitrogen, Waltham, MA), or miR mimic scramble (MiR negative control #1 MirVana, 4464059, Invitrogen, Waltham, MA) with equal volume of lipofectamine 2000 (Thermo Fisher Scientific;

Waltham, MA) in Opti-Mem media (Thermo Fisher Scientific; Waltham, MA). When cells were treated with polymeric nanoparticles and LNPs, miR137-3p mimic was loaded into the nanoparticles and applied to cells to a final concentration of 200 nM. In all conditions, after 24h the media was replaced with complete DMEM media, and the cells were harvested 24, 48, 72, or 96h after treatment.

Transient Transfection

48h before transfection 1×10^6 Neuro2A cells were plated in 10 cm^2 plates. On the day of treatment, cells were starved with plain DMEM and incubated for 24h with plasmids containing miR137, anti-miR137, or miRNA-scramble and a red florescent protein (Cat. # CS921MR-1, SO# 103431, Systems Biosciences, Palo Alto, CA) at 1 mg/mL and polyethyleneimine at 2 mg/mL. The next day, transfected media was replaced with complete media. To create a stable cell line, RFP expressing single colony clones were isolated and selected by puromycin antibiotic selection at 30 mg/mL.

Extracellular Vesicle Isolation by Size Exclusion Chromatography

For EV isolation experiments, cell media was replaced with EV-depleted serum (System Biosciences; Palo Alto, CA) for 24 hours prior to conditioned media collection. EVs were isolated based on previously published methods (Sandau et al., 2020). Conditioned media was centrifuged at 300 x g at 4°C for 10 min, filtered in 30 kDa centrifugal filters (MRCF0R030, Millipore Sigma, Burlington, MA), centrifuged again at 10,000 x g at 4°C for 20 min, concentrated on Amicon Ultra 100K filters (Sigma-Aldrich, St. Louis, MO) and centrifuged at 4,000 x g at 4°C for 25 min, filtered through 0.1 mm Spin-X filters

(Sigma-Aldrich, St. Louis, MO), and finally centrifuged at 12,000 x g at 4°C for 3 min. 500 mL of concentrated conditioned media was loaded onto size exclusion chromatography columns (qEV original/35 nm, Izon Science, Medford, CA) according to the manufacturer's recommendations. Twelve 500 µL fractions were collected, stored on ice, and used for RT-qPCR and immunoblot experiments.

RNA Isolation, cDNA, RT-qPCR

Treated and untreated Neuro2A cells were homogenized mechanically using a pellet pestle motor (DWK Life Sciences; Millville, NJ). Total RNA was extracted from whole N2A cells or EVs following manufacturers protocol using the MagMax mirVana miRNA Isolation Kit (ThermoFisher Scientific; Waltham, MA). Total RNA concentration and quality was measured on a NanoDrop spectrophotometer, and 10 ng of RNA was transcribed to cDNA using specific mmu-miR137-3p and Sno202 RNA (endogenous control) primers with MultiScribe Reverse Transcriptase (Applied Biosystems; Waltham, MA). Samples were run in duplicate with universal TaqMan real-time quantitative PCR (StepOnePlus, Applied Biosystems; Waltham, MA) and fold change levels of miR137 were analyzed using the delta-delta Ct calculation procedure (Applied Biosystems; Waltham, MA). Statistical comparisons were made using a one-way ANOVA followed by Dunnett's multiple comparisons post-hoc test in GraphPad Prism 10.0.2. A p-value < 0.05 was considered significant.

Immunoblotting

Neuro2A whole cell and EV samples were lysed and homogenized in 1X RIPA Buffer containing 1X protease inhibitor (Roche; Branchburg, NJ), then centrifuged at 14,500 g for 10 minutes at 4°C. Supernatants were collected for use in the BCA Protein Assay Kit (Thermo Fisher Scientific; Waltham, MA). 10 mg of protein for each sample was subjected to SDS-PAGE through a 12% Bis-Tris precast gel (Bio-Rad; Hercules, CA) against Precision Plus Protein Dual Color Standards and run at 180V for 1 hour with XT MOPS (BioRad) running buffer. The gel was transferred onto a PVDF membrane with transfer buffer containing 10% methanol at 30mV overnight at 4°C then washed 3 x 5 min with Tris Buffered Saline with 0.05% Tween (TBST). Membranes were blocked with 5% nonfat dry milk in TBST at room temperature for 30 minutes. The blots were incubated overnight at 4°C with primary antibodies diluted in TBST: rabbit anti-syntenin (1:1000, ab19903, Abcam; Cambridge, UK), anti-heat shock protein 70 (HSC70) (1:1000, ab51052, Abcam; Cambridge, UK), and anti-endoplasmic reticulum protein 72 (ERP72) (1:1000, ab82587, Abcam; Cambridge, UK). The next day, after washing 3 x 10 min with TBST, the blots were incubated with donkey anti-mouse or anti-rabbit HRP secondary antibody (1:10,000 Jackson ImmunoResearch; West Grove, PA) in 5% milk in TBST solution for 1 hour at room temperature. After antibody incubation, the blots were washed again for 3 x 5 min with TBST and visualized using Clarity Western ECL Substrate (Bio-Rad; Hercules, CA) and the ChemiDoc MP Imaging detection system (Bio-Rad). Bands were analyzed by densitometry using Image J (National Institutes of Health, USA). The proteins of interest were normalized to β-actin. Statistical analysis comparing relative protein expression from each treatment group was performed using

a two-way ANOVA in GraphPad Prism 9.5.0. A p-value < 0.05 was considered significant.

Nanoparticle Tracking Analysis for Extracellular Vesicles

Relative EV quantification and size distribution was determined using the ZetaView PMX 110 (version 8.05.12 SP1, Particle Metrix; Ammersee, Germany). EV void fractions (pooled 1-6) and EV sample fractions (pooled 7-10) are diluted 1:20 in 0.22 mm filtered 0.1X phosphate buffered solution (PBS) and calibrated against 100 nm polystyrene particles (ThermoFisher Scientific; Waltham, MA). Matching capture and analysis settings were maintained for all readings: camera level 14, detection threshold 3, automatic blur size and automatic (8.1–15.9 pix) maximum jump distance. The void volume and each fraction were measured three times with 30 s acquisitions, then averaged to generate sample size (nm) and concentration (particles/ml).

Dynamic Light Scattering for Polymeric and Lipid Nanoparticles

The hydrodynamic diameter, polydispersity index, and zeta potential of the polymeric nanoparticles and LNPs were evaluated by dynamic light scattering (Malvern ZetaSizer NanoSeries, Malvern, U.K.) in PBS buffer (pH 7.4) at 25 °C.

Image Analysis

For *in vitro* live cell imaging, cells were treated with Cy7.5-labeled polymeric nanoparticles then imaged at 2h, 4h, 6h, 24h, and 48h post treatment on a Keyence BZ-X800 fluorescent microscope (Itasca, IL) at 37°C with 10% humidity and 5% CO2. The

number of Cy7.5 positive cells were counted, and the florescent intensity of those cells was quantified using the BZ-X800 Analyzer (1.1.1.8) using relative fluorescent units (RFU).

Toxicity

In vitro cell toxicity after polymeric or LNP treatment was normalized to untreated N2A cells and determined by MTT cell proliferation kit and processed according to manufacturer's protocol (AB211091, Abcam; Cambridge, UK).

Results

Mouse neuroblastoma Neuro2A (N2A) parent cell lines were transfected with a plasmid containing the mouse mature miR137 or antisense sequence (anti-miR137) designed to block endogenous miR137. Single colony clones were selected for the expression of miR137, measured by RT-qPCR, and normalized against a small endogenous RNA (SNO202). A one-way ANOVA determined a significant effect of treatment ($F (3, 8) = 284$, $p < 0.0001$) (**Fig. 1a**). Using Dunnett's multiple comparisons post-hoc test we determined a significant overexpression of miR137 in the cells that had been transfected with the miR137 sequence compared to untreated cells ($F (3, 8) = 284$, $p < 0.0001$), and a significant reduction in miR137 in the cells transfected with the anti-sense sequence ($F (3, 8) = 284$, $p < 0.0152$). Importantly, we found no effect of miR137 levels with treatment of a miR scramble control ($F (3, 8) = 284$, $p < 0.9595$).

Following stable cell line generation, EVs were isolated by applying EV depleted media to the cells 24h before collecting the conditioned cell culture media. The following

day, the concentrated media was loaded onto size exclusion chromatography columns to separate the suspended particles by size and molecular weight. The levels of miR137 in EVs were measured by RT-qPCR and compared against miR137 transfected and untreated N2A cells. An unpaired t-test showed a significant incorporation of miR137 in EVs released from miR137 transfected N2A cells compared to untreated N2A EVs ($t(4) = 3.401$, $p = .0272$) (**Fig. 1b**). Overall, this data suggests that N2A cells can overexpress miR137 and miR137 can be packaged into released EVs.

Immunoblotting for the expression known EV protein markers (alix, syntenin, and HSC70) determined fractions 7-10 contained EVs, while the media only samples and the void fraction 6 did not (**Fig. 2**). Subsequent studies will combine pooled fractions 7-10 for higher EV concentrations. Additionally, there was no presence of the endoplasmic reticulum marker ERP72 in any EV fractions since this subcellular compartment should not be enriched in vesicles released from cells.

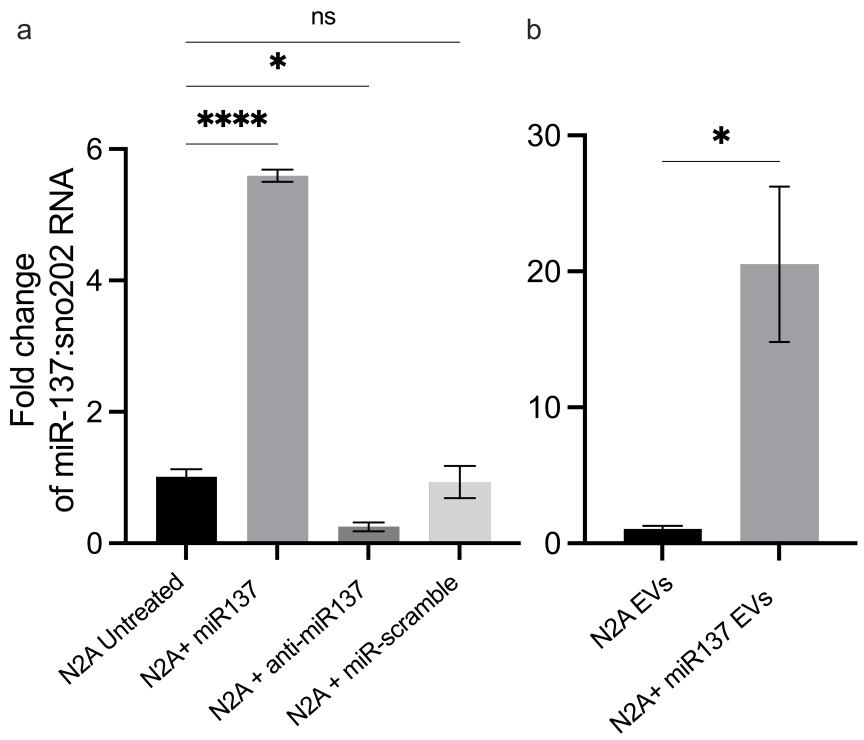

Figure 1 MicroRNA-137 overexpression in N2A cells and released extracellular vesicles

(a) RT-qPCR fold change of Neuro2A (N2A) cells were transfected with a plasmid containing miR-137, anti-miR137, or a miR-scramble control. **b)** miR137 expression in EVs collected from untreated or miR137 transfected N2A cells. All treatments are compared against sno202RNA in untreated N2A cells. n = 3 with triplicate determinations, mean ± SEM. ns, not significant: $p > 0.05$; *$p < 0.05$ and ****$p < 0.0001$.

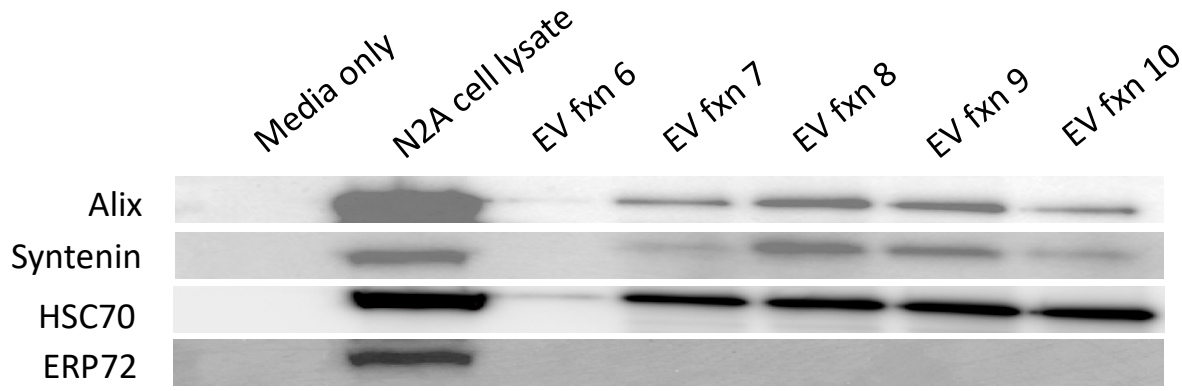

Figure 2 Extracellular vesicle markers in size exclusion chromatography fractions
EVs were collected from conditioned cell culture media from Neuro2A (N2A) cells and size exclusion chromatography fractions (fxn) 6-10 were measured. Immunoblots of known EV markers alix, syntenin, heat shock protein 71 (HSC70), and endoplasmic reticulum protein 72 (ERP72) were measured in media, N2A cell lysate, and EV fxn samples.

Lastly, we performed nanoparticle tracking analysis (NTA) to characterize the distribution of particle size (nm) in EV depleted media, PBS eluent, EV void fractions 1-6, and combined EV fractions 7-10 (N2A EVs) (**Table 1**). As expected, the EV depleted media samples had the smallest particle size with a mean of 175 nm and the lowest particle concentration at 3.2E+5 particles/mL. This value can be considered the "background noise" of particulates in the media (which might include salts, proteins, or cellular debris) that could be detected by the NTA but are not true EVs released by cells. EV fractions were eluted in PBS, so PBS was measured as a control sample in the NTA. We detected larger particle sizes (mean diameter = 356 nm) with a much higher particle concentration at 1.5E+8 particles/mL. We measured similar particle size, standard deviation (STD), standard error of mean (SEM), and concentration in replicate samples of the EV void fraction 6. As determined by immunoblots (**Fig. 2**), the EV void fraction

should not contain EVs, but could contain other biological artifacts with similar characteristics. Lastly, although cellular conditions were identical, replicates 1-5 of N2A EVs were variable in terms of particle size, STD, SEM, and concentration. Some EV samples (EV replicates 1-3) had lower final vesicle concentrations than the EV void fraction or PBS eluent control samples. This data suggests high heterogeneity and variability in EV sample preparation even when basic conditions of preparation are standardized.

Table 1 Extracellular vesicle size characterization

Nanoparticle tracking analysis measured the mean, median, standard deviation (STD), and standard error of mean (SEM) of particle size (nm) and final vesicle concentration in EV depleted media, PBS eluent, EV void fractions, and N2A EV samples.

Replicate Number	Sample	Mean Diameter (nm)	Median Diameter (nm)	STD	SEM	Final Concentration (particles/mL)
1	EV Depleted Media	175	165	104	47	3.2E+5
1	PBS Eluent	356	152	191	85	1.5E+8
1	EV Void Fraction	194	150	70	31	4.5E+8
2	EV Void Fraction	192	167	86	43	9.4E+8
1	N2A EVs	232	150	125	72	3.9E+7
2	N2A EVs	243	162	139	70	2.2E+7
3	N2A EVs	112	112	0	0	4.8E+7
4	N2A EVs	102	102	0	0	5.1E+9
5	N2A EVs	168	159	122	71	3.1E+9

Next, we encapsulated miR137 into polymeric nanoparticles. Using dynamic light scattering (DLS) analysis, we measured the particle diameter (nm), size heterogeneity by polydispersity index (PDI), and charge by ZetaPotential (mV). We found the

polymeric nanoparticles ranged in size from 120–175 nm (**Fig. 3a**), had a PDI between 0.2–0.4 (**Fig. 3b**), and a charge between -10 to -15 mV (**Fig. 3c**). The moderate PDI suggests potential aggregation of polymeric nanoparticles which is reflected in the variable size distribution. Overall, this data demonstrates polymeric nanoparticles can be synthesized with more consistent and reproduceable properties compared to EVs, but still lack some homogenous production properties.

After characterizing the polymeric nanoparticles, we treated N2A cells with polymeric nanoparticles containing an external Cy7.5 fluorophore and loaded with miR137. We used live cell imaging to measure the nanoparticle uptake by counting the number of cells that were Cy7.5+ (**Fig. 4a**) and measuring the Cy7.5 florescent intensity (**Fig. 4b**). A One-way ANOVA revealed a significant effect of treatment in the number of cells that took up the florescent polymers with increasing concentrations ($F(2, 9) = 58.4$, $p < 0.0001$). This data suggests the incorporation and uptake of polymeric nanoparticles can be visualized in live cells and is dose dependent.

Subsequently, we measured the release of miR137 from polymeric nanoparticles after treating N2A cells with increasing concentrations (**Fig. 5**). Unexpectedly, we found a decrease in release of miR137 with increasing polymer doses up to 500 nM, then a large increase at 1000 nM, suggesting the polymeric nanoparticles may have difficulty biodegrading the polymer and releasing the miR137 cargo.

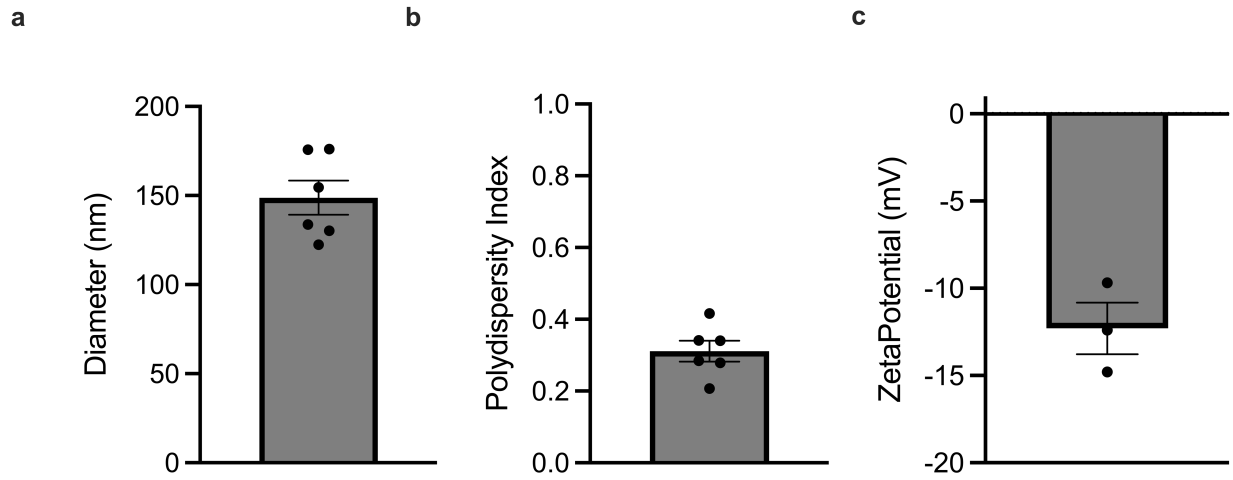

Figure 3 Polymeric nanoparticle characterization

Dynamic light scattering analysis measured the average **a)** diameter (nm), **b)** size heterogeneity (polydispersity index), **c)** and charge (zeta potential (mV)) of polymeric nanoparticles loaded with miR137. n = 3-6 with triplicate determinations, mean ± SEM.

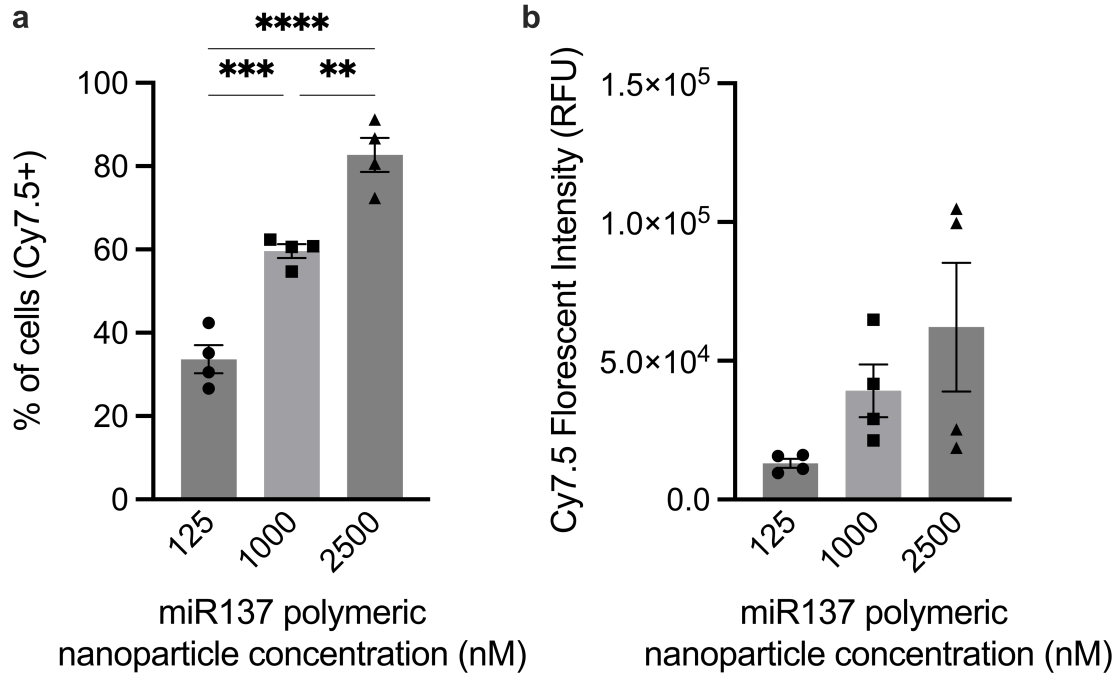

Figure 4 Cy7.5 polymeric nanoparticle uptake

N2A cells were treated with increasing concentrations of Cy7.5 tagged polymeric nanoparticles loaded with miR137 and the uptake was measured by **a)** percentage (%)

of cells Cy7.5+ and **b)** Cy7.5 florescent intensity by relative florescent units (RFU). n = 4 with triplicate determinations, mean ± SEM. ** $p < 0.01$, *** $p < 0.001$ and **** $p < 0.0001$ determined by Tukey's multiple comparisons post-hoc test.

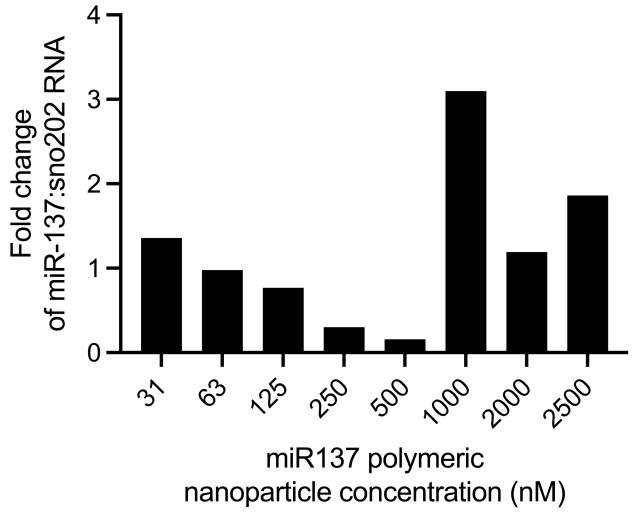

Figure 5 MiR137 release from polymeric nanoparticles

N2A cells were treated with increasing concentrations of polymeric nanoparticles loaded with miR137 and the release of miR137 was measured by RT-qPCR fold change of miR137 expression compared to sno202RNA in untreated cells. Values represent mean determinations with n = 2 in triplicate.

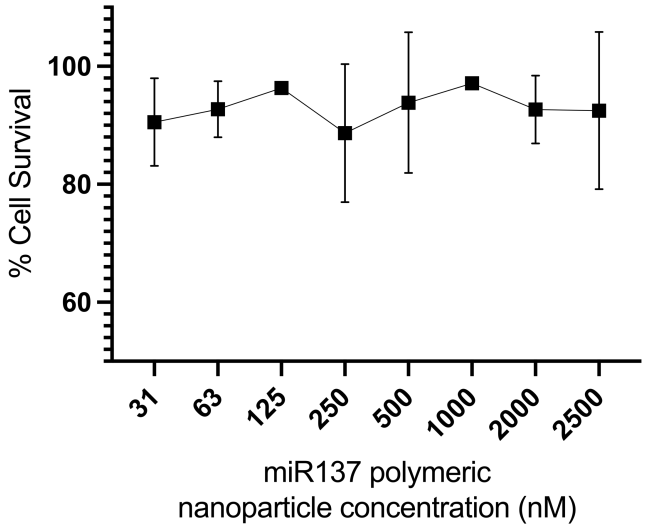

Figure 6 MiR137-loaded polymeric nanoparticle cytotoxicity

N2A cells were treated with increasing concentrations of polymeric nanoparticles loaded with miR137 and percent of cell survival was measured by MTT assay. n = 2 with triplicate determinations, mean ± SEM.

Next, we measured the toxicity of polymeric nanoparticles following treatment with increasing particle concentrations (**Fig 6**) and found mild cytotoxicity with ~ 80% of cell survival relative to untreated, but no effect of dose. Overall, these data suggest miR137 polymeric nanoparticles can encapsulate miR137, endocytose into cell cultures, and vesicle batches are more consistent and reproduceable. However, we determined miR137 polymeric nanoparticles have difficulty releasing cargo with increasing doses and are slightly toxic to N2A cells.

The last nanoparticle type we assessed were miR37-loaded lipid nanoparticles (miR137-LNP). We encapsulated miR137 into LNPs through microfluidics mixing and using DLS we measured the particle diameter (nm), size heterogeneity (PDI), charge (mV), and encapsulation efficiency (%). We found the miR137-LNPs produced consistent batches that were around ~65 nm in diameter (**Fig 7a**), PDI < 0.2 (**Fig 7b**), charge ~2 mV (**Fig 7c**), and high encapsulation efficiencies > 98% (**Fig 7d**). Importantly, miR137-LNP replicates exhibit much lower variability compared to EVs or polymeric nanoparticles, suggesting high reproducibility and consistency with miR137-LNP batches.

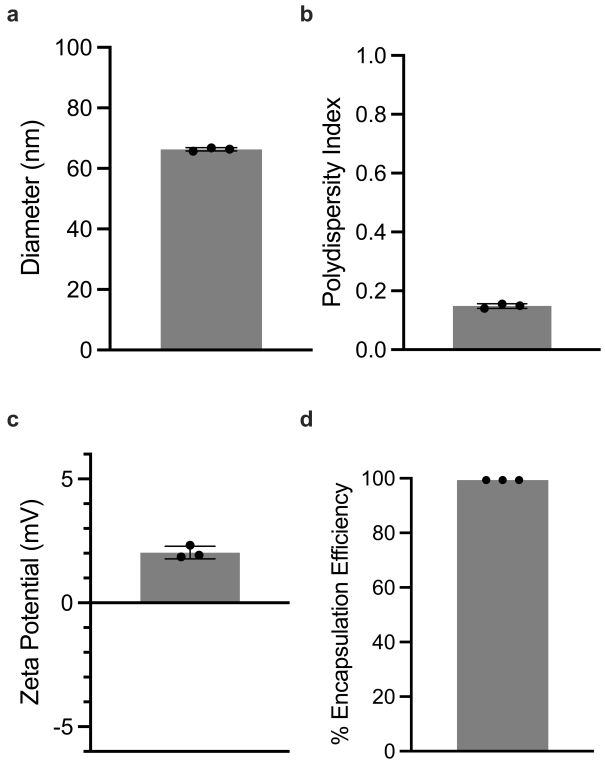

Figure 7 MiR137-loaded lipid nanoparticle characterization

Dynamic light scattering analysis measured the average **a)** diameter (nm), **b)** size heterogeneity (polydispersity index), **c)** charge (zeta potential (mV)) and **d)** encapsulation efficiency of lipid nanoparticles loaded with miR137. n = 3 with triplicate determinations, mean ± SEM.

After characterizing the properties miR137-LNPs, we measured the release of nucleic acids in N2A cells by loading miR137 or anti-miR137 into LNPs. We determined the fold change of miR137 expression compared to sno202RNA by RT-qPCR. A One-way ANOVA found a significant dose effect of miR137 levels in cells treated with miR137-LNPs ($F(2, 3) = 91.36$, $p = 0.0021$) (**Fig 8a**), and inhibition of endogenous

miR137 levels with cells treated with anti-miR137-LNPs (**Fig 8b**). These data suggest LNPs released nucleic acid cargo in a dose dependent manner.

Cytotoxicity was measured by treating N2A cells with increasing concentrations of miR137-loaded LNPs and measuring the percent of cell survival (**Fig. 9**). We found increasing doses of miR137-loaded LNPs were minimally toxic and cells maintained high cell survival rates >95%. Overall, this data demonstrates LNPs offer a delivery vector that can be synthesized with consistent and homogenous batch results, can release functional nucleic acids, and have a minimal cytotoxic effect.

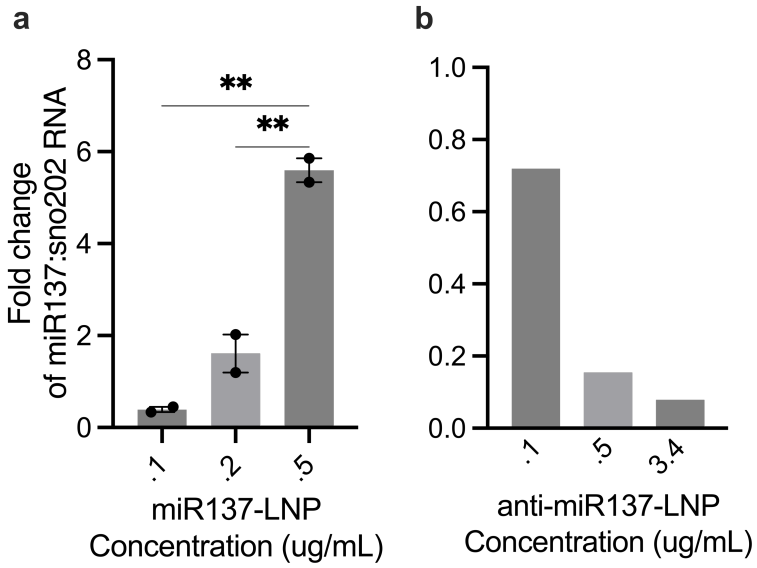

Figure 8 Release of miR137 and anti-miR137 from lipid nanoparticles

N2A cells were treated with increasing concentrations of lipid nanoparticles loaded with **a)** miR137 or **b)** anti-miR137 and the fold change of miR137 expression was measured by RT-qPCR and compared to sno202RNA. n = 1-2 with triplicate determinations, mean ± SEM. ** $p < 0.01$ determined by Tukey's multiple comparisons post-hoc test.

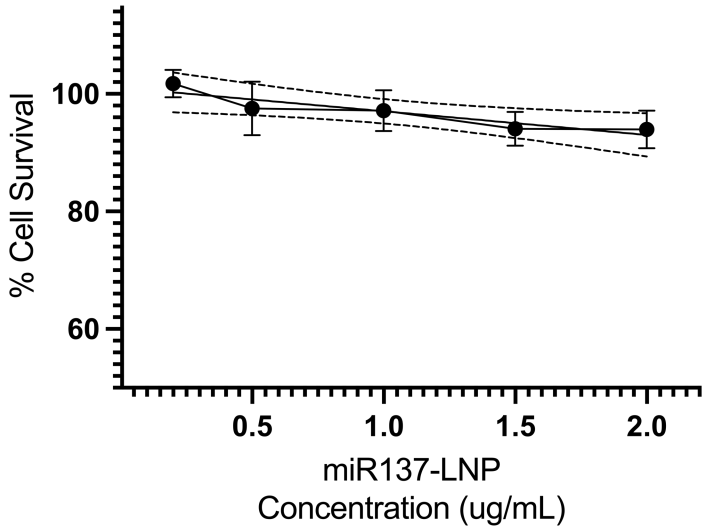

Figure 9 MiR137-loaded lipid nanoparticle cytotoxicity

N2A cells were treated with increasing concentrations of lipid nanoparticles loaded with miR137 and percent (%) cell survival was measured by the MTT assay. n = 6, mean ± SEM.

Discussion

As the burden of neurological diseases continues to increase globally ("Global, Regional, and National Burden of Neurological Disorders, 1990–2016," 2019), the number of effective treatments for heterogenous human populations is severely lacking. Furthermore, the CNS remains the most challenging system to target due to several biological barriers including the BBB, endogenous phagocytosis and immune clearance, and the interconnectivity of deep neural networks made up of many different cell types. Developing a delivery system to improve the stability of encapsulated cargoes as they are transported to the brain, while reducing the off-target side effects, and improving safety profiles, will be extremely valuable.

The use of nanomedicine has pioneered a new wave of research on drug delivery with endogenous and synthetic materials to improve drug solubility, increase

circulation time, and improve precision therapies. Here, we compared the properties of three nanoparticle types to encapsulate and deliver miR137 cargo to neuroblastoma cell cultures. Each nanoparticle material has advantages and disadvantages, some of which are discussed here, and will require careful consideration based on the target tissue application.

To start, nanoparticle size can influence distribution, bioavailability, clearance rates, and uptake in target or off-target organs (De Jong & Borm, 2008). Smaller vesicles (<100 nm) have lower off-target liver uptake and larger vesicles (200-300 nm) are cleared more rapidly by phagocytosis (Seki et al., 2004). We found LNPs had the smallest particle size (~65nm), about half the diameter of EVs or polymeric nanoparticles (100-300 nm). The inconsistency in EV size could be due to the presence of multiple EV populations, including exosomes (30-100 nm) and macrovesicles (0.1-1 mm), which vary in size and biogenesis mechanism (Ståhl et al., 2019). Furthermore, the large size range of polymeric nanoparticles could be due to vesicle aggregation or improper cargo loading. Our polymeric nanoparticles had poor apparent cargo release; however, solely detecting the expression of a delivered cargo could be misrepresenting the efficiency of the delivery system. Although cargo validation is an important step in evaluating an effective vector, future studies will need to measure the downstream functional effects of miR137 delivery by detecting the inhibition of target protein expression. It is possible that LNP delivery *in vitro* will not predict *in vivo* results (Paunovska et al., 2018), so future studies will need to optimize LNP vectors for delivery to the brain.

Another consideration includes nanoparticle charge which can affect uptake by negatively charged cell membranes and cytotoxicity (Rasmussen et al., 2020). Our studies showed polymeric nanoparticles were negatively charged at -10 to -15 mV, LNPs were neutral to slightly positive at 2 mV, and studies show EVs are charged at -30 to -50 mV depending on buffer concentrations (Midekessa et al., 2020). It's possible that polymeric nanoparticle cytotoxicity could be due to the negative vesicle charge but lack endogenous recognition properties that EVs possess. Therefore, synthetic nanoparticles may be less toxic with a neutral or slightly positive charge (Syama et al., 2022).

Synthetic nanoparticles attempt to mimic the inherent properties of EVs including cell or tissue targeting, circulation in bodily fluids, and avoidance of immune activation. However, the most common FDA-approved nanoparticles include lipid-based (21%), polymeric (29%), and liposomal (22%) drugs (Namiot et al., 2023). The lack of EV approved therapeutics could be due to issues with scale-up capabilities, laborious and costly production, and the complexity and heterogeneity of biologically produced vesicles. EVs contain a multitude of lipids, proteins, carbohydrates, cargo, and surface molecules, which may play a role in the complexity of these nano-sized particles. Furthermore, EV isolation methods are highly debated and can vary with cell type (De Sousa et al., 2023). Thus, the field lacks a basic understanding of the role of each EV component and how EVs function as biological delivery vehicles. Alternatives to overloading a biological cell system with a therapeutic cargo (as we have done with miR137 in N2A cells), include retroactively loading EVs with therapeutic agents (Walker et al., 2019). However, without the ability to control for the additional EV surface and

cargo components - some of which remain unknown - we currently do not see a clear path to using EVs as a controlled drug delivery mechanism.

On the other hand, a major advantage of using EVs as delivery vehicles, which synthetic nanoparticles have yet to match, is the endogenous nature of biological vesicles that do not activate the immune response. Our studies showed LNPs are less cytotoxic than polymeric nanoparticles, but EVs are the most compatible with the host-immune system compared other nanocarriers (C. Liu et al., 2017). Additionally, cell survival rates may not fully capture cellular stress states, so further studies will need to investigate the immunogenicity of LNPs in brain tissue. However, the spectrum of individual immune responses to the COVID-19 mRNA vaccine demonstrated the immunogenicity of LNPs may come at a tradeoff of scale-up, shelf-life stability, and therapeutic need.

Overall, the data in this study suggest LNPs are advantageous over polymeric nanoparticles and EVs in terms of scale-up properties, homogenous batch consistencies, and contain critical characteristics for effective nucleic acid delivery. Future studies should determine the *in vivo* applications of LNP biodistribution, cell-type targeting, and immunogenicity in a mouse model. LNPs have the potential to deliver cargos to the brain and improve the therapeutic possibility for neuro-nanomedicine.

Chapter 3: microRNA137-loaded lipid nanoparticles regulate synaptic protein expression in the prefrontal cortex

This chapter is adapted from the following publication:

Palumbo, M.C., Gautam, M., Sonneborn, A., Kim, K., Wilmarth, P.A., Reddy, A.P., Shi, X., Marks, D.L., Sahay, G., Abbas, A.I., Janowsky, A. (2023) MicroRNA-137 loaded lipid nanoparticles regulate synaptic proteins in the prefrontal cortex. *Molecular Therapy.* 2023; S1525-0016(23)00448–3. PMID: 37644723 PMCID: PMC10556225.

Introduction

MicroRNAs (miRNAs) are ~22 nucleotide, single-stranded, noncoding RNAs that modulate developmental processes and cellular function. MiRNAs target specific sets of messenger RNAs (mRNAs) and are key translational silencers of gene expression (Catalanotto et al., 2016). Up to 80% of human genes are regulated by miRNAs, and individual miRNA sequences can regulate complex networks of tens to hundreds of gene targets (R. C. Friedman et al., 2009; Selbach et al., 2008). MicroRNA137 (miR137) is enriched in the embryonic midbrain and forebrain across neurodevelopment (Hollins et al., 2014). In adulthood, miR137 is located in the synapto-dendritic compartment of cortical, subcortical, and hippocampal areas (Kuswanto et al., 2015; Willemsen et al., 2011), where it targets a number of synaptic and developmental mRNAs. Accordingly, over-expression of miR137 in adult mice alters synaptogenesis, synaptic ultrastructure, and synaptic function (He et al., 2018). Genetic deletion of

miR137 results in postnatal lethality; while miR137 heterozygous mice have disrupted synaptic and dendritic growth, repetitive behavior, and impaired learning and social behavior (Y. Cheng et al., 2018). Thus, miR137 dysregulation may be a factor in brain disorders associated with synaptic dysfunction (Arakawa et al., 2019; Cao & Zhen, 2018).

Schizophrenia (SCZ) is a highly heritable (Hilker et al., 2018), polygenic neuropsychiatric disorder characterized by impaired cognition (Abbas et al., 2018), deficits in sensory processing (Javitt et al., 2020), negative symptoms, and episodic psychosis (American Psychiatric Association & American Psychiatric Association, 2013). These symptoms result from synaptic pathology (OBI-NAGATA et al., 2019), and there is substantial overlap of synaptic genes that increase the risk of SCZ and those that are regulated by miR137 (Loohuis et al., 2017; Maury et al., 2023; Sakamoto & Crowley, 2018; Siegert et al., 2015; J. Yin et al., 2014). Furthermore, single nucleotide polymorphisms (SNPs) in the *MIR137* gene are also associated with an increased risk of SCZ (Ripke et al., 2011, 2013). *MIR137* allele variants are linked to SCZ clinical endophenotypes including earlier age of onset, more severe psychotic symptoms, decreased cognitive function (Cummings et al., 2013; Kuswanto et al., 2015; Lett et al., 2013), and alterations in brain structure and activity (Kuswanto et al., 2015; van Erp et al., 2014). Importantly, SNPs in the noncoding region of *MIR137* reduce the expression of miR137 (Guella et al., 2013). Since miR137 expression is decreased in some individuals with SCZ, exogenous replacement of miR137 represents an attractive therapeutic target. However, free floating miRNAs are subject to degradation so a delivery vehicle to protect and target the miRNA is needed.

The lipid nanoparticles (LNPs) encapsulating the COVID-19 mRNA vaccine demonstrated that nanocarriers can be used to traffic nucleic acids for previously unmet therapeutic needs. LNP delivery vectors exhibit the following desirable properties: (1) protection of nucleic acids from nucleases, (2) customization for tissue and cell selectivity, (3) high payload delivery, (4) low toxicity, and (5) feasibility for large scale production (J. Kim et al., 2021). LNP-delivered small nucleic acid therapeutics, including small interfering RNAs, are approved for clinical trials (Rizk & Tüzmen, 2017). Previous studies delivering miRNAs by LNPs to the brain were limited to therapeutic agents for gliomas (Jiménez-Morales et al., 2022). However, the therapeutic effect of LNP-delivered miRNA on synaptic protein networks remains a large gap in neuro-nanomedicine.

As a result, we developed an LNP-based platform to deliver miR137 to neurons, thereby modulating synaptic proteins. Our *in vitro* studies demonstrated that LNPs were effective nucleic acid delivery vehicles and confirmed the release of miR137 cargo and subsequent inhibition of target transcripts. Mouse *in vivo* studies showed that LNPs remained localized to the prefrontal cortex injection site and preferentially expressed tdTomato in Ai9 mice following cre-recombination in neurons relative to other cell types. Delivery of miR137 to the mouse prefrontal cortex significantly modulated a diverse network of pre-and post-synaptic glutamatergic proteins. This work demonstrates that LNPs offer a unique delivery mechanism for nucleic acid transportation to the brain to modulate key synaptic proteins.

Materials and Methods

Materials

Mature mmu-miR137-3p mimic (Assay ID MC10513) and miRNA scramble control (4464059) were purchased from Thermo Fisher Scientific (Waltham, MA). Cy5-mmu-miR137-3p was purchased from Creative Biogene (Shirley, NY) and Cy7.5-PEG-LNP Avanti Polar Lipids (Alabaster, AL). Ionizable lipid Dlin-MC3-DMA (MC3) was purchased from BioFine International Inc, (BC, Canada). Cationic lipid 1,2-dioleoyl-3-trimethylammoniumpropane (DOTAP; chloride salt) and 2-distearoyl-sn-glycero-3-phosphocholine (18:0 PC, DSPC) were acquired from Avanti Polar Lipids (Alabaster, AL). Cholesterol and 1,2-dimyristoyl-rac-glycero-3-methoxypolyethylene glycol-2000 (DMG-PEG2k) were purchased from Sigma Aldrich (St Louis, MO).

Nanoparticle Formulation and Characterization

To encapsulate cargo into LNPs, CleanCap Cre mRNA (5-methoxyuridine; 5-moU) - (L-7211), and CleanCap firefly luciferase (Fluc) mRNA (Fluc-L-7602) were purchased from Trilink Biotechnologies (San Diego, CA). LNPs were formulated via microfluidic mixing of one-part ethanol phase (containing the lipids) and three parts aqueous phase (containing the nucleic acid cargo). The ethanol phase contains the MC3:DOTAP:DSPC:Cholesterol:DMG-PEG2k at a molar ratio of 25:50:5:19:1.0, respectively(Kinsey et al., 2022; Mousli et al., 2022; X. Yu et al., 2023). The aqueous phase consists of the nucleic acid cargo in 50 mM citrate buffer at pH 4. Following microfluidic mixing in the NanoAssmblr^{TM} Benchtop (Precision NanoSystem; Product code: NIT0055, BC, Canada) at a 1:3 (ethanol to aqueous) flow ratio, the LNPs were

subjected to dialysis for 4 hours at room temperature with PBS (pH 7.2) using a 10 KDa Slide-A-Lyzer (Thermo Fisher Scientific; Waltham, MA) dialysis bag before being transferred to fresh PBS solution overnight at 4 °C. LNPs were then concentrated using pre-washed Amicon Ultra-15 100k MWCO (EMD Millipore) centrifugal filter tubes (Burlington, MA). The nanoparticles were stored at 4°C and used for *in vitro* and *in vivo* studies. The LNPs were characterized for hydrodynamic radius and polydispersity index (PDI) using dynamic light scattering (DLS) (Zetasizer Nano ZSP (Malvern Instruments; Malvern, UK). The cholesterol content of the LNPs was determined using Amplex® Red Cholesterol Assay Kit (Cat. # A12216, Thermo Fisher Scientific; Waltham MA) (Lima et al., 2020; Schultz et al., 2019) according to manufacturer's protocol. This assay is based on an enzyme-coupled reaction that detects the free cholesterol. For each sample, background fluorescence was corrected by subtracting the values derived from the no-cholesterol control. The plate was analyzed using Infinite® 200 PRO plate reader (TECAN; Männedorf, Switzerland) using an excitation of 560 nm and emission of 590 nm. The calculated total amount of cholesterol in LNPs was 0.45 µg/µL. Therefore, within the lipid blend, we determined the following lipid amounts in the final LNP solution: 0.99 µg/µL of MC3, 2.15 µg/µL of DOTAP, 0.24 µg/µL of DSPC, and 0.15 µg/µL of DMG-PEG-2k.

Nucleic acid encapsulation efficiency (EE) was determined by ribogreen assay using a modified Quant-iT RiboGreen RNA reagent (Life Technologies; Carlsbad, CA), which can be used to quantify both mRNA and miRNA. For the quantification process, nucleic acid and LNP stock solutions were appropriately prepared in two distinct buffers: 1x TE buffer and 2% Triton X-100 in TE buffer with RNAse-free water. The assay was

performed according to the manufacturer's protocol in a black clear bottom 96-well plate and analyzed using Infinite® 200 PRO plate reader (TECAN; Männedorf, Switzerland) at an excitation of 480 nm and emission of 520 nm. The background fluorescence was subtracted from each sample using PBS control during analysis. The nucleic acid concentration was determined by fitting our LNP sample data to the nucleic acid standard curve. The percent EE for each sample was calculated using the following equation:

$$\%EE = \left(1 - \frac{Total\ nucleic\ acid_{in\ Triton\ TE\ buffer} - Nucleic\ acid\ outside\ LNP_{in\ TE\ buffer}}{Total\ nucleic\ acid_{in\ Triton\ TE\ buffer}}\right) * 100$$

Cryo-Transmission Electron Microscopy

Cryo-TEM images were captured using Falcon III and K3 Summit cameras (Gatan; Pleasanton, CA) with DED at 300 kV. A copper lacey carbon film-coated Cryo-EM grid (Quantifoil, R1.2/1.3 300 Cu mesh) was plunge-frozen using the Vitrobot Mark IV system (FEI; Waltham, MA). To freeze the samples, 2 µL of LNPs were dispensed onto the glow discharged grids in the Vitrobot chamber, which was maintained at 23 ºC and 100% relative humidity. After 30 sec, the samples were blotted with filter paper for 3 sec before being immersed in liquid ethane cooled by liquid nitrogen. The frozen grids were carefully examined for flaws then clipped and assembled into cassettes. The images were captured at a nominal magnification of 45,000 at an electron dose of 15-20 e−/Å^2 then processed and analyzed using Fiji (ImageJ 1.53t; National Institute of Health, USA).

Cell Culture

Neuro2A (N2A) cells (ATCC, CCL-131) are neuroblasts with neuronal and amoeboid stem cell morphology isolated from mouse brain tissue. N2A cells were grown in Dulbecco's modified Eagle's medium (DMEM) containing 10% FetalClone serum (Thermo Fisher Scientific; Waltham, MA) and maintained in a humidified incubator with 10% CO_2. Two days before the treatment, cells were plated in 12-well plates with 1 × 10^6 cells/well. Cells were treated with a final concentration of 200 nM miR137-3p mimic or 200 nM miRNA scramble control with equal volume of lipofectamine 2000 (Thermo Fisher Scientific; Waltham, MA) in 0.5 µL Opti-Mem media (Thermo Fisher Scientific; Waltham, MA). When cells were treated with LNPs, miR137-3p mimic was loaded into the LNPs and applied to cells to a final concentration of 200 nM. In all conditions, after 24h the media was replaced with complete DMEM media, and the cells were harvested 24, 48, 72, or 96h after treatment.

Toxicity

In vitro cell toxicity after LNP treatment was determined by MTT cell proliferation kit and processed according to manufacturer's protocol (AB211091, Abcam; Cambridge, UK). *In vivo* LNP toxicity was determined by weighing animals pre- and post-LNP injection as well as by total animal survival rate.

RNA Isolation, cDNA, RT-qPCR

Live Neuro2A cells or flash frozen brain tissue was cut at 300 µm on a cryostat and 1 mm bilateral prefrontal cortex or cerebellar biopsy punches (Ted Pella; Redding, CA,

USA) were homogenized mechanically using a pellet pestle motor (DWK Life Sciences; Millville, NJ). Total RNA was extracted following manufacturers protocol using the MagMax mirVana miRNA Isolation Kit (ThermoFisher Scientific; Waltham, MA). Total RNA concentration and quality was measured on a NanoDrop spectrophotometer, and 10 ng of RNA was transcribed to cDNA using specific mmu-miR137-3p and Sno202 RNA (endogenous control) primers with MultiScribe Reverse Transcriptase (Applied Biosystems; Waltham, MA). Samples were run in duplicated with universal TaqMan real-time quantitative PCR (StepOnePlus, Applied Biosystems; Waltham, MA) and fold change levels of miR137 were analyzed using the delta-delta Ct calculation procedure (Applied Biosystems; Waltham, MA). Statistical comparisons were made using a two-way ANOVA followed by Sidak's multiple comparisons post-hoc test in GraphPad Prism 9.5.0. A p-value < 0.05 was considered significant.

Immunoblotting

Neuro2A cell samples were lysed and homogenized in 1X RIPA Buffer containing 1X protease inhibitor (Roche; Branchburg, NJ), and then centrifuged at 14,500g for 10 minutes at 4°C. Supernatants were collected for use in the BCA Protein Assay Kit (Thermo Fisher Scientific; Waltham, MA). 10 mg of protein for each sample was subjected to SDS-PAGE through a 12% Bis-Tris precast gel (Bio-Rad; Hercules, CA) against Precision Plus Protein Dual Color Standards and run at 180V for 1 hour with XT MOPS (BioRad) running buffer. The gel was transferred onto a PVDF membrane with transfer buffer containing 10% methanol at 30mV overnight at 4°C then washed 3 x 5 min with Tris Buffered Saline with 0.05% Tween (TBST). Membranes were blocked with

5% nonfat dry milk in TBST at room temperature for 30 minutes. The blots were incubated overnight at 4°C with primary antibodies diluted in TBST: rabbit anti-GluA1 (1:250, AB1504, Millipore Sigma; Burlington, MA), rabbit anti-β-actin (1:1000, AB6276, Abcam; Cambridge, UK), rabbit anti-PSD95 (1:1000, AB238135, Abcam; Cambridge, UK), rabbit anti-TCF4 (1:1000, 185736, Abcam; Cambridge, UK), mouse anti-SYT1 (1:1000, 105011, Synaptic Systems; Gottingen, Germany), mouse anti-CACNA1C (1:1000, AC84814, Abcam; Cambridge, UK), rabbit anti-CPLX1 (1:1000, 10246-2-AP, ProteinTech; Rosemont, IL), and rabbit anti-FMRP (1:1000, AB17722, Abcam; Cambridge, UK). The next day, after washing 3 x 10 min with TBST, the blots were incubated with donkey anti-mouse or anti-rabbit HRP secondary antibody (1:10,000 Jackson ImmunoResearch; West Grove, PA) in 5% milk in TBST solution for 1 hour at room temperature. After antibody incubation, the blots were washed again for 3 x 5 min with TBST and visualized using Clarity Western ECL Substrate (Bio-Rad; Hercules, CA) and the ChemiDoc MP Imaging detection system (Bio-Rad). Bands were analyzed by densitometry using Image J (National Institutes of Health, USA). The proteins of interest were normalized to β-actin as an internal control. Statistical analysis comparing relative protein expression from each treatment group was performed using a two-way ANOVA in GraphPad Prism 9.5.0. A p-value < 0.05 was considered significant.

Animals

Male and female C57BL/6J or Ai9 mice (strain #007909) (Jackson Labs; Bar Harbor, ME) were maintained on a 12-hour light/12-hour dark cycle with lights on at 7 am. Food and water were available ad libitum. All experimental procedures followed the protocols

approved by the Institutional Animal Care and Use Committee at Oregon Health & Science University and the Veterans Affairs Portland Health Care System Institutional Animal Care and Use Committee. Mice were deeply anesthetized with 3% vaporized isoflurane in oxygen (1L/min) until sedated and sacrificed using rapid cervical dislocation and brains were rapidly extracted, flash frozen with liquid nitrogen, and stored at −80°C for further processing.

Injections

Mice were deeply anesthetized with 3% vaporized isoflurane in oxygen (1L/min) until sedated and placed in a stereotaxic apparatus. For the duration of the surgery, isoflurane was maintained at 1%, and mice were kept warm on a heating pad. Carprofen (0.11mL/25g body weight) and dexium (0.01mL/1g body weight) were injected subcutaneously before the surgery. Lidoject (0.2mL/incision) was administered at the surgery site before making an incision. Mice were injected with LNPs containing Firefly luciferase mRNA (0.0023 mg/kg, L-7602, Trilink Biotechnologies), mmu-miR137-3p (0.0018 mg/kg, Life Technologies; Carlsbad, CA), or Cre mRNA (0.0014 mg/kg, L-7211,Trilink Biotechnologies; San Diego, CA) at three locations within the mPFC bilaterally (+/−0.4 medial/lateral, +1.94 anterior/posterior, 1.0, 1.6 and 2.6 depth below brain surface; 0.5 µL nanoparticle per injection site), at a rate of 100 nL per minute.

In vivo Bioluminescent Imaging and Quantification

Mice were injected intraperitoneally with 150 mg Pierce D-Luciferin/kg (Thermo Fisher Scientific; Waltham, MA) body weight according to manufacturer's protocol.

Bioluminescent imaging was conducted on the same animals at 1h, 3h, 5h, 7h, 9h, 24h, 48h, and 96h post LNP injection on the IVIS Spectrum In Vivo Imaging System (PerkinElmer; Waltham, MA). The mouse skull was shaved prior to surgery, but no other parts of the animal required shaving. Image analysis for region of interest (ROI) measurement was performed on Living Image Software (PerkinElmer; Waltham, MA)) and was reported as average radiance (the sum of the radiance from each pixel inside the ROI/number of pixels or super pixels; photons/sec/cm2/sr). Statistical analysis comparing average radiance of fLuc in the brain and the liver at each time point was performed using a two-way ANOVA in GraphPad Prism 9.5.0. A p-value < 0.05 was considered significant.

Immunohistochemistry

Brains were extracted and immediately post fixed overnight in 4% paraformaldehyde in 1X PBS then cryoprotected in 30% sucrose in 1X PBS until the tissue sank. 40 µm sections were cut on a cryostat and free-floating sections were stored in 1X PBS at 4°C until used for immunohistochemistry experiments. Sections were incubated with Tris-EDTA for 20 min at room temperature, then permeabilized for 3 x 5 min with 1X PBS and 0.3% Triton-X. Tissue was then blocked in 1X PBS, 0.3% Trixon-X, and 5% Normal Goat Serum for 1 hr at room temperature. Primary antibodies (mouse anti-NeuN (1:1000, AB104224, Abcam; Cambridge, UK) and rabbit anti-Iba1 (1:1000, AB178846, Abcam; Cambridge, UK) were added to 1X PBS and 0.3% Trixton-X and incubated overnight at 4°C. The next day, tissue was washed in 1X PBS and 0.3% Trixton-X for 3 x 5 min and secondary antibodies (1:1000, Alexa 488 goat anti-rabbit, AB150077,

Abcam; Cambridge, UK) and Alexa 647 goat anti-mouse (1:1000, AB150115, Abcam; Cambridge, UK) were added for 2 hours at room temperature. Sections were washed with 1X PBS, mounted, coverslipped, and dried overnight before imaging. Negative control samples were run with no primary antibodies.

Neuronal Cell Measurements

Mice (n = 2/treatment) were treated every day for five days with PBS or miR137-LNPs. On day 8, brains were extracted and immediately post fixed in 4% paraformaldehyde then cryoprotected in 30% sucrose. 40 µm sections were cut on a cryostat and free-floating sections were processed based on manufacturer's protocol using a Hematoxylin and Eosin staining kit (Vector Laboratories; Newark, CA) (Garman, 2011). Prefrontal cortex tissues sections were imaged on a Keyence BZ-X800 fluorescent microscope. Three sections per animal were analyzed for neuronal cell density based on the prominent nucleus and pale cytoplasm staining. An unpaired t-test was performed using mean neuronal cell densities in PBS or miR137-LNP animals by area field of view (μm^2).

Image Analysis

For *in vitro* live cell imaging, cells were washed with PBS and imaged on a Keyence BZ-X800 fluorescent microscope (Itasca, IL) at 37°C with 10% humidity and 5% CO2 and imaged at 2h, 4h, 6h, 24h, and 48h post treatment. For immunohistochemistry imaging, slides were imaged on a Zeiss ApoTome.2 Axio Imager (Oberkochen, Germany) with standardized exposure levels for each fluorescent channel. The ApoTome imaging

system generates three fluorescent images in one optical section, which helps maintain higher homogenous resolution across the field-of-view compared to a laser scanning confocal microscope (Weigel et al., 2009). Four animals with six images per animal were analyzed for each condition. All images were quantified at 20x magnification. Due to the potential microglial or astrocyte recruitment to the needle tract injection site, the brain tissue directly adjacent (100-200 μm) (Rungta et al., 2013) to the injection site was quantified so overlapping cell type expression would not be skewed. The expression of NeuN (a neuron-specific nuclear marker), Iba1 (a microglia-specific protein marker), GFAP (an astrocyte-specific cell body and extension marker), and tdTomato (a cytoplasmic reporter protein specific to cells where cre-mRNA is translated) was determined as overlapping if the same cell labeled one or more indicated cellular markers. Co-expression was determined by separating each channel and counting fluorescence that overlapped for each cell. Using GraphPad Prism 9.5.0, an ordinary one-way ANOVA with a post-hoc Tukey's multiple comparisons test was used to compare conditions. A p-value < 0.05 was considered significant.

Quantitative proteomics sample preparation

Mass spectrometric analysis was performed by the OHSU Proteomics Shared Resource. Whole brain mouse tissue samples were flash frozen 72h after treatment (PBS n = 6, blank LNP n = 6, miR137-LNP n = 6; 3 males/3 females/group). Blank LNPs include all the same lipid components as the miR137-LNPs, but do not contain any nucleic acid. The brain tissue was cut at 300 μm on a cryostat and 1 mm bilateral prefrontal cortex (Ted Pella; Redding, CA) samples were homogenized in 200ul of 5%

SDS, 50mM triethyl ammonium bicarbonate buffer using Bioruptor Pico and heated to 95C for 5min. Samples were cooled and centrifuged for 5min at 16,000g and supernatant transferred to an Eppendorf lobind tube. Protein concentrations were determined using the Pierce BCA assay. 50ug/sample was digested using trypsin (1:16, trypsin: protein) overnight using S-Trap micro cartridge (Protifi Inc; Farmingdale, NY), after reduction with dithiothreitol, and alkylation with iodoacetamide. Peptides were eluted from the S-Trap using 40ul each of 50mM TEAB, 0.2% aqueous formic acid, and 50% Acetonitrile containing 0.2% formic acid, pooled, and dried in a speedvac. Each sample was suspended in 100ul of HPLC water and a peptide assay was done using Pierce Quantitative Colorimetric Peptide Assay Kit (Thermo Fisher Scientific; Waltham, MA).

TMT labeling and mass spectrometric analysis

In preparation for tandem mass tag (TMT) labeling, 18 dried unfractionated peptide samples (15ug/sample) were dissolved in 20 µL of 100 mM triethylammonium bicarbonate buffer, and TMT 18-plex reagents (Thermo Fisher Scientific; Waltham, MA) were dissolved at a concentration of 9.6µg/µL in anhydrous ACN. Each of the samples was then labeled by adding 12 µL (115 µg) of an individual TMT reagent, followed by shaking at room temperature for 1 hr. Two µL of each labeled sample in each group were then pooled, 2 µL of 5% hydroxylamine added, the samples incubated for 15 min, dried by vacuum centrifugation, dissolved in 33.8 µL of 5% formic acid, and 2µg peptides analyzed by a single 40-min LC-MS/MS method using an Orbitrap Fusion as described below. This run was performed to normalize the total reporter ion intensity of

each multiplexed sample and to check labeling efficiency. After the normalization and efficiency run, the remaining unmixed samples were then combined in adjusted volumes to yield equal summed reporter ion intensities during the subsequent two-dimensional liquid chromatography/mass spectrometry analysis (2DLC/MS). Following volume-based normalization, the combined samples (45.6µg) were dried by vacuum centrifugation, TMT-labeled samples were reconstituted in 40µL of 10mM ammonium formate, pH 9 and separated by two-dimensional nano reverse-phase liquid chromatography/mass spectrometry (2D-LC/MS) using a Dionex NCS-3500RS UltiMate RSLCnano UPLC and Orbitrap Fusion Tribrid mass spectrometer (Thermo Scientific; Waltham, MA). TMT labeled peptides were eluted from the first dimension high pH column using sequential injections of 20 µL volumes of 17%, 20%, 21%, 22%, 23%, 24%, 25%, 26%, 27%, 28%, 29%, 30%, 31%, 32%, 33%, 34%, 35%, 40%, 50%, and 90% ACN in 10 mM ammonium formate (pH 9) at a 3 µl/min flow rate. Eluted peptides were diluted at a tee with a mobile phase containing 0.1% formic acid at a 24 ul/min flow rate. Peptides were delivered to an Acclaim PepMap 100 µm x 2 cm NanoViper C18, 5 µm trap on a switching valve. After 10 min of loading, the trap column was switched on-line to a PepMap RSLC C18, 2 µm, 75 µm x 25 cm EasySpray column (Thermo Scientific; Waltham, MA). Peptides were then separated at low pH in the 2nd dimension using a 5-25% ACN gradient over 100 min in mobile phase containing 0.1% formic acid at a 300 nl/min flow rate. Tandem mass spectrometry data was collected using an Orbitrap Fusion Tribrid instrument (Thermo Scientific; Waltham, MA). Peptides were separated using the instrument's EasySpray NanoSource, survey scans performed in the Orbitrap mass analyzer, and data-dependent MS2 scans performed in the linear ion

trap using collision-induced dissociation following isolation with the instrument's quadrupole. Reporter ion detection was performed in the Orbitrap mass analyzer using MS3 scans following synchronous precursor isolation in the linear ion trap, and higher-energy collisional dissociation in the instrument's ion-routing multipole.

Proteomic data analysis

The protein sequences searched were canonical mouse reference FASTA sequences (21,968 proteins) downloaded December 26, 2022 from www.UniProt.org. Common contaminants (175 sequences) were added, and sequence-reversed entries were concatenated for a final protein FASTA file of 44,286 sequences.

The 20-fraction TMT 18-plex sample produced 20 instrument files that were processed with the PAW pipeline (Wilmarth et al., 2009) (https://github.com/pwilmart/PAW_pipeline). Binary files were converted to text files using MSConvert (Chambers et al., 2012). Python scripts extracted TMTpro reporter ion peak heights and fragment ion spectra in MS2 format (McDonald et al., 2004). There were 334,353 linked MS2/MS3 scans acquired. The Comet search engine (version 2016.03) (Eng et al., 2013) was used: 1.25 Da monoisotopic peptide mass tolerance, 1.0005 Da monoisotopic fragment ion tolerance, fully tryptic cleavage with up to two missed cleavages, variable oxidation of methionine residues, static alkylation of cysteines, and static modifications for TMTpro labels (at peptide N-termini and at lysine residues).

Top-scoring peptide spectrum matches (PSMs) were filtered to a 1% false discovery rate (FDR) using an interactive GUI application to set thresholds in delta-mass histograms and conditional Peptide-prophet-like linear discriminant function

(Keller et al., 2002) score histograms where incorrect delta-mass and score histogram distributions were estimated using the target/decoy method (Elias & Gygi, 2007). The 115,725 filtered PSMs were assembled into protein lists using basic and extended parsimony principles and required two distinct peptides per protein per plex. The final list of identified proteins, protein groups (indistinguishable peptide sets), and protein families (highly homologous peptide sets) were used to define unique and shared peptides for quantitative use. Total (summed) reporter ion intensities were computed from the PSMs associated with all unique peptides (final grouped protein context) for each protein.

The protein intensity values for each biological sample in each biological condition were compared for differential protein expression using the Bioconductor package edgeR (Robinson et al., 2010) within Jupyter notebooks. Result tables contained typical proteomics summaries, reporter ion intensities, and statistical testing results. Further investigation of comparing proteomic distributions across biological groups determined two outlier samples (PBS, miR137-LNP). A Grubb's test was used to determine putative sample outliers based on the relative protein abundance levels of house-keeping genes (Beta tubulin, GAPDH, DJ-1, actin) (Wiśniewski & Mann, 2016). Subsequent data was interpreted with the removal of these two samples from further analysis. A two-sample t-test was used to compare abundance differences of individual a priori proteins of interest between biological conditions.

The mass spectrometry proteomics data have been deposited to the ProteomeXchange Consortium (http://proteomecentral.proteomexchange.org) via the

PRIDE partner repository (Perez-Riverol et al., 2022) with the dataset identifier PXD041648.

Biological Network Analysis

Following Tandem TMT mass spectrometry analysis of samples treated with miR137-LNP, blank LNPs, or PBS (n = 5-6/group) public databases were used to determine differentially expressed protein cellular location and biological process enrichment. The STRING 11.5 (Szklarczyk et al., 2023) database creates networks of known and predicted protein-protein interactions from over 24.5 million proteins. Following input of differentially expressed proteins, we sought to determine network scale protein enrichment in functional classifications defined by Gene Ontology including biological process (https://www.informatics.jax.org/vocab/gene_ontology/GO:0008150), subcellular components (https://www.informatics.jax.org/vocab/gene_ontology/GO:0005575), and molecular function (https://www.informatics.jax.org/vocab/gene_ontology/GO:0003674). Similarly, SynGO (Koopmans et al., 2019) was used to investigate subcellular compartmentalization of differentially expressed proteins and where genes of interest are translated, either in the neuropil or the soma (Glock et al., 2021). Finally, when comparing differentially expressed proteins after miR137 treatment to GWAS hits for SCZ risk, the FUMA 1.5.3 GENE2FUNC was cross referenced (Watanabe et al., 2017).

Data Availability

All data associated with this study are available in the main text or the supplemental material. All quantitative proteomics data have been submitted to the ProteomeXchange Consortium via the PRIDE partner repository (Perez-Riverol et al., 2022) with the dataset identifier PXD041648.

Results

We first synthesized and characterized LNPs to modulate synapses in the brain. Initial testing of LNP formulations compared LNPs composed of MC3 (ionizable) only, SM102 (ionizable cationic) only, SM102 and DOTAP (cationic), or MC3 and DOTAP lipids. We found LNP formulations combining MC3 and DOTAP lipids were the most efficient at cargo release (data not shown). Subsequent formulations used MC3 and DOTAP lipids to self-assemble into LNPs with nucleic acid cargo via intermolecular interactions using microfluidics along with structural lipids (DSPC), sterols (cholesterol), and PEG-lipids (DMG-PEG2k) (**Fig. 10A**). LNPs with three nucleic acid cargos were tested with consistent batch results: firefly luciferase mRNA (fLuc-mRNA-LNP), Cre mRNA (cre-mRNA-LNP), and microRNA137 (miR137-LNP). Dynamic light scattering analysis of LNP formulations demonstrated homogenous particle sizes (~70 nm) with low polydispersity index (<0.2) (**Fig. 10B**), slightly positive charge (~2 mV) (**Fig. 10C**), and high encapsulation efficiencies (>98%) (**Fig. 10D**). One-way ANOVA determined no significant variation in LNP zeta potential ($F(2, 6) = 1.024$, $p = 0.4142$). Cryo-transmission electron microscopy images of miR137-LNPs showed concentric multilamellar “onion-like” structures with internal aqueous space (**Fig. 10E**). Overall, reliable LNP batch consistencies suggest this preparation method is suitable for various

nucleic acid cargos.

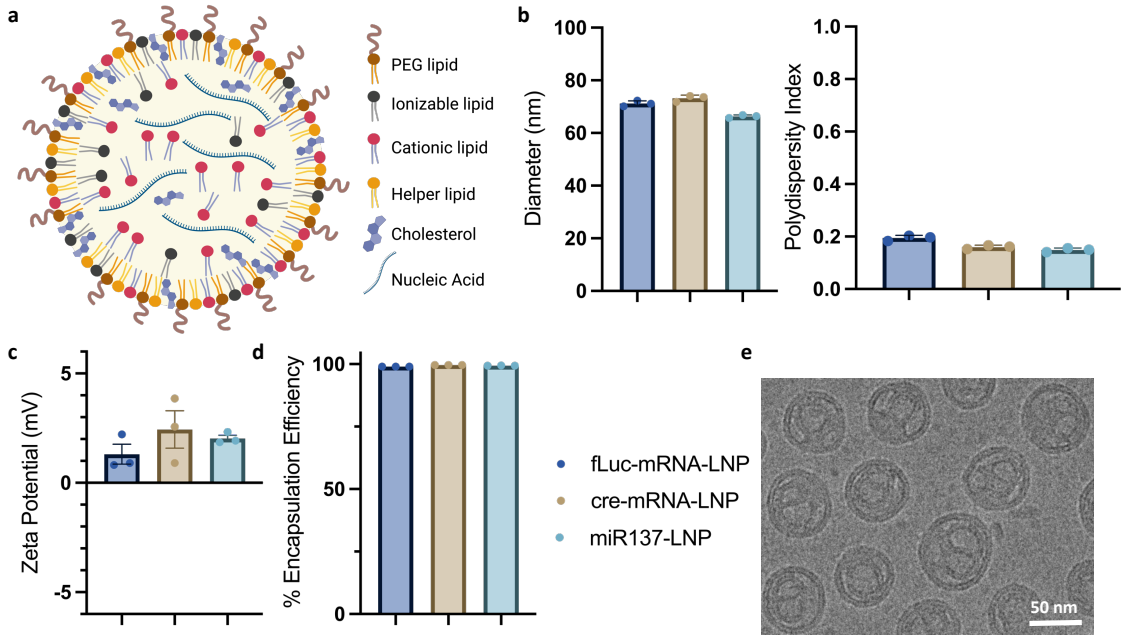

Figure 10 Lipid nanoparticle characterization

A) Schematic of an LNP comprised of lipid components and an encapsulated nucleic acid. Dynamic light scattering analysis characterizing LNPs with **B)** hydrodynamic size (nm) and particle heterogeneity (polydispersity index), **C)** zeta potential (mV), and **D)** nucleic acid encapsulation efficiency (%). **E)** Cryo-TEM image of miR137-LNP scale bars: 50 μm. n = 3 with triplicate determinations, mean ± SEM. Firefly luciferase mRNA (fLuc-mRNA-LNP), Cre mRNA (cre-mRNA-LNP), and microRNA137 (miR137-LNP)

By using a fluorophore tagged to PEG-lipids or the mature miR137 sequence, we visualized LNP uptake, intracellular trafficking, and endosomal escape of miR137 in live cells (**Fig. 11A**). Mouse neuroblastoma Neuro2A (N2A) cells endocytosed Cy7.5

tagged-LNPs (Cy7.5-LNP, magenta), which did not sequester to the lysosomal compartment (LysoTracker, blue) at 6h. Importantly, miR137 cargo (Cy5-miR137, magenta) was visualized in the cytosol and perhaps was released in the cytoplasm through endosomal escape (nuclear stain, DAPI, blue) (**Fig. 11B**). Treating N2A cells with increasing concentrations of miR137-LNPs was non-toxic with high cell survival (**Fig. 9**). At 24h, a one-way ANOVA determined that adding 200nMscramble miRNA in lipofectamine to N2A cells did not change the expression of miR137 levels compared to untreated cells ($p > 0.999$). Adding miR137 loaded in LNPs significantly increased miR137 levels ($F (3, 61) = 11.18$, $p < 0.0001$) and improved the transfection efficiency compared to adding the miR137 mimics in lipofectamine ($F (3, 61) = 11.18$, $p < 0.0001$) (**Fig. 11C**). A two-way ANOVA demonstrated an effect of treatment that miR137 expression persisted for 96h post treatment ($F (3, 39) = 6.011$, $p = 0.0018$) (**Fig. 16 A1A**) and was dose dependent (**Fig. 16 A1B**).

Compared to N2A untreated cells, a two-way ANOVA with Dunnett's multiple comparisons test determined treatment with miR137 mimics in lipofectamine significantly inhibited translation of several miR137 synaptic protein targets: transcription factor 4 (TCF4) ($F (3, 62) = 45.35$, $p = 0.0177$), synaptotagmin 1 (SYT1) ($F (3, 62) = 45.35$, $p < 0.0001$), and the voltage-gated calcium channel a1C (CACNa1C) ($F (3, 62) = 45.35$, $p = 0.0003$) (**Fig. 11D**) (**Fig. 17 A3)**, in addition to other synaptic protein targets such as the glutamate receptor 1 (GluA1) ($F (1, 48) = 87.33$, $p = 0.0141$), synaptophysin (Syn) ($F (1, 48) = 87.33$, $p = 0.0245$), complexin 1 (CPLX1) ($F (1, 48) = 87.33$, $p < 0.0001$), and the Fragile X mental retardation protein (FMRP) ($F (1, 48) = 87.33$, $p = 0.0008$) (**Fig. 17 A3A, A3B**). Treatment with miR137-LNPs showed an even

larger inhibition of TCF4 (F (3, 62) = 45.35, p < 0.0001), SYT1 (F (3, 62) = 45.35, p < 0.0001), and CACNa1C (F (3, 62) = 45.35, p < 0.0001), while miRNA scramble had no effect on TCF4 (F (3, 62) = 45.35, p = 0.9171), SYT1 (F (3, 62) = 45.35, p = 0.9971), or CACNa1C (F (3, 62) = 45.35, p = 0.9953) (**Fig. 11D**). Importantly, expression of a protein that is not a target of miR137, post synaptic density 95 (PSD95), was unaffected (F (1, 48) = 87.33, p > 0.9999) by miR137 mimic or miR137-LNPs, demonstrating the specificity of miR137 to target specific transcripts. From this, we concluded that LNPs endocytosed into neuroblastoma cell cultures and released functional miR137 cargo capable of targeting downstream transcripts.

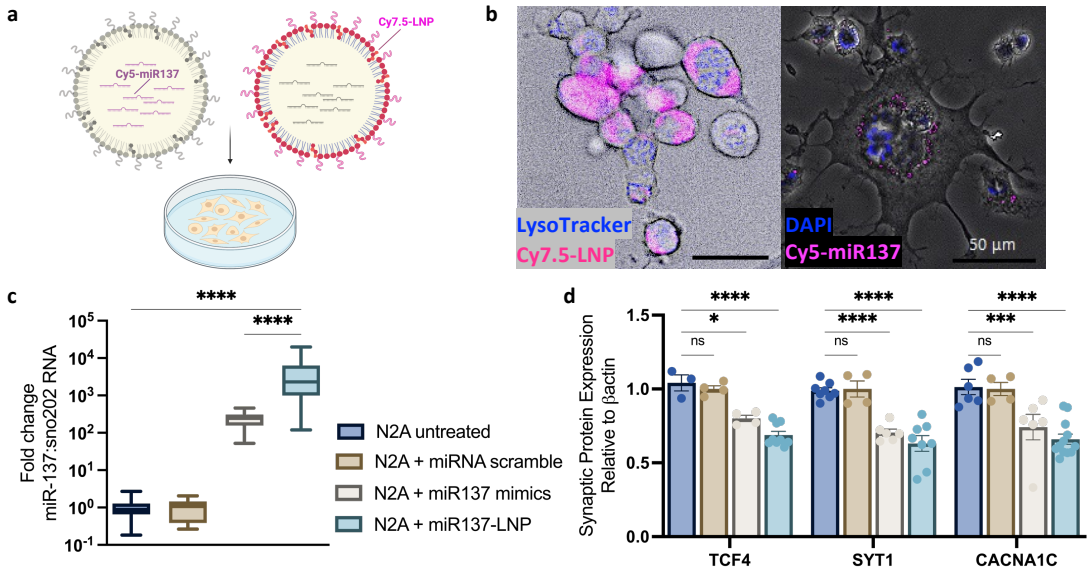

Figure 11 Lipid nanoparticle delivery and miR137 release in cell culture

a) Schematic of fluorophore tagging of LNPs (Cy7.5-LNP) or miR-137 cargo (Cy5-miR137) in Neuro2A cells. **b)** Live cell imaging of LNP uptake (Cy7.5-LNP, magenta) at 6h without lysosomal compartment sequestering (LysoTracker, blue) and cytoplasmic release of miR137 (Cy5-miR137, magenta) cargo (nuclear stain, DAPI, blue). **c)** RT-qPCR fold change miR137 expression compared to sno202RNA in N2A cells at 24h

after treatment with 200nM of miRNA scramble, miR137 mimic, or miR137-LNPs. **d)** Translational inhibition of target synaptic proteins transcription factor 4 (TCF4), synaptotagmin 1 (SYT1), and voltage gated calcium channel α1c (CACNA1C) after treatment with 200nM miR137 mimic, miR137-LNPs or miRNA scramble compared to untreated N2A cells. n = 3-8 with triplicate determinations, mean ± SEM. ns, not significant: $p > 0.05$; *$p < 0.05$; ***$p < 0.001$ and ****$p < 0.0001$.

To study the *in vivo* biodistribution and pharmacokinetics of LNPs in the brain, we bilaterally injected firefly luciferase mRNA encapsulated in LNPs (fLuc-mRNA-LNP) into the mouse prefrontal cortex (PFC). A two-way ANOVA revealed robust luminescent radiance near the injection site with no detectable expression in the liver ($F (1, 26) = 89.99$, $p < 0.0001$) or other off-target organs (**Fig. 12A**, **12B**). The same experimental animals were repeatedly measured, and radiance peaked between 9h and 24h ($F (7, 26) = 10.77$, $p < 0.0001$) post injection, and returned to baseline by 96h (**Fig. 12C**). Thus, LNP nucleic acid cargo is bilaterally and locally expressed at the direct PFC injection site without detectable off-target expression. We did not detect any overt toxicity as all experimental animals survived until the experimental endpoint, two weeks following LNP injection (**Fig. 12D**) and did not lose more than 5% of their original body weight (g) (**Fig. 12E**). In separate experiments, we found that delivery of miR137-LNPs every day for five days did not result in weight loss (g) (**Fig. 12F**) or cellular anatomical disruptions determined by neural cell density counts (S. Liu et al., 2014) (unpaired t-test, $t(12) = 1.175$, $p = 0.2629$) (**Fig. 18 A3**), demonstrating the potential use of repeated LNP treatments in the brain.

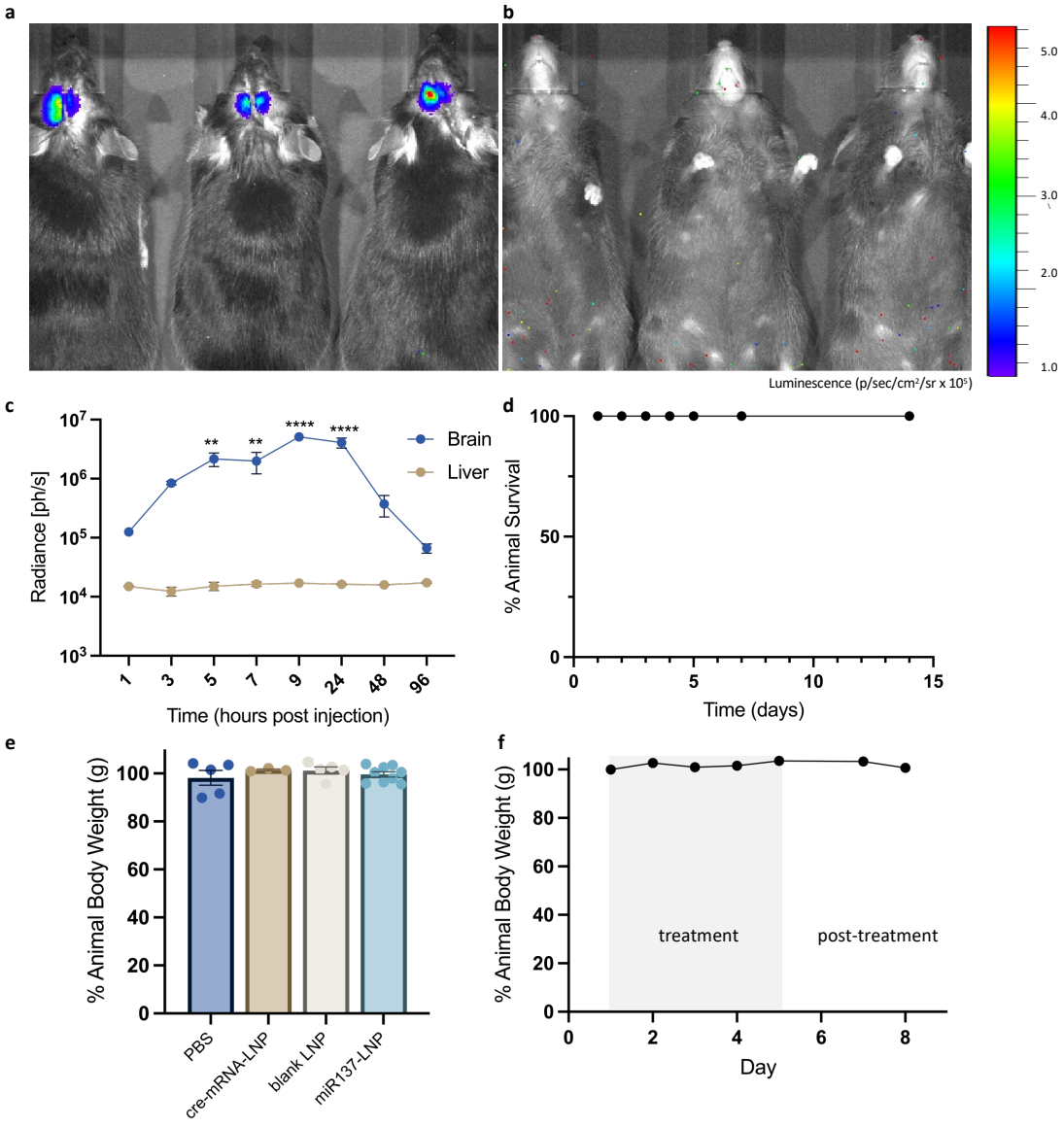

Figure 12 Lipid nanoparticle mediated transfection and toxicity in vivo

Representative **a)** dorsal and **b)** ventral images of luciferase bioluminescence in mouse brain and other tissues 24h post a single injection in the prefrontal cortex with firefly luciferase mRNA LNPs. **c)** Time curve (hours post injection) of luciferase radiance (photons/second) in the brain and the liver. n = 3, mean ± SEM; $^{**}p < 0.01$ and $^{****}p < 0.0001$. **d)** Percent animal survival after a single bilateral intracerebral injection with LNPs. n = 6, mean ± SEM **e)** Percent change in animal body weight after single bilateral intracerebral injection with PBS, cre-mRNA-LNP, blank LNP, or miR137-LNPs. n = 3-10,

mean ± SEM. In separate experiments, animals received five consecutive bilateral intracerebral injections with miR137-LNPs (Day 1-5) **f)** and the percent change in animal body weight was measured up to 8 days. n = 2, mean ± SEM

Using immunohistochemistry to multiplex neuron (NeuN+), microglia (Iba1+), and astrocyte (GFAP+) markers in sectioned PFC tissue, we determined LNP cargo expression in specific cell types. We delivered cre-mRNA-LNPs to Ai9 mice, a Cre reporter strain with a loxP-flanked STOP cassette preventing transcription of a CAG promoter within the ubiquitously expressed ROSA26 locus. Ai9 mice express robust tdTomato fluorescence following cre-mediated recombination. In this case, there is no fluorophore tagging of the LNP itself, thus there is no way to visualize the uptake of LNPs. Instead, we rely on visualizing the expression of the cre-mRNA as it is translated to the tdTomato reporter protein. To focus our analysis on LNP-induced effects, rather than tissue damage and microglial recruitment to the needle tract, we quantified tdTomato expression in the adjacent 100-200 μm from the injection site (**Fig. 19 A4A, A4B**) (Rungta et al., 2013). Low magnification fluorescent microscopy images showed robust bilateral tdTomato+ (red) cells at the PFC injection site (**Fig. 13A**). 81.11% of tdTomato+ cells were NeuN+, 15.64% of tdTomato+ cells were Iba1+, and 3.25% of tdTomato+ cells were GFAP+. One-way ANOVA indicated a significant effect of cell marker (NeuN/Iba1/GFAP) on tdTomato+ expression ($F(2, 66) = 427.4$, $p < 0.0001$) (**Fig. 13B**-**13D**). Post-hoc analysis using Tukey's multiple comparisons test indicated that tdTomato expression differed significantly by cell marker (NeuN vs Iba1, $p < 0.0001$); (NeuN vs GFAP, $p < 0.0001$); (GFAP vs Iba1, $p < 0.0001$). These data suggest LNP nucleic acid cargo is preferentially expressed in neurons in the mouse PFC.

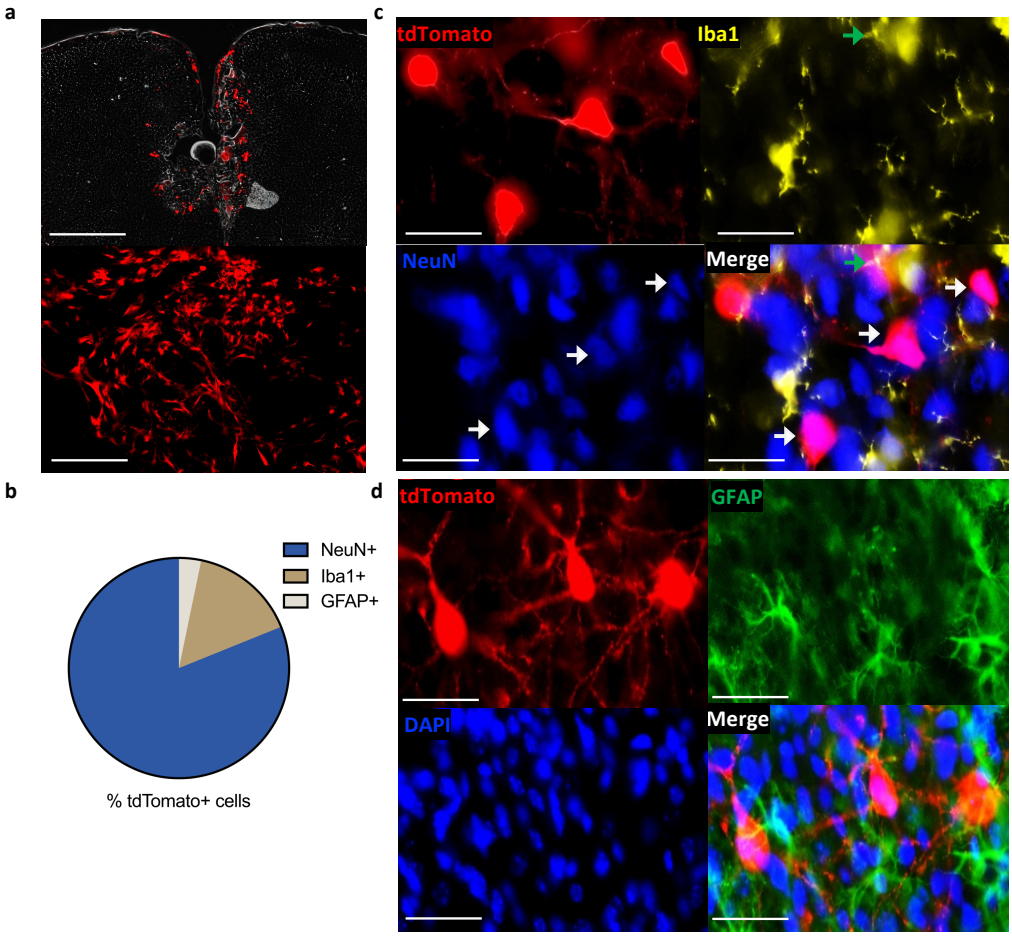

Figure 13 Lipid nanoparticle cell type expression in the brain

Mice received bilateral intracerebral injections in the prefrontal cortex with cre-mRNA-LNPs which express tdTomato (red) following cre-recombination. **a)** High (top) and low (bottom) magnification of tdTomato florescence and injection placements in the prefrontal cortex. scale bars: 500 µm **b)** Quantification of tdTomato+ cells preferentially co-expressed with neuronal (NeuN+, blue) over microglial (Iba1+, yellow) or astrocyte (GFAP+, green) markers (nuclear stain, DAPI, blue). **c)** TdTomato+ cells overlap slightly with Iba1+ cells (green arrows), but mostly co-express with NeuN+ cells (white arrows). **d)** TdTomato+ cells do not co-label with GFAP+ cells. scale bars: 5 µm; n = 4, mean ± SEM; ****$p < 0.0001$.

Following confirmation that LNPs can effectively deliver nucleic acids to PFC neurons *in vivo*, we sought to determine if miR137-LNPs can alter synaptic protein expression. Mice received bilateral injections of miR137-LNPs or PBS into the PFC. After 24h, a two-way ANOVA with Tukey's test for post-hoc comparisons determined miR137 levels were significantly upregulated in the PFC compared to small nucleolar RNA 202 (sno202) with no detectable changes in cerebellar tissue ($F(1, 25) = 2.865$, $p = 0.0391$) (**Fig. 14A**). Unbiased isobaric-labeling quantitative proteomics of PFC biopsy punches was used to compare 4,807 proteins after 72h from three experimental groups (n = 5-6/group): PBS, blank LNPs, or miR137-LNPs. This experimental design allowed us to determine the proteomic effects of the LNPs alone (PBS vs. blank LNP) and of the miR137 alone (blank LNP vs. miR137-LNP). Comparing differentially expressed proteins (DEPs) from blank LNP and miR137-LNP treatments indicated that 224 proteins were altered with 105 upregulated (red) and 119 downregulated (blue) (**Fig. 14B**). The STRING (Szklarczyk et al., 2023), Gene Ontology, SynGo (Koopmans et al., 2019), and FUMA GENE2FUNC (Watanabe et al., 2017) databases generated functional and structural classifications of known protein-protein network interactions based on the DEPs from miR137-LNP compared to blank LNP treatments. The databases confirmed that 52% of the total DEP from miR137-LNPs were involved in neuronal development (GO:0032502) including neurogenesis and neuron differentiation (**Fig. 20 A6**) although the experimental animals were adults, where we might expect the majority of neuronal development to have already occurred (Semple et al., 2013). Additionally, 23% DEP from miR137-LNPs were in neuronal synapses (GOCC:0045202) (**Fig. 21 A7A**). MiR137-LNPs affected both pre-and post-synaptic proteins (**Fig. 14C**)

with the majority of the DEPs translated in the neuropil (dendrites and axons) compared to the soma (**Fig. 21 A7B**) (Glock et al., 2021), suggesting local translation of synaptic proteins. Further investigation determined 67% of synaptic DEPs from miR137-LNP were glutamatergic (GOCC:0098978). Our findings support previous work demonstrating that miR137 modulates genes and proteins involved in neuronal development (Loohuis et al., 2017) and glutamatergic synaptic function (Olde Loohuis et al., 2015).

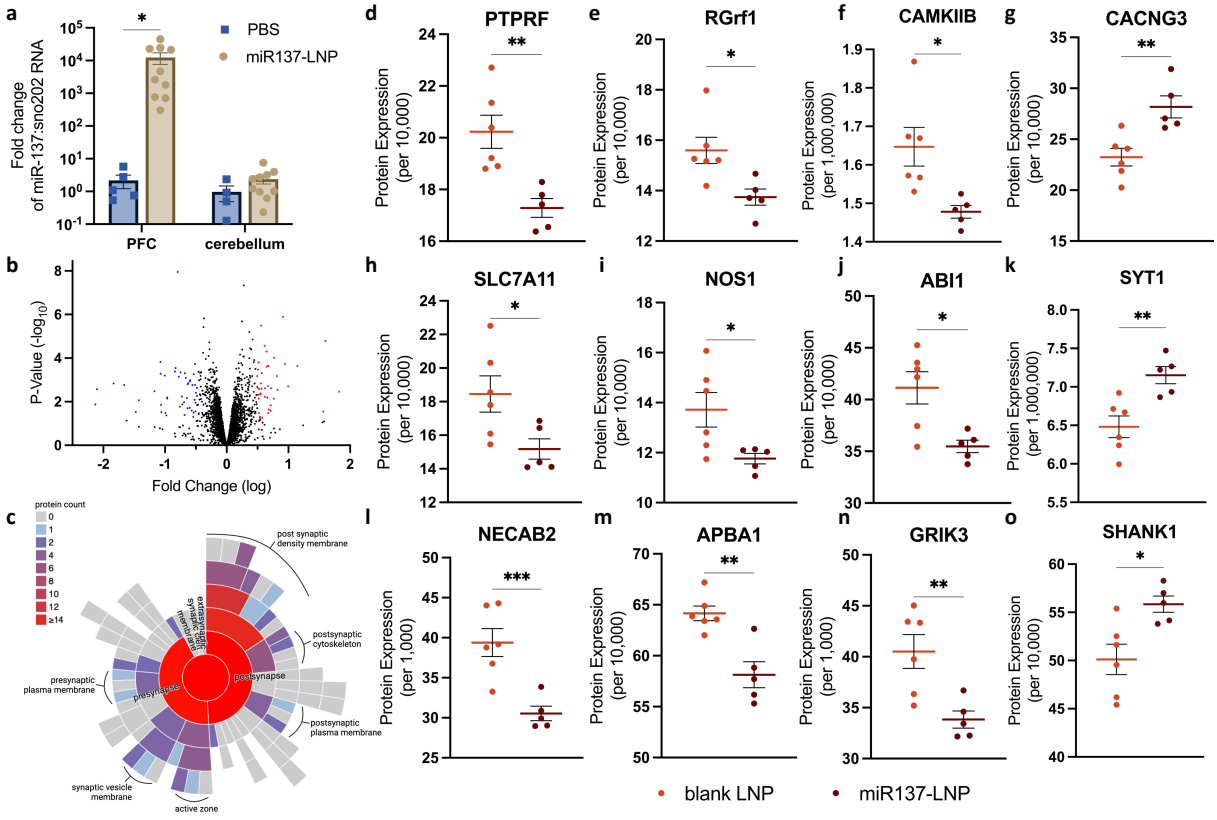

Figure 14 Lipid nanoparticle delivery and proteomic analysis of miR137 in the brain

Mice received bilateral intracerebral injections in the prefrontal cortex with miR137-LNPs or PBS. **a)** RT-qPCR fold change miR137 expression compared to sno202RNA at 24h. n = 4-10; mean ± SEM *$p < 0.05$. TMT proteomics comparing

prefrontal cortex biopsies of animals who received miR137-LNP or blank LNPs at 72h. **b)** Volcano plot of differentially expressed proteins between blank LNP and miR137-LNP (Log2Fold Change and adjusted *p* values < 0.05). **c)** Pre- and post-synaptic location of differentially expressed proteins by count following miR137-LNP treatment. Treatment with miR137-LNPs disrupts glutamatergic synaptic proteins compared to blank LNPs including **d)** receptor-type tyrosine-protein phosphatase F (PTPRF), **e)** Ras-specific guanine nucleotide-releasing factor 1 (RGrf1), **f)** calcium/calmodulin dependent protein kinase II beta (CAMKIIB), **g)** voltage-dependent calcium channel gamma-3 (CACNG3), **h**) solute carrier family 7 member 11 (SLC7A11), **i)** nitric oxide synthase 1 (NOS1), **j)** Abl interactor 1 (ABI1), **k)** synaptotagmin 1 (SYT1), **l)** N-terminal EF-hand calcium-binding protein 2 (NECAB2), **m)** amyloid beta A4 precursor protein (APBA1), **n)** glutamate receptor, ionotropic kainate 3 (GRIK3), and **o)** SH3 (SHANK1). n = 5-6/group, mean ± SEM *$p < 0.05$, **$p < 0.01$, ***$p < 0.001$.

A two-sample t-test found specific glutamatergic synaptic proteins were significantly inhibited in miR137-LNP treatments compared to blank LNPs (**Fig. 14D-14O**) including receptor-type tyrosine-protein phosphatase F (PTPRF) (t(9) = 3.778, p = .0044) (**Fig. 14D**), Ras-specific guanine nucleotide-releasing factor 1 (RGrf1) (t(9) = 2.877, p = .0183) (**Fig. 14E**), calcium/calmodulin dependent protein kinase II beta (CAMKIIB) (t(9) = 2.937, p = .0166) (**Fig. 14F**), solute carrier family 7 member 11 (SLC7A11) (t(9) = 2.5, p = .0338) (**Fig. 14H**), nitric oxide synthase 1 (NOS1) (t(9) = 2.487, p = .0346) (**Fig. 14I**), Abl interactor 1 (ABI1) (t(9) = 3.123, p = .0123) (**Fig. 14J**), N-terminal EF-hand calcium-binding protein 2 (NECAB2) (t(9) = 4.241, p = .0022) (**Fig. 14L**), amyloid beta A4 precursor protein (APBA1) (t(9) = 4.303, p = .0020) (**Fig. 14M**), and the glutamate receptor ionotropic kainate 3 (GRIK3) (t(9) = 3.356, p = .0084) (**Fig. 14N**). Three glutamatergic synaptic proteins were upregulated in miR137-LNP treatments compared to blank LNPs including the voltage-dependent calcium channel

gamma-3 (CACNG3) (t(9) = 3.611, p = .0056) (**Fig. 14G**), synaptotagmin 1 (SYT1) (t(9) = 3.606, p = .0057) (**Fig. 14K**), and SH3 (SHANK1) (t(9) = 3.027, p = .0143) (**Fig. 14O**). Many of the altered glutamatergic proteins effected by miR137-LNPs are in the postsynaptic density including CACNG3 (GO:0099061), PTPRF (GO:0099061), NOS1 (GO:0099092), CAMKIIB (GO:0014069), ABI1 (GO:0014069), and SHANK1 (GO:0014069). This data suggests miR137 delivered to neurons using LNPs modulates the expression of proteins involved in synaptic glutamate neurotransmission.

Lastly, we investigated the effect of blank LNPs on the proteome. Compared to PBS, we found blank LNPs induced differential expression of 1,536 proteins (923 upregulated (red) and 613 downregulated (blue)) (**Fig. 15A**). Based on the FUMA GENE2FUNC (Watanabe et al., 2017) database, the top GO molecular functions from DEPs following blank LNP treatment included binding of cell adhesion molecules, protein complexes, RNA, and lipids (**Fig. 15B**). Additionally, the SynGo database confirmed the cellular function of DEPs from blank LNPs include synaptic organization, cellular signaling, metabolism, and transport (**Fig. 15C**). This finding was validated though the biological pathway analysis which determined an upregulation of proteins involved in lipid metabolism (GO:0006629, GO:0044255, GO:0006644), response to lipids (GO:0033993), and lipid transport (GO:0006869) (**Table 2 A1**). The Reactome pathways indicated activation of 44% of the complement (MMU-166658) (**Fig. 15D**) and 16.54% of the cytokine (MMU-1280215) cascades (**Fig. 15E**) (**Table 3 A2**). It appears the cytokine and complement activation are driven by the LNP itself, as the blank LNP and miR137-LNP treatments show similar trends in protein activation compared to PBS. However, the DEPs involved in these immune pathways only made up 1.45% and

4.14% of the total DEPs in blank LNPs, respectively. To determine if LNPs activate microglia, we quantified five proteins known to be upregulated in activated microglia (Jurga et al., 2020; Rayaprolu et al., 2020). A two-way ANOVA with Sidak's multiple comparisons found enrichment of activated microglia proteins: cluster of differentiation 44 (CD44) ($F(4, 45) = 3.224$, $p = 0.0004$), moesin (MSN) ($F(4, 45) = 3.224$, $p = 0.0036$), profilin 1 (PFN1) ($F(4, 45) = 3.224$, $p = 0.6957$), myosin heavy chain 9 (MYH9) ($F(4, 45) = 3.224$, $p = 0.0011$), and cluster of differentiation 11 (CD11) ($F(4, 45) = 3.224$, $p < 0.0001$) after blank LNP treatment compared to PBS (**Fig. 19 A4C**). Of note, this analysis does not differentiate between microglia recruited to sites of damaged tissue due to the injection and cells specifically affected by LNPs. Finally, in agreement with previous proteomic analysis using the cationic DOTAP lipid in the LNP formulation (Dilliard et al., 2021), our proteomics data showed elevation of vitronectin, fibrinogen gamma chain, fibrinogen beta chain, clusterin, and alpha-s1-casein. Our mass spectrometry proteomics data have been deposited to the ProteomeXchange Consortium (http://proteomecentral.proteomexchange.org) via the PRIDE partner repository (Perez-Riverol et al., 2022) with the dataset identifier PXD041648.

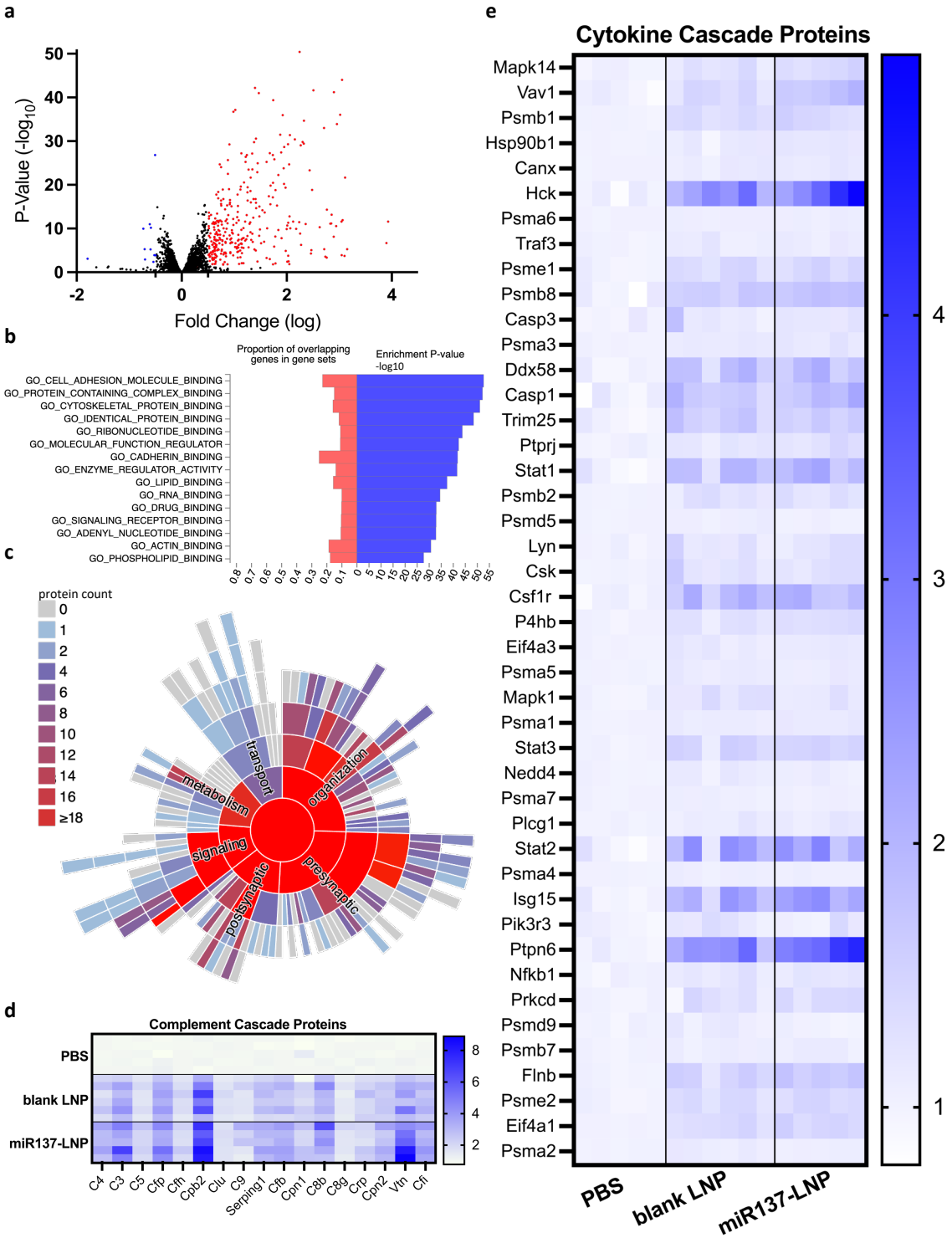
a
P-Value (-log10)
Fold Change (log)
b
Proportion of overlapping genes in gene sets
Enrichment P-value -log10
GO_CELL_ADHESION_MOLECULE_BINDING
GO_PROTEIN_CONTAINING_COMPLEX_BINDING
GO_CYTOSKELETAL_PROTEIN_BINDING
GO_IDENTICAL_PROTEIN_BINDING
GO_RIBONUCLEOTIDE_BINDING
GO_MOLECULAR_FUNCTION_REGULATOR
GO_CADHERIN_BINDING
GO_ENZYME_REGULATOR_ACTIVITY
GO_LIPID_BINDING
GO_RNA_BINDING
GO_DRUG_BINDING
GO_SIGNALING_RECEPTOR_BINDING
GO_ADENYL_NUCLEOTIDE_BINDING
GO_ACTIN_BINDING
GO_PHOSPHOLIPID_BINDING
c
protein count
0
1
2
4
6
8
10
12
14
16
≥18
transport
organization
metabolism
signaling
postsynaptic
presynaptic
d
Complement Cascade Proteins
PBS
blank LNP
miR137-LNP
C4
C3
C5
Cfp
Cfh
Cpb2
Clu
C9
Serping1
Cfb
Cpn1
C8b
C8g
Crp
Cpn2
Vtn
Cfi
e
Cytokine Cascade Proteins
Mapk14
Vav1
Psmb1
Hsp90b1
Canx
Hck
Psma6
Traf3
Psme1
Psmb8
Casp3
Psma3
Ddx58
Casp1
Trim25
Ptprj
Stat1
Psmb2
Psmd5
Lyn
Csk
Csf1r
P4hb
Eif4a3
Psma5
Mapk1
Psma1
Stat3
Nedd4
Psma7
Plcg1
Stat2
Psma4
Isg15
Pik3r3
Ptpn6
Nfkb1
Prkcd
Psmd9
Psmb7
Flnb
Psme2
Eif4a1
Psma2
PBS
blank LNP
miR137-LNP

Figure 15 Proteomic analysis of blank LNPs in the brain

Quantitative proteomics comparing prefrontal cortex biopsies of animals who received PBS or blank LNPs. **a)** Volcano plot of differentially expressed proteins between PBS and blank LNPs (Log2Fold Change and adjusted *p* values < 0.05). **b)** Gene Ontology (GO) molecular functions of enriched proteins by count from blank LNPs. **c)** Functional enrichment of differentially expressed proteins from blank LNPs. Heat map of activated protein expression in PBS, blank LNP, and miR137-LNP groups involved in **d)** complement and **e)** cytokine cascade pathways normalized to PBS. n = 5-6/group.

Discussion

The risk for developing schizophrenia (SCZ) is linked to single nucleotide polymorphisms in *MIRNA137,* which decreases miR137 expression, causing dysregulation of target synaptic proteins (Guella et al., 2013; van Erp et al., 2014). Many miR137 target transcripts are implicated in GWAS studies and linked to an increased risk of SCZ (Coyle et al., 2020). Polygenic disorders such as SCZ may benefit from the therapeutic application of miRNAs as broad-spectrum genetic regulators. Delivering replacement miRNA, or miRNA cocktails designed to tune synaptic function, is a path towards treatment of SCZ. Development of a transportation vehicle is required to protect and deliver therapeutic nucleic acid cargo to the appropriate location and cell type. Lipid nanoparticles (LNPs) are attractive delivery vectors due to their customizable size, charge, cargo loading, high bioavailability, and targeting capability (Herrera-Barrera, Ryals, et al., 2023; S. Patel et al., 2019).

Here we evaluated LNP delivery of nucleic acids to the prefrontal cortex (PFC) and the effects of miR137 on protein expression in the mouse brain. After confirming that LNP nanocarriers could successfully deliver miR137 to neuroblastoma cells *in vitro*,

we showed that miR137 modulated downstream synaptic proteins. In follow-up studies *in vivo*, we administered several types of nucleic acid cargo to the brain including small molecules (miR137) and large gene constructs (firefly luciferase mRNA and Cre-mRNA). We injected LNPs containing firefly luciferase mRNA into the PFC and found that the LNPs remained in the brain. Additional studies found Cre-mRNA delivered by LNPs predominantly expressed their cargo in neurons and to a lesser extent in microglia. Lastly, quantitative proteomic analysis of PFC tissues indicated that LNPs containing miR137 modulated glutamatergic synaptic proteins.

One key aspect of SCZ pathology is glutamatergic synaptic dysfunction in cortical neurons (Parellada & Gassó, 2021; Uno & Coyle, 2019). Disrupted excitatory neurotransmission due to aberrant expression of miR137 could impact synaptic function and result in behavioral abnormalities found in SCZ (Forsyth & Lewis, 2017). However, no tool currently exists to restore the synaptic glutamatergic circuits to normal levels. Our proteomic analysis determined miR137 delivered by LNPs altered pre-and post-synaptic glutamatergic proteins involved in neurotransmitter and receptor gating, binding, release, trafficking, and glutamate-dependent synaptic plasticity. Interestingly, a subset of the glutamatergic synaptic proteins, whose expression was modulated by miR137, are identified in GWAS studies that increase the risk for SCZ including PTPRF, SHANK1, CAMKIIB, C4, GRIK3, and CACNAα1C (Coyle et al., 2020; Fromer et al., 2014; Singh et al., 2020; Trubetskoy et al., 2022). Unexpectedly, some known targets of miR137 did not respond *in vivo* as they did *in vitro* (including TCF4, GluA1, Syn, CPLX1, and FMRP), suggesting that the pattern of synaptic protein modulation *in vivo* may be different than *in vitro*. One possibility is that the timing of protein homeostasis *in*

vivo could be driven by exogenously inflating the miRNA machinery (Cursons et al., 2018). Future studies varying the dose or timing of miRNA treatments will be required to establish long-term neural network or behavioral effects.

A complementary hypothesis in SCZ pathology suggests aberrant neuronal glutamate release leads to microglial activation through the complement cascade, implicating the immune system (Parellada & Gassó, 2021). In some individuals, modulation of complement genes may be therapeutic, as mutations in complement C4 genes have been linked to excessive synaptic pruning in SCZ (Woo et al., 2020; Yilmaz et al., 2021). We found that ~15% of the mRNA cargo delivered by LNPs was expressed in microglia, which play a role in synaptic pruning. It is possible the mRNA cargo expressed in microglia may be due to LNP phagocytosis at the injection site. To determine if LNPs are recruiting and activating microglia, future experiments could isolate cells expressing LNP cargo and measure 1) if the acceptor cells express activated microglial proteins and 2) if activated microglia are pro- or anti-inflammatory. Additionally, further studies could analyze microglial morphological changes (e.g. ramified, bushy, amoeboid microglia) due to LNP exposure. We found stimulation of cytokine and complement proteins was driven by the LNP itself, although these proteins accounted for less than 5% of all differentially expressed proteins. Our findings warrant further studies on the long-term biological consequences of the LNP immunogenicity (Mohamed et al., 2019) in the brain. Current genetic modulators, such as adeno-associated viruses (AAVs), significantly activate the innate immune response (Muhuri et al., 2021), but additional studies are required to directly compare LNP immune activation to AAVs. Nonetheless, future research directed at reducing immunogenic

responses – for example, by decorating the particle surface with anti-inflammatory agents or endogenous cell membranes from neuronal tissue – would be valuable (Y. Han et al., 2021).

Gene therapies in lipid based nanoplatforms are FDA approved to treat hereditary transthyretin-mediated amyloidosis with siRNA (J. Yang, 2019) and SARS-CoV-2 with mRNA vaccines (Schoenmaker et al., 2021). However, only a few studies have evaluated the safety and efficiency of LNP-based RNA therapies for central nervous system disorders. Previous studies have systemically injected selective organ targeting (SORT) LNPs and showed targeted lung, spleen, and liver tropism (Q. Cheng et al., 2020). Improving on first-generation SORT LNPs, we formulated LNPs with a mixture of DOTAP and Dlin-MC3 ionizable lipids and selectively showed high brain expression for ~ 24h with no detectable clearance to systemic organs (Brown et al., 2018; Campani et al., 2020; Hald Albertsen et al., 2022; Rungta et al., 2013). Our LNPs have distinct "onion-like" morphologies possibly due to the cationic lipids, which could be highly solvated and promote the formation of aqueous internal domains. Another possible reason is the arrangement of concentric phospholipid bilayers enclosing an aqueous core can form an onion-like multilayer structure. Maintaining exogenous long-term RNA expression in the brain could require multiple weekly treatments with potential risk for inflammation or cytotoxicity (Verbeke et al., 2022). However, our studies with single or multiple doses of miR137-LNP administrations found no toxicity in terms of body weight loss or change in tissue integrity. To design the next generation of noninvasive gene therapies, future studies will investigate the systemic delivery of targeted LNPs to cross the BBB. However, traversing the BBB will require careful

evaluation of the cost that off-target tissues could be affected. To target specific cell-types, LNPs could be coated with ligands, antibodies, or peptides (L. Han & Jiang, 2021), which would significantly improve drug delivery systems and therapies for brain disorders.

Overall, the evidence presented here encourages further research of miRNAs in pathological conditions. Using delivery of miR137 by LNPs, we have modulated neuronal glutamatergic synaptic protein networks connected to SCZ risk. These studies provide promising support for using LNPs as customizable tools for gene and protein therapies in the brain.

Chapter 4: General Discussion

Overview

This chapter concludes the findings of this dissertation comparing three nanoparticle nucleic acid delivery vehicles and the effects of miR137-LNPs in the mouse brain. This discussion will begin with a summary of findings followed by the potential clinical implications for psychiatric and other neurological disorders. The limitations of the provided studies will be discussed, as well as the direction for future studies given what this work has added to the understanding of nanoparticles in the brain. Finally, this chapter will conclude with closing remarks about the utility of LNPs in neuroscience and beyond.

Summary of Findings

The goal of Chapter 2 was to characterize three nanoparticle formulations that most effectively encapsulate and transport nucleic acids to N2A cells. These studies compared endogenous EVs, polymeric nanoparticles, and LNPs. After measuring particle characteristics, batch consistencies, toxicity, and miR137 cargo release, we found LNPs are the most reproduceable and effective delivery vehicles. Based on the findings in Chapter 2, all subsequent *in vivo* studies were conducted with LNPs. The goal of Chapter 3 was to determine the biodistribution, cell-type specific cargo expression, and proteomic effect of miR137-loaded LNPs in the PFC. We found LNPs are localized to the PFC injection site for about 24h without detectable expression in off-target organs. Furthermore, LNPs preferentially express nucleic acid cargo in neurons in the PFC compared to microglia or astrocytes. We found significant proteomic

changes in synaptic and developmental proteins after miR137-LNP treatment in the PFC. Interestingly, we found an overlap in the altered glutamatergic synaptic proteins after miR137-LNP treatment with SCZ risk genes. Finally, we found blank LNPs activate RNA, drug, and lipid binding mechanisms and initiate a neuroimmune response with enrichment of cytokine and complement cascade pathways. This discussion will address the findings of the aforementioned studies and the direction neuro-nanomedicine should take for future research.

Clinical Implications

There are over 600 CNS disorders ranging from developmental to degenerative, from infections to traumatic brain injury, and from cancer to psychiatric conditions (National Library of Medicine, 2014). A diagnosis of a brain disorder is a severe and often fatal sentence. Thus, there is a need for innovative research on therapeutics for CNS diseases.

The field of nanotherapeutics offers promising new avenues to develop drugs and technologies for previously unmet clinical needs. Currently, there are four nanocrystal treatments used for SCZ in the clinic. Nanocrystals are not newly synthesized drugs, but instead are known drug compounds thought to have therapeutic effects yet exhibit low aqueous solubility. However, these drug nanocrystals still lack receptor specificity, and have actions on serotonin, dopaminergic, and glutamatergic neurotransmitter systems. Thus, “third-generation antipsychotics” are not devoid of severe side effects. Aripiprazole lauroxil is a long-acting intramuscular injectable nanocrystal. However, because it is a prodrug with slow release, treatment regimens

require oral supplementation for the first 21 days (Krogmann et al., 2019). Non-adherence, weight gain, akathisia, and motor issues are still common side effects for patients (Preda & Shapiro, 2020). The hydrophilicity of the nanocrystal paliperidone palmitate - a metabolite of risperidone - alters mitochondrial function, synaptic plasticity and neuronal firing (Corena-McLeod, 2015). Thus, it appears nanocrystal technology is not an improvement on current antipsychotic drugs and is associated with unique issues and challenges.

Long-acting injectable antipsychotics are concentrated drug formulations which are injected intramuscularly and slowly released over time. The first generation of long-acting injectable antipsychotics, such as haloperidol and risperidone, are encased in degradable polymer microspheres dissolved in an oily delivery vehicle. However, the oily polymeric substance is associated with high rates of pain and injection site reactions (Zolezzi et al., 2021). Due to non-adherence of daily oral medications in patients with SCZ, new studies are inventing novel methods to deliver polymeric long-acting injectable drugs such as solid implants, inserts, transdermal patches, and wafers (Abdelkader et al., 2021).

A potential therapy for CNS disorders includes introducing foreign genetic material to target cells against a pathological gene of interest, or to augment a genetic deficiency. Viruses evolved to incorporate and change the genome of the infected host cells. Viral vector-based gene therapies are functionally like nano-vehicles and are commonly investigated delivery systems. Currently, three viral vector strategies are approved for clinical use and include adeno-associated viruses, adenoviruses, and lentiviruses (Zhao et al., 2021). Almost all viral gene therapy products are marketed as

cancer treatments, with very few therapies targeting the brain. This could be due to several challenges that limit using viral delivery systems such as: high immunotoxicity, high cost, impractical production strategies, inefficient transduction, and high off-target tissue effects (Li et al., 2023). Thus, to combat these viral-vector limitations, scientific investigation has turned to non-viral approaches for therapeutic delivery to the brain.

Three current gene therapies in lipid-based nanoplatforms are FDA approved. In 2018, Onpattro was the first LNP nucleic acid delivery vehicle used to treat hereditary transthyretin-mediated amyloidosis with siRNA (Akinc et al., 2019; J. Yang, 2019). The ionizable lipid used in the Onpattro formulation is the same MC3 lipid used in these dissertation studies. From a regulatory standpoint, using lipid components that are currently FDA approved for a new application, such as a CNS delivery vehicle, would be advantageous. However, Onpattro patients must be repeatedly dosed every three weeks; thus, successive generations could improve the half-life of the therapeutic siRNA.

The next sequential FDA approved LNP platforms were designed to treat SARS-CoV-2 with mRNA vaccines (Schoenmaker et al., 2021). The global use of COVID-19 mRNA vaccines delivered by LNPs sparked widespread interest using LNPs for a variety of previously unmet clinical needs. However, to remain protected from the infectious virus, multiple booster vaccines are needed and could inhibit the long-term adaptive immune response (Qin et al., 2022). The initial reported side effects after vaccine administration were thought to generate from the patients' adaptive immune response against the SARS-CoV-2 virus. However, further work suggests that the

ionizable and PEG lipid components of the LNP are responsible for the inflammatory effect (Mohamed et al., 2019; Ndeupen et al., 2021).

The COVID-19 vaccines were delivered intramuscularly, which would likely only affect the peripheral immune system. Depending on the delivery route, transporting cargo to the brain presents additional central immune system challenges that must be considered and tested in clinical populations. The studies in this dissertation focus solely on CNS immune factors as LNPs were directly injected into the mouse brain. However, intranasal and intrathecal methods are being investigated as possible LNP delivery routes (Correia et al., 2022). If the risks and side effects of systemic LNP delivery outweigh the rewards, future studies should investigate combining intracerebral LNP delivery with current treatment strategies. Some disorders, such as focal pediatric epilepsy, require surgery and placement of electrodes or subdural grids to monitor and treat frequent seizures that cannot be managed by diet and medication (Rugg-Gunn et al., 2020). During surgical procedures, LNPs loaded with therapeutic cargo could be delivered into the affected brain parenchyma for localized and long-term relief of seizure symptoms. Overall, there are many unanswered questions about the clinical utility of LNPs in the CNS which warrant further research.

Limitations

The findings in these dissertation studies have limitations which highlight the need for future studies to investigate the effects of nanoparticles as nucleic acid delivery vehicles in the brain. In Chapter 2, due to the difficulty in EV production, our studies were unable to compare the cytotoxicity, uptake and miR137 cargo release of EVs, as

was done for polymeric nanoparticles and LNPs. Following EV release and collection, previous studies have genetically and chemically modified EV membranes with aptamers, antibodies, or fluorophores (Mohammadi et al., 2023). However, conjugating fluorophores to nanoparticle lipids and visualizing florescence may give a false representation of intracellular cargo release mechanisms. Instead, relying on the expression of delivered reporter cargo may be more critical in determining functional nanoparticle delivery. Thus, visualizing vesicle biodistribution and measuring functional cargo readouts are both necessary steps in understanding vesicle delivery mechanisms.

Testing the effects of different nanoparticles in primary cell cultures with microglia and astrocytes present might have improved our understanding of the immunogenicity of various nanoparticles in cells that support neuronal activity. To test nanoparticle immunogenicity in a mouse macrophage cell line, future work could use RAW-Blue cells that express a reporter gene once the immunogenic NF-kB signal is stimulated (R. E. Lewis et al., 2014). Using this reporter cell line over the conventional MTT cell proliferation assay could be useful in quantifying high-throughput cell enumeration. Finally, another challenge researchers must consider is that *in vitro* LNP delivery does not predict *in vivo* LNP efficiency (Paunovska et al., 2018). Thus, initial LNP testing should continue with *in vitro* models, but the clinical application of an LNP system should be determined by results of *in vivo* models.

All *in vitro* studies in Chapters 2 and 3 were conducted in mouse neuroblastoma N2A cells. To fully capture the complexity and inter-dynamic activity of multiple cell types in the brain, N2A cells could have been differentiated into various neuronal sub-types, or

an additional neuronal cell line could be tested. It was unknown how miR137-loaded LNPs function in the brain, thus these studies used untargeted LNPs. However, targeting specific neuronal sub-populations such as glutamatergic, dopaminergic, or serotonergic neurons, could be beneficial in developing personalized therapies for disorders such as SCZ. To date, only one study has successfully altered neuron-specific glutamatergic NMDAR *in vivo* by LNPs (Rungta et al., 2013). However, this study did not actively target LNPs to neurons. LNP cellular uptake is dependent on ApoE and the LDLR, an endogenous uptake mechanism in neurons (Hayashi, 2011). Furthermore, Rungta et al. did not measure the effect of LNPs on microglia, so it could be that LNPs were taken up by microglia but was not reported. Efficiently delivering gene therapy cargo to specific neuronal cell types, via a targeted ligand, peptide, or cell-coating mechanism would significantly improve the utility of LNPs in the brain and for CNS disorders.

This dissertation addresses some unknown effects of LNPs in the brain, but some uncertainties remain. For example, in Chapter 3, we found challenges ensuring cell-type specific targeting in the brain. Although we found preferential expression of nucleic acid cargo in neurons in the PFC, ~15% of mRNA cargo was co-expressed with microglia, suggesting potential phagocytosis of LNPs. In all tissue types, macrophages may be the first and primary cell types that process nanoparticles and mediate host immunological responses (Gustafson et al., 2015). To combat this issue, previous studies coated LNPs with macrophage membranes to mimic the immunological characteristics of macrophages and camouflage LNPs from elimination (Y. Han et al., 2021). Further studies should examine the effect of LNPs on microglia *in vivo*. For

instance, LNP microglial activation and recruitment could be analyzed based on microglia morphological changes (e.g. ramified, bushy, amoeboid) (Jurga et al., 2020). Isolating specific cell types in the brain after LNP treatment, by florescent activated cell sorting, would give a detailed indication of the percentage of LNPs lost in debris clearance and not biologically activate in neurons. Thus, understanding how nanomaterials are distributed, internalized, and processed by macrophages will be important in the utility of LNPs for a variety of disease states.

The largest factor impeding LNP-based nucleic acid therapies for clinical applications is the immunogenicity of LNP formulations. In Chapter 3, we show activation of cytokine and complement cascade proteins following administration of LNPs in the brain. Some studies have attempted to work around this issue by co-administering or incorporating immunosuppressive agents into LNP systems (Yoneda et al., 2022). The presence of dexamethasone suppressed pro-inflammatory cytokines following intravenous LNP-siRNA administration (Chen et al., 2018). Including immunosuppressants into LNP formulations could act as an additional adjuvant and boost nanoparticle transfection at target tissues. Furthermore, our proteomic studies were limited to analysis at a single time point with a single LNP administration. Determining the appropriate miRNA dose and timing needed for desired outcomes will need to balance how the immune system will respond to potential repeated treatments in the brain.

In Chapter 3, we determined LNPs do not diffuse far from the injection site, which could be another limitation of LNP applications in the brain. We found LNPs travel 100-200 μm from the injection site, which could be advantageous for targeting a small brain

region such as the ventral tegmental area. However, to target a larger brain region such as the hippocampus, LNP diffusion and spread may need to improve. One study in the mouse brain found increasing the PEG-lipid anchor length improved LNP diffusion up to 1 mm from the injection site (E. Waggoner et al., 2023). “Short” C14 anchored PEG-lipids are quickly desorbed from the LNP once in circulation (Wilson et al., 2015). Thus, trafficking LNPs for long distances in the brain may benefit from “long” C18 anchored PEG-lipids with slower desorption kinetics, longer circulation times, and less accumulation in reticuloendothelial organs (Mui et al., 2013).

Delivering miRNAs could be a genetic tool to regulate a network of gene targets. For a polygenic disorder such as SCZ, miRNAs could be advantageous over current pharmacological manipulations that possess low receptor and cell type specificity. The proteomic analysis performed in these studies was useful in determining the effect of miR137, as miRNAs are inhibitors of target transcription. However, protein and mRNA expression profiles differ quantitatively, temporally and spatially (Abreu et al., 2009), due to post-transcriptional mRNA regulation (Vogel & Marcotte, 2012). Furthermore, protein-mRNA correlation coefficients only reach 0.47 in complex tissues like the brain (Maier et al., 2009). Comprehensive single-cell transcriptional analysis could be useful in conjugation with proteomics to determine the effect of miR137-LNPs on the genome and proteome, respectively.

Each conserved miRNA, including miR137, typically reduces expression of a given target by ~20% (Selbach et al., 2008). This modest effect may be due to a single gene containing several miRNA-binding sites. Gene repression is multiplicative when multiple sites are active (Grimson et al., 2007). Thus, co-targeting of closely spaced

miRNA sites with distinct seed sequences could further enhance gene repression. It is likely that miR137 is involved in a cooperative cluster of miRNAs that have overlapping brain-enriched targets. For example, miR137, miR124, and miR128 can synergistically regulate neuronal proliferation and differentiation (Santos et al., 2016). The co-targeting pair, miR137 and miR138, have significant overlapping targets and differentiate glutamatergic neurons (Cherone et al., 2019). Additional miRNA clusters are altered in SCZ including the miR29 family (Camkurt et al., 2016), the large genomic miR379/410 cluster (Winter, 2015), and the miR137/miR2682 locus is associated with SCZ allele variants and decreased miR137 expression (Duan et al., 2014). Therefore, further work should investigate the potential additive effect of gene repression with co-administering a cluster of miRNAs including miR137.

The current tools available to detect delivered nucleic acids are not able to determine their functional half-life intracellularly. For example, we measured fLuc mRNA and miR137 expression in the brain after LNP delivery and determined maximal expression about 24h post injection. However, the downstream cascades, including protein turnover rates, may vary with target applications. Studies suggest the half-life of miRNAs range from 28 to 220 h (Z. Zhang et al., 2012). To extend the expression of miRNAs and reduce delivery frequency, using a plasmid DNA could provide prolonged transgene expression (Scholz & Wagner, 2012). Further work should investigate the long-term effects of elevated RNAs in the brain.

One limitation of using miRNAs lies in the inherent properties of miRNAs being regulators of tens to hundreds of transcripts simultaneously. In Chapter 3, there were no apparent deleterious effects of miR137 replacement *in vitro* or *in vivo*. However, it's

possible that sustained elevation of miR137 could trigger activation of undesirable pathways. Studying the effect of miRNA dose when artificially inflating the miRNA machinery will be useful to measure potential off-target effects. For example, miR137 is highly implicated in the development and prognosis for glioma. Downregulation of miR137 is associated with a variety of tumors including breast cancer, cervical cancer, ovarian cancer, non-small cell lung cancer, and gastrointestinal stromal tumors. Thus, replacement of miR137 could be protective and inhibit proliferation of malignant differentiation (Y. Wang et al., 2020). Thus, depending on the area of focus, researchers may be unintentionally missing off-target effects of miR137 levels in the brain.

Due to the limited research of LNPs in the brain, the results of these dissertation studies significantly improve our understanding in the scientific field. The lack of new therapeutic treatments for SCZ creates a unique space for interdisciplinary fields to combine technological advances. Before LNPs are modified with targeting agents and delivered to every organ in the body, it is necessary to understand how LNPs work in each target tissue. The studies presented, although not without limitations, provide an important steppingstone to developing LNP-based platforms for CNS disorders.

Future directions

The results from these studies will inform future neuro-nanotechnology research on the effects of LNPs directly injected into the brain parenchyma. Future studies will use these results as the backbone for the next generation of LNPs targeted to the brain. Using machine learning or artificial intelligence-based systems to scan curated libraries of LNP components might be useful in synthesizing and categorizing lipid properties for

brain targeted delivery. For example, modifying LNP components during the initial formulation stage can improve the discovery pipeline and predict appropriate polar heads, functional groups, and linkers for specific target tissue applications (Altınoglu et al., 2015). Previous work determined the LNP's chemical structure is dependent for tissue-specific selective organ targeted (SORT) nanoparticles to extra-hepatic organs (Q. Cheng et al., 2020). Altering the chemical nature of LNP molecules controlled the biodistribution, acid dissociation constant (pK_a), and serum protein interactions of SORT nanoparticles (Dilliard et al., 2021). This model-based screening approach will reduce *in vivo* testing of many combinations of lipid formulations and improve clinical translation of LNP delivery systems.

Although most current work focuses on improving properties of the nanocarrier, future work should continue to enhance the pharmacological properties of the cargo. RNA exhibits higher turnover rates and is more labile than DNA (Wada & Becskei, 2017). Synthesis of structural RNA modifications, such as locked nucleic acids, have increased the stability of therapeutic RNAs against enzymatic degradation (Hagedorn et al., 2018). Furthermore, increasing the binding affinity of nucleic acid products to their target can significantly improve cargo potency (Swayze et al., 2007). Additional strategies utilize active tissue targeting by conjugating ligands directly to the therapeutic nucleotides. This mechanism removes the need for a delivery vehicle which is endogenously trafficked through passive biological targeting. The most promising ligand-conjugated system targets liver hepatocytes via the *N*-acetylgalactosamine (GalNAc)-asialoglycoprotein interaction (Cui et al., 2021). However, conjugating ligands or antibodies directly to nucleic acids or drugs is limited due to the necessary - but

challenging - covalent bond linking the molecules. Synthesizing a therapeutic nucleic acid LNP transportation system to the brain may require advancements in both RNA biology and LNP delivery.

Emerging work has investigated delivering complex payloads using LNPs, such as co-encapsulation with therapeutic gene editing and guide RNA technology (Herrera-Barrera, Gautam, et al., 2023). Recent studies successfully edited the mouse cornea genome by delivering CRISPR-Cas9 with LNPs (Mirjalili Mohanna et al., 2022). SORT LNPs with CRISPR-based technology have selectively edited epithelial cells, endothelial cells, B cells, T cells and hepatocytes in the lung, spleen, and liver (Q. Cheng et al., 2020). Furthermore, combining LNP-based technology with RNA-sensing mechanisms to ubiquitously edit all animal cell types has widespread applications in reprogrammable RNA medicine (Qian et al., 2022). As selective gene and RNA editing continues to improve, future work should focus on delivering therapeutic materials across the BBB, in a cell- or brain region-specific manner, by a non-invasive delivery method.

To improve selectivity and reduce off-target effects, LNPs could be coated with a targeting agent to a specific receptor or cell type. If LNPs can selectively target the brain with systemic delivery, we could reduce the need for invasive brain surgeries. Previous work investigated LNP targeting by attaching antibodies, ligands, or peptides via conjugation to the PEG lipid on the LNP surface. Incorporating a receptor in a specific conformation can aid in LNP antibody affinity (Chang et al., 2021). Additionally, peptide targeted LNPs have successfully delivered mRNA cargo to retinal cells in rodents and nonhuman primates (Herrera-Barrera, Ryals, et al., 2023). However, using click chemistry will be necessary to ensure the proper orientation of any targeted moieties on

the LNP surface. Adding long chain PEG-lipid linkers to LNP formulations, then attaching antibodies to the PEG lipids is a successful method of ensuring conjugation of antibodies in the correct orientation (Sakurai et al., 2022). Ensuring nanoparticle accumulation in specific tissue or cell-types would significantly improve clinical translation of brain-targeted LNPs.

The BBB is the largest biological barrier to developing new therapeutics for CNS disorders. The low nanoparticle brain tropism and high off-target organ expression remain a substantial issue for LNPs in the brain. The clinical translation of LNPs would significantly improve if LNPs could traverse the BBB (Pardridge, 2023). Transferrin receptors only line brain capillary endothelial cells in the BBB, and mediate cellular iron uptake in the brain by receptor-mediated transport. Previous studies have found the most success crossing the BBB with nanoparticles targeting transferrin receptors (Wiley et al., 2013; X. Yang et al., 2009). Interestingly, altering the affinity of transferrin can improve nanoparticle transportation across the BBB (Niewoehner et al., 2014; Y. J. Yu et al., 2011). Alternatively, previous work proposed that nanoparticle circulation time can extend by hitchhiking onto red blood cells to cross the BBB (Gao et al., 2020). However, once LNPs cross the BBB, directing nanoparticles to their target cell-type or brain region of interest presents another challenge.

Investigating the mechanism of LNP uptake by alternative delivery methods will improve nanoparticle technology for a wide range of patient populations. Intraparenchymal infusion remains the most common clinical approach to deliver therapeutic small nucleic acids to the brain (Hudry & Vandenberghe, 2019). These dissertation studies investigated the local intracerebral administration of LNPs in the

brain, since intracerebral methods are clinically performed for a variety of neurological applications including Parkinson's disease (Freed et al., 2001), glioma (Chaichana et al., 2015), epilepsy (Gernert & Feja, 2020), and ischemic stroke (Noh et al., 2020).

Delivery methods such as intranasal, intramuscular, intrathecal, or intravenous administration should be investigated. Importantly, the brain region and disease of interest must be considered when evaluating LNP delivery routes. For example, delivery strategies directly to the cerebrospinal fluid (CSF) (intracerebroventricular or intracisternal) or bloodstream could be a useful strategy for multifocal diseases. With intravenous administration, a unique protein corona profile forms around the LNP when delivered to specific tissues (Dilliard et al., 2021). Therefore, future studies could investigate the absorbed protein rich layer following intravenous brain delivery. Intranasal LNP delivery may accumulate in olfactory and prefrontal cortical regions in the rodent (Chung et al., 2020), and could be advantageous for disorders localized in the forebrain. Intrathecal delivery routes may accumulate in caudal brain epithelium such as the cerebellum (Belur et al., 2021), and could be desirable for lysosomal storage disorders, such as Niemann-Pick disease, which affects cerebellar Purkinje cells (Berry-Kravis, 2021). Meanwhile, intramuscular delivery routes could provide novel treatment options for some motor neuron diseases. Therefore, it's possible that one delivery strategy may not be appropriate for all CNS disorders.

An additional tool utilizes barcoded peptides encoding mRNA into distinct LNP formulations and could test multiple delivery techniques in the same animal. Each formulation is independently quantified by protein production and analyzed by mass spectrometry in distinct tissue and cell types (Rhym et al., 2023). This batch-based

method can screen multiple simultaneous LNP formulations, administered by various delivery techniques, within the same animal, and reduces the need for transgenic reporter animal models. Furthermore, this approach could quantify LNP targeting to all organs simultaneously based on the delivery route.

Many questions remain about therapeutic nucleic acids delivered by LNPs and should be the focal point of biomedical research going forward. For instance, future work should investigate if/how specific cell types are able to sense LNPs. It's possible there is a recognition mechanism for specific tissues, such as the immune system, to sense LNPs as non-native invaders. By understanding this biological process, we can work to reverse or inhibit that signal and mimic native molecules in the tissue of interest to reduce phagocytosis. Additional questions remain as to how cells process excessive nucleic acids or lipids. Accumulation of intracellular lipid storage can be pathological (Schulze & Sandhoff, 2011), and lipidoses affect the same endo-lysosomal processing as LNPs. Designing technology to determine how each lipid in the LNP formulation is metabolized by the cell would be advantageous.

Conclusions

The experiments presented in this dissertation provide significant novel evidence that LNPs can be used as nucleic acid delivery vehicles to the brain. Despite many advances, many brain disorders do not have available treatments or the treatment options are insufficient. Addressing this issue will require merging fields in materials science, nanotechnology, and neuroscience to help to maximize new bioengineering discoveries for severe brain disorders. The experiments presented in this dissertation

leverage such interdisciplinary technologies, providing significant new evidence that LNPs can be used as nucleic acid delivery vehicles in the brain to modify cellular functioning. These findings emphasize that developing new nanotechnologies is - and will continue to remain - critical to advancing treatments for brain disorders.

Appendix

These data are additional experiments associated with Chapter 3

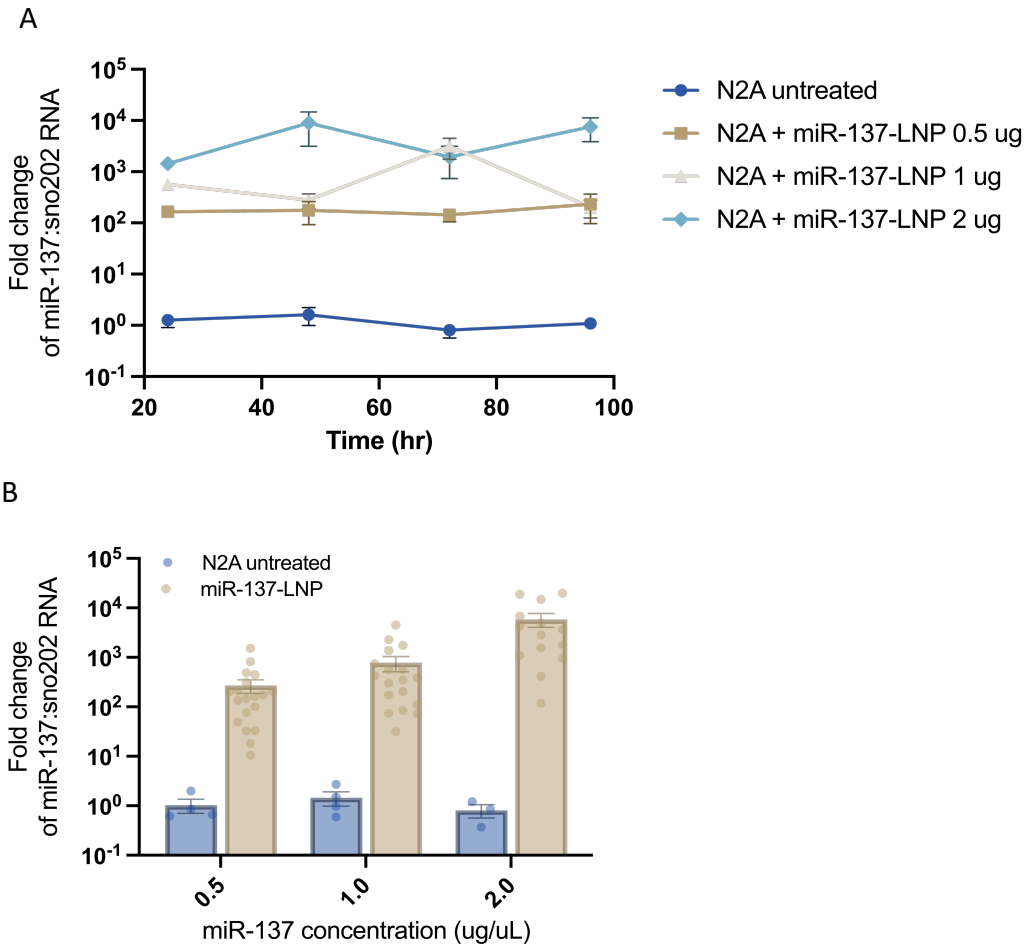

Figure 16 A1 Lipid nanoparticle concentration and time course in neuronal cell culture

a) Time course of RT-qPCR fold change of miR-137 expression to sno202RNA after treatment with **b)** 0.5ug, 1ug, or 2ug of miR-137-LNPs in Neuro2A cell culture. n = 3-19, mean ± SEM

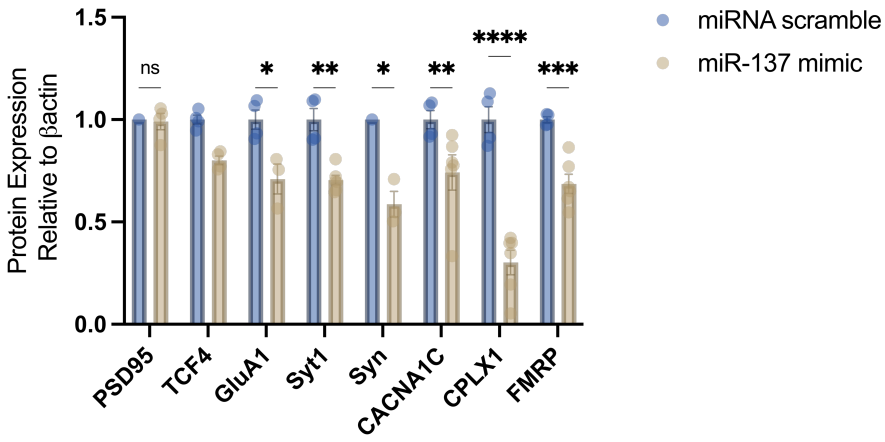

Figure 17 A2 MiR-137 synaptic protein inhibition

Treatment with miR-137 mimic in N2A cells and western blot analysis of target synaptic proteins transcription factor 4 (TCF4), glutamate receptor 1 (GluA1), synaptotagmin 1 (SYT1), synaptophysin (SYN), voltage gated calcium channel alpha 1C (CACNA1C), complexin 1 (CPLX1), fragile X mental retardation protein (FMRP), and post synaptic density 95 (PSD95) expression compared to treatment with miRNA scramble. All protein levels are normalized to beta actin in miRNA scramble. n = 3-6, mean ± SEM; ns, not significant: $p > 0.05$; *$p < 0.05$; **$p < 0.01$; ***$p < 0.001$ and ****$p < 0.0001$.

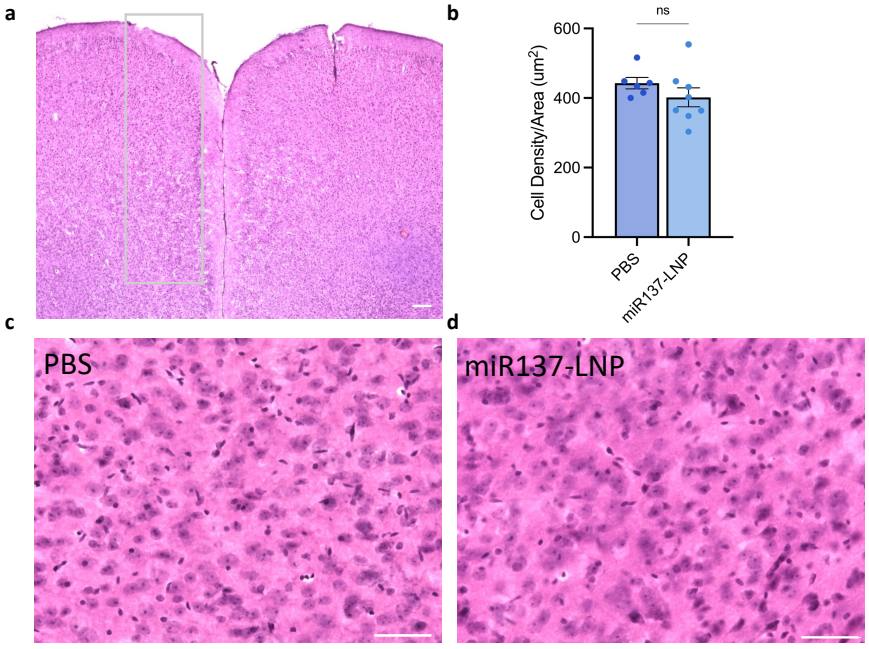

Figure 18 A3 Cellular lipid nanoparticle toxicity *in vivo*

H&E stain from **a)** mouse prefrontal cortex brain tissue. scale bar: 200 μm **b**) Quantification of neuronal cell density per section area (μm^2) after 5 consecutive days of

c) PBS or **d**) miR137-LNP treatments. scale bars: 100 µm. n = 2/treatment; mean ± SEM; ns, not significant

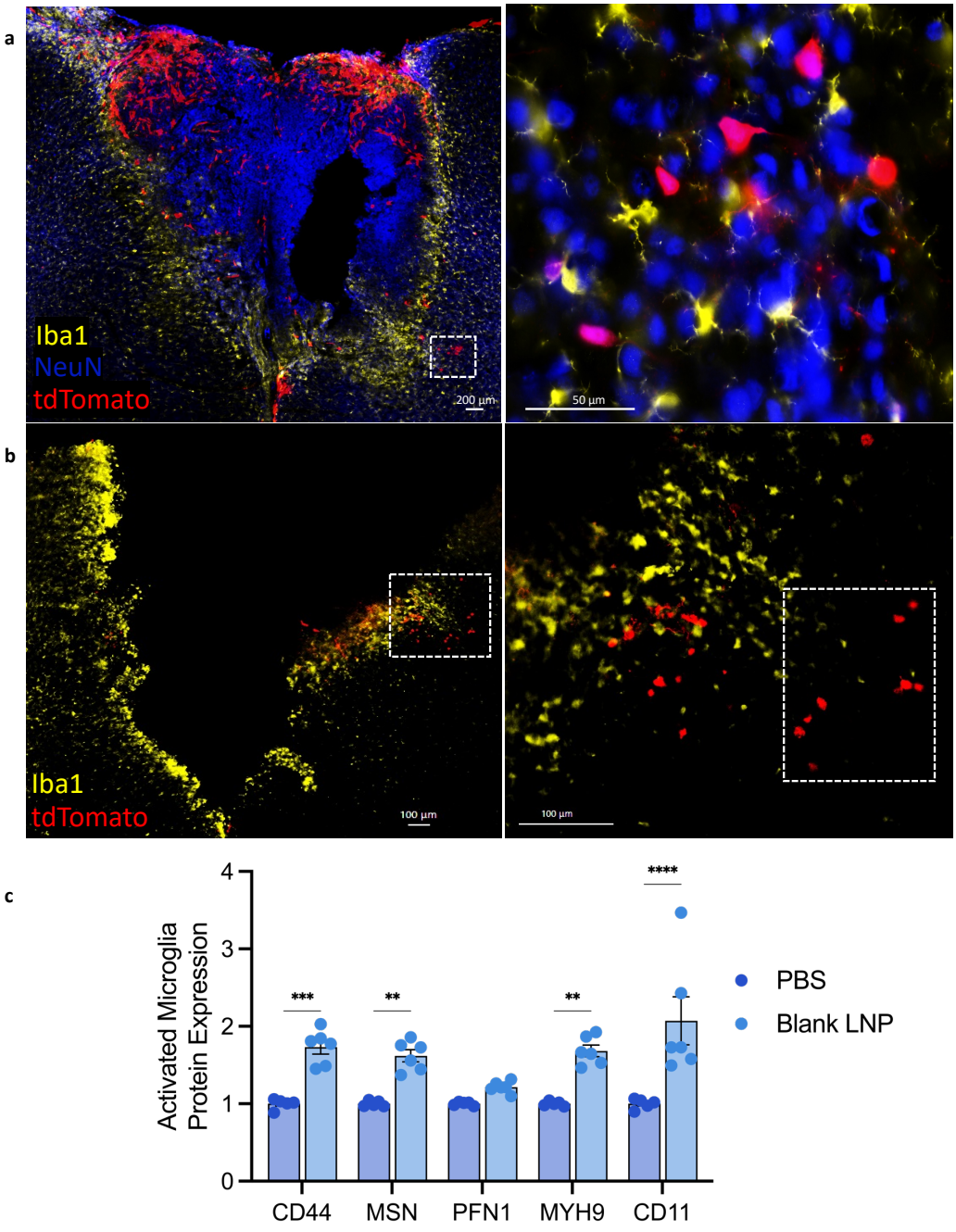

Figure 19 A4 Microglia Quantification and Activation

Representative florescent images **a)** and **b)** of injection tract marks in the prefrontal cortex and adjacent quantified region (white box) for tdTomato (red), Iba1 (yellow), or

NeuN (blue) co-labeling. **c)** Proteomic quantification of activated microglia protein expression comparing prefrontal cortex biopsies of animals who received PBS or blank LNPs: cluster of differentiation 44 (CD44), moesin (MSN), profilin 1 (PFN1), myosin heavy chain 9 (MYH9), and cluster of differentiation 11 (CD11) normalized to PBS. n = 5-6/group. mean ± SEM; ***p* < 0.01, ****p* < 0.001 and *****p* < 0.0001.

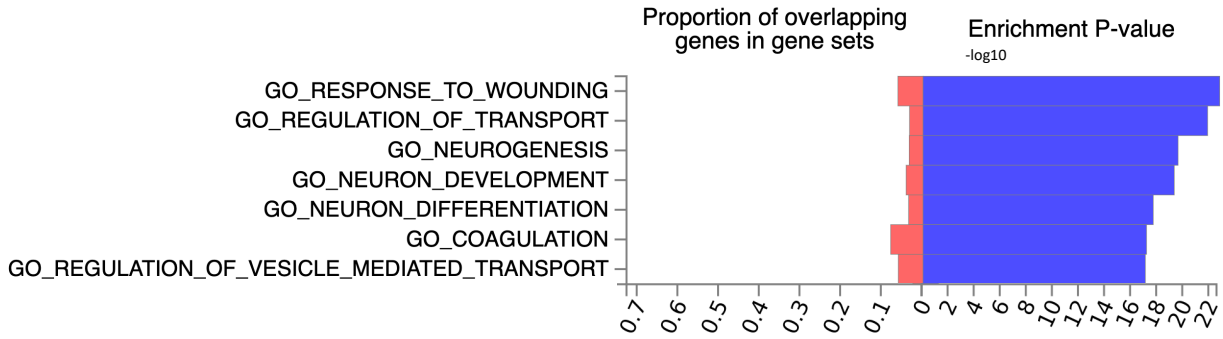

Figure 20 A5 miR137-LNP GO Biological Process

Quantitative proteomics comparing prefrontal cortex biopsies of animals who received miR137-LNP or blank LNPs. GO biological process of enriched proteins from miR-137-LNPs involved in neuronal development. n = 5-6/group.

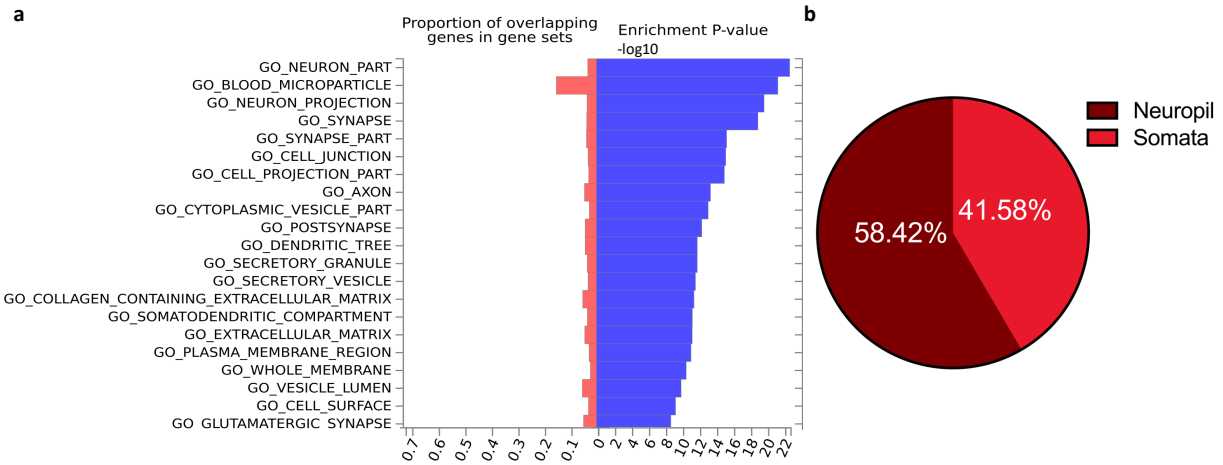

Figure 21 A6 miR137-LNP GO Cellular Compartment

Quantitative proteomics comparing prefrontal cortex biopsies of animals who received miR137-LNP or blank LNPs. **a)** GO cellular compartment of enriched proteins from miR-137-LNPs located in neuronal synapses. **b)** The majority of DEP miR137-LNP proteins are translated in the neuropil compared to the somata. n = 5-6/group.

Table 2 A1 Blank LNP Reactome pathway enrichment in the brain

Differentially expressed proteins (DEP) comparing blank LNPs to PBS treatments. False discovery rate (FDR).

LNP Reactome Pathways

GO-term	Term description	% network activation	% total DEP	FDR
MMU-168256	Immune system	17.95	19.14	2.92E-43
MMU-76002	Platelet activation, signaling and aggregation	29.64	4.93	6.18E-20
MMU-2262752	Cellular responses to stress	17.97	4.67	8.19E-10
MMU-166658	Complement cascade	44.0	1.45	1.91E-08
MMU-1280215	Cytokine signaling in immune system	16.54	4.14	1.12E-07

Table 3 A2 Blank LNP biological process enrichment in the brain

Differentially expressed proteins (DEP) comparing blank LNPs to PBS treatments. False discovery rate (FDR).

LNP Biological Process

GO-term	Term description	% network activation	% total DEP	FDR
GO:0033993	Response to lipid	12.04	6.91	4.92E-06
GO:0006629	Lipid metabolic process	11.14	7.56	3.61E-05
GO:0044255	Cellular lipid metabolic process	11.17	5.86	0.00042
GO:0006869	Lipid transport	13.57	2.30	0.0049
GO:0006644	Phospholipid metabolic process	12.71	2.50	0.0081

REFERENCES

Abbas, A. I., Sundiang, M. J. M., Henoch, B., Morton, M. P., Bolkan, S. S., Park, A. J., Harris, A. Z., Kellendonk, C., & Gordon, J. A. (2018). Somatostatin Interneurons Facilitate Hippocampal-Prefrontal Synchrony and Prefrontal Spatial Encoding. *Neuron*, *100*(4), 926-939.e3. https://doi.org/10.1016/j.neuron.2018.09.029

Abdelkader, H., Fathalla, Z., Seyfoddin, A., Farahani, M., Thrimawithana, T., Allahham, A., Alani, A. W. G., Al-Kinani, A. A., & Alany, R. G. (2021). Polymeric long-acting drug delivery systems (LADDS) for treatment of chronic diseases: Inserts, patches, wafers, and implants. *Advanced Drug Delivery Reviews*, *177*, 113957. https://doi.org/10.1016/j.addr.2021.113957

Abram, S. V., Wisner, K. M., Fox, J. M., Barch, D. M., Wang, L., Csernansky, J. G., MacDonald, A. W., & Smith, M. J. (2017). Fronto-temporal connectivity predicts cognitive empathy deficits and experiential negative symptoms in schizophrenia. *Human Brain Mapping*, *38*(3), 1111–1124. https://doi.org/10.1002/hbm.23439

Abreu, R. de S., Penalva, L. O., Marcotte, E. M., & Vogel, C. (2009). Global signatures of protein and mRNA expression levels. *Molecular bioSystems*, *5*(12), 1512–1526. https://doi.org/10.1039/b908315d

Akinc, A., Maier, M. A., Manoharan, M., Fitzgerald, K., Jayaraman, M., Barros, S., Ansell, S., Du, X., Hope, M. J., Madden, T. D., Mui, B. L., Semple, S. C., Tam, Y. K., Ciufolini, M., Witzigmann, D., Kulkarni, J. A., van der Meel, R., & Cullis, P. R. (2019). The Onpattro story and the clinical translation of nanomedicines containing nucleic acid-based drugs. *Nature Nanotechnology*, *14*(12), Article 12. https://doi.org/10.1038/s41565-019-0591-y

Akinc, A., Querbes, W., De, S., Qin, J., Frank-Kamenetsky, M., Jayaprakash, K. N., Jayaraman, M., Rajeev, K. G., Cantley, W. L., Dorkin, J. R., Butler, J. S., Qin, L., Racie, T., Sprague, A., Fava, E., Zeigerer, A., Hope, M. J., Zerial, M., Sah, D. W. Y., … Maier, M. A. (2010). Targeted delivery of RNAi therapeutics with endogenous and exogenous ligand-based mechanisms. *Molecular Therapy: The Journal of the American Society of Gene Therapy*, *18*(7), 1357–1364. https://doi.org/10.1038/mt.2010.85

Altınoglu, S., Wang, M., & Xu, Q. (2015). Combinatorial library strategies for synthesis of cationic lipid-like nanoparticles and their potential medical applications. *Nanomedicine (London, England)*, *10*(4), 643–657. https://doi.org/10.2217/nnm.14.192

American Psychiatric Association, & American Psychiatric Association (Eds.). (2013). *Diagnostic and statistical manual of mental disorders: DSM-5* (5th ed). American Psychiatric Association.

Anastasiades, P. G., & Carter, A. G. (2021). Circuit organization of the rodent medial prefrontal cortex. *Trends in Neurosciences*, *44*(7), 550–563. https://doi.org/10.1016/j.tins.2021.03.006

Andrade, C. (2016). Antipsychotic Drugs in Schizophrenia: Relative Effects in Patients With and Without Treatment Resistance. *The Journal of Clinical Psychiatry*, *77*(12), e1656–e1660. https://doi.org/10.4088/JCP.16f11328

Arakawa, Y., Yokoyama, K., Tasaki, S., Kato, J., Nakashima, K., Takeyama, M., Nakatani, A., & Suzuki, M. (2019). Transgenic mice overexpressing miR-137 in the brain show schizophrenia-associated behavioral deficits and transcriptome profiles. *PloS One*, *14*(7), e0220389. https://doi.org/10.1371/journal.pone.0220389

Astruc, D. (2015). Introduction to Nanomedicine. *Molecules*, *21*(1), 4. https://doi.org/10.3390/molecules21010004

Barbas, H., & Zikopoulos, B. (2007). The prefrontal cortex and flexible behavior. *The Neuroscientist : A Review Journal Bringing Neurobiology, Neurology and Psychiatry*, *13*(5), 532–545. https://doi.org/10.1177/1073858407301369

Bassett, A. S., & Chow, E. W. C. (2008). Schizophrenia and 22q11.2 deletion syndrome. *Current Psychiatry Reports*, *10*(2), 148–157. https://doi.org/10.1007/s11920-008-0026-1

Belur, L. R., Romero, M., Lee, J., Podetz-Pedersen, K. M., Nan, Z., Riedl, M. S., Vulchanova, L., Kitto, K. F., Fairbanks, C. A., Kozarsky, K. F., Orchard, P. J., Frey, W. H., Low, W. C., & McIvor, R. S. (2021). Comparative Effectiveness of Intracerebroventricular, Intrathecal, and Intranasal Routes of AAV9 Vector Administration for Genetic Therapy of Neurologic Disease in Murine Mucopolysaccharidosis Type I. *Frontiers in Molecular Neuroscience*, *14*. https://www.frontiersin.org/articles/10.3389/fnmol.2021.618360

Berry-Kravis, E. (2021). Niemann-Pick Disease, Type C: Diagnosis, Management and Disease-Targeted Therapies in Development. *Seminars in Pediatric Neurology*, *37*, 100879. https://doi.org/10.1016/j.spen.2021.100879

Birnbaum, R., & Weinberger, D. R. (2020). A Genetics Perspective on the Role of the (Neuro)Immune System in Schizophrenia. *Schizophrenia Research*, *217*, 105–113. https://doi.org/10.1016/j.schres.2019.02.005

Brachya, G., Yanay, C., & Linial, M. (2006). Synaptic proteins as multi-sensor devices of neurotransmission. *BMC Neuroscience*, *7 Suppl 1*(Suppl 1), S4. https://doi.org/10.1186/1471-2202-7-S1-S4

Brown, R. A. M., Richardson, K. L., Kalinowski, F. C., Epis, M. R., Horsham, J. L., Kabir, T. D., De Pinho, M. H., Beveridge, D. J., Stuart, L. M., Wintle, L. C., & Leedman, P. J. (2018). Evaluation of MicroRNA Delivery In Vivo. *Methods in Molecular Biology (Clifton, N.J.)*, *1699*, 155–178. https://doi.org/10.1007/978-1-4939-7435-1_12

Camkurt, M. A., Karababa, F., Erdal, M. E., Bayazıt, H., Kandemir, S. B., Ay, M. E., Kandemir, H., Ay, Ö. İ., Çiçek, E., Selek, S., & Taşdelen, B. (2016). Investigation of Dysregulation of Several MicroRNAs in Peripheral Blood of Schizophrenia Patients. *Clinical Psychopharmacology and Neuroscience*, *14*(3), 256–260. https://doi.org/10.9758/cpn.2016.14.3.256

Campani, V., Zappavigna, S., Scotti, L., Abate, M., Porru, M., Leonetti, C., Caraglia, M., & De Rosa, G. (2020). Hybrid lipid self-assembling nanoparticles for brain delivery of microRNA. *International Journal of Pharmaceutics*, *588*, 119693. https://doi.org/10.1016/j.ijpharm.2020.119693

Cao, T., & Zhen, X.-C. (2018). Dysregulation of miRNA and its potential therapeutic application in schizophrenia. *CNS Neuroscience & Therapeutics*, *24*(7), 586–597. https://doi.org/10.1111/cns.12840

Carey, R. J., Pinheiro-Carrera, M., Dai, H., Tomaz, C., & Huston, J. P. (1995). L-DOPA and psychosis: Evidence for L-DOPA-induced increases in prefrontal cortex dopamine and in serum corticosterone. *Biological Psychiatry*, *38*(10), 669–676. https://doi.org/10.1016/0006-3223(94)00378-5

Catalanotto, C., Cogoni, C., & Zardo, G. (2016). MicroRNA in Control of Gene Expression: An Overview of Nuclear Functions. *International Journal of Molecular Sciences*, *17*(10). https://doi.org/10.3390/ijms17101712

Chaichana, K. L., Pinheiro, L., & Brem, H. (2015). Delivery of local therapeutics to the brain: Working toward advancing treatment for malignant gliomas. *Therapeutic Delivery*, *6*(3), 353–369. https://doi.org/10.4155/tde.14.114

Chambers, M. C., Maclean, B., Burke, R., Amodei, D., Ruderman, D. L., Neumann, S., Gatto, L., Fischer, B., Pratt, B., Egertson, J., Hoff, K., Kessner, D., Tasman, N., Shulman, N., Frewen, B., Baker, T. A., Brusniak, M.-Y., Paulse, C., Creasy, D., … Mallick, P. (2012). A cross-platform toolkit for mass spectrometry and proteomics. *Nature Biotechnology*, *30*(10), 918–920. https://doi.org/10.1038/nbt.2377

Chang, H.-Y., Wu, S., Li, Y., Zhang, W., Burrell, M., Webster, C. I., & Shah, D. K. (2021). Brain pharmacokinetics of anti-transferrin receptor antibody affinity variants in rats determined using microdialysis. *mAbs*, *13*(1), 1874121. https://doi.org/10.1080/19420862.2021.1874121

Chen, S., Zaifman, J., Kulkarni, J. A., Zhigaltsev, I. V., Tam, Y. K., Ciufolini, M. A., Tam, Y. Y. C., & Cullis, P. R. (2018). Dexamethasone prodrugs as potent suppressors of the immunostimulatory effects of lipid nanoparticle formulations of nucleic acids. *Journal of Controlled Release: Official Journal of the Controlled Release Society*, *286*, 46–54. https://doi.org/10.1016/j.jconrel.2018.07.026

Cheng, Q., Wei, T., Farbiak, L., Johnson, L. T., Dilliard, S. A., & Siegwart, D. J. (2020). Selective organ targeting (SORT) nanoparticles for tissue-specific mRNA delivery and CRISPR-Cas

gene editing. *Nature Nanotechnology*, *15*(4), 313–320. https://doi.org/10.1038/s41565-020-0669-6

Cheng, Y., Wang, Z.-M., Tan, W., Wang, X., Li, Y., Bai, B., Li, Y., Zhang, S.-F., Yan, H.-L., Chen, Z.-L., Liu, C.-M., Mi, T.-W., Xia, S., Zhou, Z., Liu, A., Tang, G.-B., Liu, C., Dai, Z.-J., Wang, Y.-Y., … Jin, P. (2018). Partial loss of psychiatric risk gene miR-137 in mice causes repetitive behavior and impairs sociability and learning via increased Pde10a. *Nature Neuroscience*, *21*(12), 1689–1703. https://doi.org/10.1038/s41593-018-0261-7

Cherone, J. M., Jorgji, V., & Burge, C. B. (2019). Cotargeting among microRNAs in the brain. *Genome Research*, *29*(11), 1791–1804. https://doi.org/10.1101/gr.249201.119

Chokhawala, K., & Stevens, L. (2023). Antipsychotic Medications. In *StatPearls*. StatPearls Publishing. http://www.ncbi.nlm.nih.gov/books/NBK519503/

Chong, H. Y., Teoh, S. L., Wu, D. B.-C., Kotirum, S., Chiou, C.-F., & Chaiyakunapruk, N. (2016). Global economic burden of schizophrenia: A systematic review. *Neuropsychiatric Disease and Treatment*, *12*, 357–373. https://doi.org/10.2147/NDT.S96649

Chung, E. P., Cotter, J. D., Prakapenka, A. V., Cook, R. L., DiPerna, D. M., & Sirianni, R. W. (2020). Targeting Small Molecule Delivery to the Brain and Spinal Cord via Intranasal Administration of Rabies Virus Glycoprotein (RVG29)-Modified PLGA Nanoparticles. *Pharmaceutics*, *12*(2), Article 2. https://doi.org/10.3390/pharmaceutics12020093

Corena-McLeod, M. (2015). Comparative Pharmacology of Risperidone and Paliperidone. *Drugs in R&D*, *15*(2), 163–174. https://doi.org/10.1007/s40268-015-0092-x

Correia, A. C., Monteiro, A. R., Silva, R., Moreira, J. N., Sousa Lobo, J. M., & Silva, A. C. (2022). Lipid nanoparticles strategies to modify pharmacokinetics of central nervous system

targeting drugs: Crossing or circumventing the blood–brain barrier (BBB) to manage neurological disorders. *Advanced Drug Delivery Reviews*, *189*, 114485. https://doi.org/10.1016/j.addr.2022.114485

Cowan, M., & Petri, W. A. (2018). Microglia: Immune Regulators of Neurodevelopment. *Frontiers in Immunology*, *9*, 2576. https://doi.org/10.3389/fimmu.2018.02576

Coyle, J. T., Ruzicka, W. B., & Balu, D. T. (2020). Fifty Years of Research on Schizophrenia: The Ascendance of the Glutamatergic Synapse. *American Journal of Psychiatry*, *177*(12), 1119–1128. https://doi.org/10.1176/appi.ajp.2020.20101481

Crowley, J. J., Collins, A. L., Lee, R. J., Nonneman, R. J., Farrell, M. S., Ancalade, N., Mugford, J. W., Agster, K. L., Nikolova, V. D., Moy, S. S., & Sullivan, P. F. (2015). Disruption of the microRNA 137 primary transcript results in early embryonic lethality in mice. *Biological Psychiatry*, *77*(2), e5-7. https://doi.org/10.1016/j.biopsych.2014.05.022

Cui, H., Zhu, X., Li, S., Wang, P., & Fang, J. (2021). Liver-Targeted Delivery of Oligonucleotides with N-Acetylgalactosamine Conjugation. *ACS Omega*, *6*(25), 16259–16265. https://doi.org/10.1021/acsomega.1c01755

Cummings, E., Donohoe, G., Hargreaves, A., Moore, S., Fahey, C., Dinan, T. G., McDonald, C., O'Callaghan, E., O'Neill, F. A., Waddington, J. L., Murphy, K. C., Morris, D. W., Gill, M., & Corvin, A. (2013). Mood congruent psychotic symptoms and specific cognitive deficits in carriers of the novel schizophrenia risk variant at MIR-137. *Neuroscience Letters*, *532*, 33–38. https://doi.org/10.1016/j.neulet.2012.08.065

Cursons, J., Pillman, K. A., Scheer, K. G., Gregory, P. A., Foroutan, M., Hediyeh-Zadeh, S., Toubia, J., Crampin, E. J., Goodall, G. J., Bracken, C. P., & Davis, M. J. (2018). Combinatorial

Targeting by MicroRNAs Co-ordinates Post-transcriptional Control of EMT. *Cell Systems*, *7*(1), 77-91.e7. https://doi.org/10.1016/j.cels.2018.05.019

De Jong, W. H., & Borm, P. J. (2008). Drug delivery and nanoparticles: Applications and hazards. *International Journal of Nanomedicine*, *3*(2), 133–149.

De Sousa, K. P., Rossi, I., Abdullahi, M., Ramirez, M. I., Stratton, D., & Inal, J. M. (2023). Isolation and characterization of extracellular vesicles and future directions in diagnosis and therapy. *Wiley Interdisciplinary Reviews. Nanomedicine and Nanobiotechnology*, *15*(1), e1835. https://doi.org/10.1002/wnan.1835

Dilliard, S. A., Cheng, Q., & Siegwart, D. J. (2021). On the mechanism of tissue-specific mRNA delivery by selective organ targeting nanoparticles. *Proceedings of the National Academy of Sciences of the United States of America*, *118*(52), e2109256118. https://doi.org/10.1073/pnas.2109256118

Doyle, L. M., & Wang, M. Z. (2019). Overview of Extracellular Vesicles, Their Origin, Composition, Purpose, and Methods for Exosome Isolation and Analysis. *Cells*, *8*(7). https://doi.org/10.3390/cells8070727

Duan, J., Shi, J., Fiorentino, A., Leites, C., Chen, X., Moy, W., Chen, J., Alexandrov, B. S., Usheva, A., He, D., Freda, J., O'Brien, N. L., Molecular Genetics of Schizophrenia collaboration, Genomic Psychiatric Cohort consortium, McQuillin, A., Sanders, A. R., Gershon, E. S., DeLisi, L. E., Bishop, A. R., … Gejman, P. V. (2014). A rare functional noncoding variant at the GWAS-implicated MIR137/MIR2682 locus might confer risk to schizophrenia and bipolar disorder. *American Journal of Human Genetics*, *95*(6), 744–753. https://doi.org/10.1016/j.ajhg.2014.11.001

Egerton, A., Murphy, A., Donocik, J., Anton, A., Barker, G. J., Collier, T., Deakin, B., Drake, R., Eliasson, E., Emsley, R., Gregory, C. J., Griffiths, K., Kapur, S., Kassoumeri, L., Knight, L., Lambe, E. J. B., Lawrie, S. M., Lees, J., Lewis, S., … Howes, O. D. (2021). Dopamine and Glutamate in Antipsychotic-Responsive Compared With Antipsychotic-Nonresponsive Psychosis: A Multicenter Positron Emission Tomography and Magnetic Resonance Spectroscopy Study (STRATA). *Schizophrenia Bulletin*, *47*(2), 505–516. https://doi.org/10.1093/schbul/sbaa128

Elias, J. E., & Gygi, S. P. (2007). Target-decoy search strategy for increased confidence in large-scale protein identifications by mass spectrometry. *Nature Methods*, *4*(3), 207–214. https://doi.org/10.1038/nmeth1019

Eng, J. K., Jahan, T. A., & Hoopmann, M. R. (2013). Comet: An open-source MS/MS sequence database search tool. *Proteomics*, *13*(1), 22–24. https://doi.org/10.1002/pmic.201200439

E. Waggoner, L., F. Miyasaki, K., & J. Kwon, E. (2023). Analysis of PEG-lipid anchor length on lipid nanoparticle pharmacokinetics and activity in a mouse model of traumatic brain injury. *Biomaterials Science*, *11*(12), 4238–4253. https://doi.org/10.1039/D2BM01846B

Forsyth, J. K., & Lewis, D. A. (2017). Mapping the Consequences of Impaired Synaptic Plasticity in Schizophrenia through Development: An Integrative Model for Diverse Clinical Features. *Trends in Cognitive Sciences*, *21*(10), 760–778. https://doi.org/10.1016/j.tics.2017.06.006

Freed, C. R., Greene, P. E., Breeze, R. E., Tsai, W.-Y., DuMouchel, W., Kao, R., Dillon, S., Winfield, H., Culver, S., Trojanowski, J. Q., Eidelberg, D., & Fahn, S. (2001). Transplantation of

Embryonic Dopamine Neurons for Severe Parkinson's Disease. *New England Journal of Medicine*, *344*(10), 710–719. https://doi.org/10.1056/NEJM200103083441002

Friedman, N. P., & Robbins, T. W. (2022). The role of prefrontal cortex in cognitive control and executive function. *Neuropsychopharmacology: Official Publication of the American College of Neuropsychopharmacology*, *47*(1), 72–89. https://doi.org/10.1038/s41386-021-01132-0

Friedman, R. C., Farh, K. K.-H., Burge, C. B., & Bartel, D. P. (2009). Most mammalian mRNAs are conserved targets of microRNAs. *Genome Research*, *19*(1), 92–105. https://doi.org/10.1101/gr.082701.108

Fromer, M., Pocklington, A. J., Kavanagh, D. H., Williams, H. J., Dwyer, S., Gormley, P., Georgieva, L., Rees, E., Palta, P., Ruderfer, D. M., Carrera, N., Humphreys, I., Johnson, J. S., Roussos, P., Barker, D. D., Banks, E., Milanova, V., Grant, S. G., Hannon, E., … O'Donovan, M. C. (2014). De novo mutations in schizophrenia implicate synaptic networks. *Nature*, *506*(7487), Article 7487. https://doi.org/10.1038/nature12929

Gao, C., Wang, Y., Sun, J., Han, Y., Gong, W., Li, Y., Feng, Y., Wang, H., Yang, M., Li, Z., Yang, Y., & Gao, C. (2020). Neuronal mitochondria-targeted delivery of curcumin by biomimetic engineered nanosystems in Alzheimer's disease mice. *Acta Biomaterialia*, *108*, 285–299. https://doi.org/10.1016/j.actbio.2020.03.029

Garman, R. H. (2011). Histology of the central nervous system. *Toxicologic Pathology*, *39*(1), 22–35. https://doi.org/10.1177/0192623310389621

GBD 2016 Disease and Injury Incidence and Prevalence Collaborators. (2017). Global, regional, and national incidence, prevalence, and years lived with disability for 328 diseases and

injuries for 195 countries, 1990-2016: A systematic analysis for the Global Burden of Disease Study 2016. *Lancet (London, England)*, *390*(10100), 1211–1259. https://doi.org/10.1016/S0140-6736(17)32154-2

Gernert, M., & Feja, M. (2020). Bypassing the Blood–Brain Barrier: Direct Intracranial Drug Delivery in Epilepsies. *Pharmaceutics*, *12*(12), Article 12. https://doi.org/10.3390/pharmaceutics12121134

Glausier, J. R., & Lewis, D. A. (2013). Dendritic Spine Pathology in Schizophrenia. *Neuroscience*, *251*, 90–107. https://doi.org/10.1016/j.neuroscience.2012.04.044

Global, regional, and national burden of neurological disorders, 1990–2016: A systematic analysis for the Global Burden of Disease Study 2016. (2019). *The Lancet. Neurology*, *18*(5), 459–480. https://doi.org/10.1016/S1474-4422(18)30499-X

Glock, C., Biever, A., Tushev, G., Nassim-Assir, B., Kao, A., Bartnik, I., Tom Dieck, S., & Schuman, E. M. (2021). The translatome of neuronal cell bodies, dendrites, and axons. *Proceedings of the National Academy of Sciences of the United States of America*, *118*(43), e2113929118. https://doi.org/10.1073/pnas.2113929118

Gonzalez-Burgos, G., & Lewis, D. A. (2008). GABA neurons and the mechanisms of network oscillations: Implications for understanding cortical dysfunction in schizophrenia. *Schizophrenia Bulletin*, *34*(5), 944–961. https://doi.org/10.1093/schbul/sbn070

Grace, A. A. (2016). Dysregulation of the dopamine system in the pathophysiology of schizophrenia and depression. *Nature Reviews. Neuroscience*, *17*(8), 524–532. https://doi.org/10.1038/nrn.2016.57

Granot, Y., & Peer, D. (2017). Delivering the right message: Challenges and opportunities in lipid nanoparticles-mediated modified mRNA therapeutics—An innate immune system standpoint. *Seminars in Immunology*, *34*, 68–77. https://doi.org/10.1016/j.smim.2017.08.015

Grimson, A., Farh, K. K.-H., Johnston, W. K., Garrett-Engele, P., Lim, L. P., & Bartel, D. P. (2007). MicroRNA Targeting Specificity in Mammals: Determinants beyond Seed Pairing. *Molecular Cell*, *27*(1), 91–105. https://doi.org/10.1016/j.molcel.2007.06.017

Guella, I., Sequeira, A., Rollins, B., Morgan, L., Torri, F., van Erp, T. G. M., Myers, R. M., Barchas, J. D., Schatzberg, A. F., Watson, S. J., Akil, H., Bunney, W. E., Potkin, S. G., Macciardi, F., & Vawter, M. P. (2013). Analysis of miR-137 expression and rs1625579 in dorsolateral prefrontal cortex. *Journal of Psychiatric Research*, *47*(9), 1215–1221. https://doi.org/10.1016/j.jpsychires.2013.05.021

Gulyaeva, L. F., & Kushlinskiy, N. E. (2016). Regulatory mechanisms of microRNA expression. *Journal of Translational Medicine*, *14*(1), 143. https://doi.org/10.1186/s12967-016-0893-x

Gustafson, H. H., Holt-Casper, D., Grainger, D. W., & Ghandehari, H. (2015). Nanoparticle Uptake: The Phagocyte Problem. *Nano Today*, *10*(4), 487–510. https://doi.org/10.1016/j.nantod.2015.06.006

Hagedorn, P. H., Persson, R., Funder, E. D., Albæk, N., Diemer, S. L., Hansen, D. J., Møller, M. R., Papargyri, N., Christiansen, H., Hansen, B. R., Hansen, H. F., Jensen, M. A., & Koch, T. (2018). Locked nucleic acid: Modality, diversity, and drug discovery. *Drug Discovery Today*, *23*(1), 101–114. https://doi.org/10.1016/j.drudis.2017.09.018

Hald Albertsen, C., Kulkarni, J. A., Witzigmann, D., Lind, M., Petersson, K., & Simonsen, J. B. (2022). The role of lipid components in lipid nanoparticles for vaccines and gene therapy. *Advanced Drug Delivery Reviews*, *188*, 114416. https://doi.org/10.1016/j.addr.2022.114416

Han, L., & Jiang, C. (2021). Evolution of blood-brain barrier in brain diseases and related systemic nanoscale brain-targeting drug delivery strategies. *Acta Pharmaceutica Sinica. B*, *11*(8), 2306–2325. https://doi.org/10.1016/j.apsb.2020.11.023

Han, Y., Gao, C., Wang, H., Sun, J., Liang, M., Feng, Y., Liu, Q., Fu, S., Cui, L., Gao, C., Li, Y., Yang, Y., & Sun, B. (2021). Macrophage membrane-coated nanocarriers Co-Modified by RVG29 and TPP improve brain neuronal mitochondria-targeting and therapeutic efficacy in Alzheimer's disease mice. *Bioactive Materials*, *6*(2), 529–542. https://doi.org/10.1016/j.bioactmat.2020.08.017

Hanna, J., Hossain, G. S., & Kocerha, J. (2019). The Potential for microRNA Therapeutics and Clinical Research. *Frontiers in Genetics*, *10*. https://www.frontiersin.org/articles/10.3389/fgene.2019.00478

Hauberg, M. E., Roussos, P., Grove, J., Børglum, A. D., Mattheisen, M., & Schizophrenia Working Group of the Psychiatric Genomics Consortium. (2016). Analyzing the Role of MicroRNAs in Schizophrenia in the Context of Common Genetic Risk Variants. *JAMA Psychiatry*, *73*(4), 369–377. https://doi.org/10.1001/jamapsychiatry.2015.3018

Hayashi, H. (2011). Lipid metabolism and glial lipoproteins in the central nervous system. *Biological & Pharmaceutical Bulletin*, *34*(4), 453–461. https://doi.org/10.1248/bpb.34.453

He, E., Lozano, M. A. G., Stringer, S., Watanabe, K., Sakamoto, K., den Oudsten, F., Koopmans, F., Giamberardino, S. N., Hammerschlag, A., Cornelisse, L. N., Li, K. W., van Weering, J., Posthuma, D., Smit, A. B., Sullivan, P. F., & Verhage, M. (2018). MIR137 schizophrenia-associated locus controls synaptic function by regulating synaptogenesis, synapse maturation and synaptic transmission. *Human Molecular Genetics*, *27*(11), 1879–1891. https://doi.org/10.1093/hmg/ddy089

Herrera-Barrera, M., Gautam, M., Lokras, A., Vlasova, K., Foged, C., & Sahay, G. (2023). Lipid Nanoparticle-Enabled Intracellular Delivery of Prime Editors. *The AAPS Journal*, *25*(4), 65. https://doi.org/10.1208/s12248-023-00833-2

Herrera-Barrera, M., Ryals, R. C., Gautam, M., Jozic, A., Landry, M., Korzun, T., Gupta, M., Acosta, C., Stoddard, J., Reynaga, R., Tschetter, W., Jacomino, N., Taratula, O., Sun, C., Lauer, A. K., Neuringer, M., & Sahay, G. (2023). Peptide-guided lipid nanoparticles deliver mRNA to the neural retina of rodents and nonhuman primates. *Science Advances*, *9*(2), eadd4623. https://doi.org/10.1126/sciadv.add4623

Hilker, R., Helenius, D., Fagerlund, B., Skytthe, A., Christensen, K., Werge, T. M., Nordentoft, M., & Glenthøj, B. (2018). Heritability of Schizophrenia and Schizophrenia Spectrum Based on the Nationwide Danish Twin Register. *Biological Psychiatry*, *83*(6), 492–498. https://doi.org/10.1016/j.biopsych.2017.08.017

Ho, P. T. B., Clark, I. M., & Le, L. T. T. (2022). MicroRNA-Based Diagnosis and Therapy. *International Journal of Molecular Sciences*, *23*(13), 7167. https://doi.org/10.3390/ijms23137167

Hollins, S. L., Goldie, B. J., Carroll, A. P., Mason, E. A., Walker, F. R., Eyles, D. W., & Cairns, M. J. (2014). Ontogeny of small RNA in the regulation of mammalian brain development. *BMC Genomics*, *15*(1), 777. https://doi.org/10.1186/1471-2164-15-777

Hudry, E., & Vandenberghe, L. H. (2019). Therapeutic AAV Gene Transfer to the Nervous System: A Clinical Reality. *Neuron*, *101*(5), 839–862. https://doi.org/10.1016/j.neuron.2019.02.017

Javitt, D. C., Siegel, S. J., Spencer, K. M., Mathalon, D. H., Hong, L. E., Martinez, A., Ehlers, C. L., Abbas, A. I., Teichert, T., Lakatos, P., & Womelsdorf, T. (2020). A roadmap for development of neuro-oscillations as translational biomarkers for treatment development in neuropsychopharmacology. *Neuropsychopharmacology*, *45*(9), Article 9. https://doi.org/10.1038/s41386-020-0697-9

Jia, X., Wang, F., Han, Y., Geng, X., Li, M., Shi, Y., Lu, L., & Chen, Y. (2016). miR-137 and miR-491 Negatively Regulate Dopamine Transporter Expression and Function in Neural Cells. *Neuroscience Bulletin*, *32*(6), 512–522. https://doi.org/10.1007/s12264-016-0061-6

Jiménez-Morales, J. M., Hernández-Cuenca, Y. E., Reyes-Abrahantes, A., Ruiz-García, H., Barajas-Olmos, F., García-Ortiz, H., Orozco, L., Quiñones-Hinojosa, A., Reyes-González, J., & Abrahantes-Pérez, M. D. C. (2022). MicroRNA delivery systems in glioma therapy and perspectives: A systematic review. *Journal of Controlled Release: Official Journal of the Controlled Release Society*, *349*, 712–730. https://doi.org/10.1016/j.jconrel.2022.07.027

Jurga, A. M., Paleczna, M., & Kuter, K. Z. (2020). Overview of General and Discriminating Markers of Differential Microglia Phenotypes. *Frontiers in Cellular Neuroscience*, *14*. https://www.frontiersin.org/articles/10.3389/fncel.2020.00198

Kadakia, A., Catillon, M., Fan, Q., Williams, G. R., Marden, J. R., Anderson, A., Kirson, N., & Dembek, C. (2022). The Economic Burden of Schizophrenia in the United States. *The Journal of Clinical Psychiatry*, *83*(6), 22m14458. https://doi.org/10.4088/JCP.22m14458

Kantrowitz, J., & Javitt, D. C. (2012). Glutamatergic transmission in schizophrenia: From basic research to clinical practice. *Current Opinion in Psychiatry*, *25*(2), 96–102. https://doi.org/10.1097/YCO.0b013e32835035b2

Kaur, A., Basavanagowda, D. M., Rathod, B., Mishra, N., Fuad, S., Nosher, S., Alrashid, Z. A., Mohan, D., & Heindl, S. E. (2020). Structural and Functional Alterations of the Temporal lobe in Schizophrenia: A Literature Review. *Cureus*, *12*(10), e11177. https://doi.org/10.7759/cureus.11177

Keller, A., Nesvizhskii, A. I., Kolker, E., & Aebersold, R. (2002). Empirical statistical model to estimate the accuracy of peptide identifications made by MS/MS and database search. *Analytical Chemistry*, *74*(20), 5383–5392. https://doi.org/10.1021/ac025747h

Khadimallah, I., Jenni, R., Cabungcal, J.-H., Cleusix, M., Fournier, M., Beard, E., Klauser, P., Knebel, J.-F., Murray, M. M., Retsa, C., Siciliano, M., Spencer, K. M., Steullet, P., Cuenod, M., Conus, P., & Do, K. Q. (2022). Mitochondrial, exosomal miR137-COX6A2 and gamma synchrony as biomarkers of parvalbumin interneurons, psychopathology, and neurocognition in schizophrenia. *Molecular Psychiatry*, *27*(2), 1192–1204. https://doi.org/10.1038/s41380-021-01313-9

Khan, I., Saeed, K., & Khan, I. (2019). Nanoparticles: Properties, applications and toxicities. *Arabian Journal of Chemistry*, *12*(7), 908–931. https://doi.org/10.1016/j.arabjc.2017.05.011

Kim, J., Eygeris, Y., Gupta, M., & Sahay, G. (2021). Self-assembled mRNA vaccines. *Advanced Drug Delivery Reviews*, *170*, 83–112. https://doi.org/10.1016/j.addr.2020.12.014

Kim, Y. S., Choi, J., & Yoon, B.-E. (2020). Neuron-Glia Interactions in Neurodevelopmental Disorders. *Cells*, *9*(10), 2176. https://doi.org/10.3390/cells9102176

Kinon, B. J., & Lieberman, J. A. (1996). Mechanisms of action of atypical antipsychotic drugs: A critical analysis. *Psychopharmacology*, *124*(1–2), 2–34. https://doi.org/10.1007/BF02245602

Kinsey, C., Lu, T., Deiss, A., Vuolo, K., Klein, L., Rustandi, R. R., & Loughney, J. W. (2022). Determination of lipid content and stability in lipid nanoparticles using ultra high-performance liquid chromatography in combination with a Corona Charged Aerosol Detector. *ELECTROPHORESIS*, *43*(9–10), 1091–1100. https://doi.org/10.1002/elps.202100244

Kokkinou, M., Irvine, E. E., Bonsall, D. R., Natesan, S., Wells, L. A., Smith, M., Glegola, J., Paul, E. J., Tossell, K., Veronese, M., Khadayate, S., Dedic, N., Hopkins, S. C., Ungless, M. A., Withers, D. J., & Howes, O. D. (2021). Reproducing the dopamine pathophysiology of schizophrenia and approaches to ameliorate it: A translational imaging study with ketamine. *Molecular Psychiatry*, *26*(6), 2562–2576. https://doi.org/10.1038/s41380-020-0740-6

Koopmans, F., Nierop, P. van, Andres-Alonso, M., Byrnes, A., Cijsouw, T., Coba, M. P., Cornelisse, L. N., Farrell, R. J., Goldschmidt, H. L., Howrigan, D. P., Hussain, N. K., Imig, C., Jong, A. P. H. de, Jung, H., Kohansalnodehi, M., Kramarz, B., Lipstein, N., Lovering, R. C., MacGillavry, H., … Verhage, M. (2019). SynGO: An Evidence-Based, Expert-Curated

Knowledge Base for the Synapse. *Neuron*, *103*(2), 217-234.e4. https://doi.org/10.1016/j.neuron.2019.05.002

Krogmann, A., Peters, L., Hardenberg, L. von, Bödeker, K., Nöhles, V. B., & Correll, C. U. (2019). Keeping up with the therapeutic advances in schizophrenia: A review of novel and emerging pharmacological entities. *CNS Spectrums*, *24*(S1), 38–69. https://doi.org/10.1017/S109285291900124X

Kuswanto, C. N., Sum, M. Y., Qiu, A., Sitoh, Y.-Y., Liu, J., & Sim, K. (2015). The impact of genome wide supported microRNA-137 (MIR137) risk variants on frontal and striatal white matter integrity, neurocognitive functioning, and negative symptoms in schizophrenia. *American Journal of Medical Genetics. Part B, Neuropsychiatric Genetics: The Official Publication of the International Society of Psychiatric Genetics*, *168B*(5), 317–326. https://doi.org/10.1002/ajmg.b.32314

Lett, T. A., Chakravarty, M. M., Chakavarty, M. M., Felsky, D., Brandl, E. J., Tiwari, A. K., Gonçalves, V. F., Rajji, T. K., Daskalakis, Z. J., Meltzer, H. Y., Lieberman, J. A., Lerch, J. P., Mulsant, B. H., Kennedy, J. L., & Voineskos, A. N. (2013). The genome-wide supported microRNA-137 variant predicts phenotypic heterogeneity within schizophrenia. *Molecular Psychiatry*, *18*(4), 443–450. https://doi.org/10.1038/mp.2013.17

Lewis, B. P., Burge, C. B., & Bartel, D. P. (2005). Conserved seed pairing, often flanked by adenosines, indicates that thousands of human genes are microRNA targets. *Cell*, *120*(1), 15–20. https://doi.org/10.1016/j.cell.2004.12.035

Lewis, R. E., Liao, G., Young, K., Douglas, C., & Kontoyiannis, D. P. (2014). Macrophage Reporter Cell Assay for Screening Immunopharmacological Activity of Cell Wall-Active Antifungals.

Antimicrobial Agents and Chemotherapy, *58*(3), 1738–1743. https://doi.org/10.1128/AAC.02408-13

Li, X., Le, Y., Zhang, Z., Nian, X., Liu, B., & Yang, X. (2023). Viral Vector-Based Gene Therapy. *International Journal of Molecular Sciences*, *24*(9), 7736. https://doi.org/10.3390/ijms24097736

Li, X., Zhang, J., Li, D., He, C., He, K., Xue, T., Wan, L., Zhang, C., & Liu, Q. (2021). Astrocytic ApoE reprograms neuronal cholesterol metabolism and histone-acetylation-mediated memory. *Neuron*, *109*(6), 957-970.e8. https://doi.org/10.1016/j.neuron.2021.01.005

Liao, W.-W., Asri, M., Ebler, J., Doerr, D., Haukness, M., Hickey, G., Lu, S., Lucas, J. K., Monlong, J., Abel, H. J., Buonaiuto, S., Chang, X. H., Cheng, H., Chu, J., Colonna, V., Eizenga, J. M., Feng, X., Fischer, C., Fulton, R. S., … Paten, B. (2023). A draft human pangenome reference. *Nature*, *617*(7960), Article 7960. https://doi.org/10.1038/s41586-023-05896-x

Lima, T., Bernfur, K., Vilanova, M., & Cedervall, T. (2020). Understanding the Lipid and Protein Corona Formation on Different Sized Polymeric Nanoparticles. *Scientific Reports*, *10*(1), Article 1. https://doi.org/10.1038/s41598-020-57943-6

Liu, B., Zhang, X., Hou, B., Li, J., Qiu, C., Qin, W., Yu, C., & Jiang, T. (2014). The Impact of MIR137 on Dorsolateral Prefrontal–Hippocampal Functional Connectivity in Healthy Subjects. *Neuropsychopharmacology*, *39*(9), 2153–2160. https://doi.org/10.1038/npp.2014.63

Liu, C., Gao, H., Lv, P., Liu, J., & Liu, G. (2017). Extracellular vesicles as an efficient nanoplatform for the delivery of therapeutics. *Human Vaccines & Immunotherapeutics*, *13*(11), 2678–2687. https://doi.org/10.1080/21645515.2017.1363935

Liu, S., Grigoryan, M. M., Vasilevko, V., Sumbria, R. K., Paganini-Hill, A., Cribbs, D. H., & Fisher, M. J. (2014). Comparative Analysis of H&E and Prussian Blue Staining in a Mouse Model of Cerebral Microbleeds. *Journal of Histochemistry and Cytochemistry*, *62*(11), 767–773. https://doi.org/10.1369/0022155414546692

Liu, S., Zhang, F., Wang, X., Shugart, Y. Y., Zhao, Y., Li, X., Liu, Z., Sun, N., Yang, C., Zhang, K., Yue, W., Yu, X., & Xu, Y. (2017). Diagnostic value of blood-derived microRNAs for schizophrenia: Results of a meta-analysis and validation. *Scientific Reports*, *7*(1), Article 1. https://doi.org/10.1038/s41598-017-15751-5

Loohuis, N. F. O., Kasri, N. N., Glennon, J. C., van Bokhoven, H., Hébert, S. S., Kaplan, B. B., Martens, G. J., & Aschrafi, A. (2017). The Schizophrenia Risk Gene MIR137 Acts as a Hippocampal Gene Network Node Orchestrating the Expression of Genes Relevant to Nervous System Development and Function. *Progress in Neuro-Psychopharmacology & Biological Psychiatry*, *73*, 109–118. https://doi.org/10.1016/j.pnpbp.2016.02.009

Mahmoudi, E., Atkins, J. R., Quidé, Y., Reay, W. R., Cairns, H. M., Fitzsimmons, C., Carr, V. J., Green, M. J., & Cairns, M. J. (2020). The MIR137 VNTR rs58335419 Is Associated With Cognitive Impairment in Schizophrenia and Altered Cortical Morphology. *Schizophrenia Bulletin*. https://doi.org/10.1093/schbul/sbaa123

Mahmoudi, E., & Cairns, M. J. (2017). MiR-137: An important player in neural development and neoplastic transformation. *Molecular Psychiatry*, *22*(1), 44–55. https://doi.org/10.1038/mp.2016.150

Mahmoudi, E., Fitzsimmons, C., Geaghan, M. P., Shannon Weickert, C., Atkins, J. R., Wang, X., & Cairns, M. J. (2019). Circular RNA biogenesis is decreased in postmortem cortical gray

matter in schizophrenia and may alter the bioavailability of associated miRNA. *Neuropsychopharmacology*, *44*(6), 1043–1054. https://doi.org/10.1038/s41386-019-0348-1

Maier, T., Güell, M., & Serrano, L. (2009). Correlation of mRNA and protein in complex biological samples. *FEBS Letters*, *583*(24), 3966–3973. https://doi.org/10.1016/j.febslet.2009.10.036

Margolis, L., & Sadovsky, Y. (2019). The biology of extracellular vesicles: The known unknowns. *PLoS Biology*, *17*(7), e3000363. https://doi.org/10.1371/journal.pbio.3000363

Maric, N. P., Jovicic, M. J., Mihaljevic, M., & Miljevic, C. (2016). Improving Current Treatments for Schizophrenia. *Drug Development Research*, *77*(7), 357–367. https://doi.org/10.1002/ddr.21337

Maury, E. A., Sherman, M. A., Genovese, G., Gilgenast, T. G., Kamath, T., Burris, S. J., Rajarajan, P., Flaherty, E., Akbarian, S., Chess, A., McCarroll, S. A., Loh, P.-R., Phillips-Cremins, J. E., Brennand, K. J., Macosko, E. Z., Walters, J. T. R., O'Donovan, M., Sullivan, P., Marshall, C. R., … Walsh, C. A. (2023). Schizophrenia-associated somatic copy-number variants from 12,834 cases reveal recurrent NRXN1 and ABCB11 disruptions. *Cell Genomics*, *0*(0). https://doi.org/10.1016/j.xgen.2023.100356

McCutcheon, R. A., Abi-Dargham, A., & Howes, O. D. (2019). Schizophrenia, Dopamine and the Striatum: From Biology to Symptoms. *Trends in Neurosciences*, *42*(3), 205–220. https://doi.org/10.1016/j.tins.2018.12.004

McCutcheon, R. A., Krystal, J. H., & Howes, O. D. (2020). Dopamine and glutamate in schizophrenia: Biology, symptoms and treatment. *World Psychiatry*, *19*(1), 15–33. https://doi.org/10.1002/wps.20693

McCutcheon, R. A., Reis Marques, T., & Howes, O. D. (2020). Schizophrenia-An Overview. *JAMA Psychiatry*, *77*(2), 201–210. https://doi.org/10.1001/jamapsychiatry.2019.3360

McDonald, W. H., Tabb, D. L., Sadygov, R. G., MacCoss, M. J., Venable, J., Graumann, J., Johnson, J. R., Cociorva, D., & Yates, J. R. (2004). MS1, MS2, and SQT-three unified, compact, and easily parsed file formats for the storage of shotgun proteomic spectra and identifications. *Rapid Communications in Mass Spectrometry: RCM*, *18*(18), 2162–2168. https://doi.org/10.1002/rcm.1603

McKelvey, K. J., Powell, K. L., Ashton, A. W., Morris, J. M., & McCracken, S. A. (2015). Exosomes: Mechanisms of Uptake. *Journal of Circulating Biomarkers*, *4*, 7. https://doi.org/10.5772/61186

Mei, Y.-Y., Wu, D. C., & Zhou, N. (2018). Astrocytic Regulation of Glutamate Transmission in Schizophrenia. *Frontiers in Psychiatry*, *9*, 544. https://doi.org/10.3389/fpsyt.2018.00544

Midekessa, G., Godakumara, K., Ord, J., Viil, J., Lättekivi, F., Dissanayake, K., Kopanchuk, S., Rinken, A., Andronowska, A., Bhattacharjee, S., Rinken, T., & Fazeli, A. (2020). Zeta Potential of Extracellular Vesicles: Toward Understanding the Attributes that Determine Colloidal Stability. *ACS Omega*, *5*(27), 16701–16710. https://doi.org/10.1021/acsomega.0c01582

Mills, R. E., Walter, K., Stewart, C., Handsaker, R. E., Chen, K., Alkan, C., Abyzov, A., Yoon, S. C., Ye, K., Cheetham, R. K., Chinwalla, A., Conrad, D. F., Fu, Y., Grubert, F., Hajirasouliha, I.,

Hormozdiari, F., Iakoucheva, L. M., Iqbal, Z., Kang, S., … Korbel, J. O. (2011). Mapping copy number variation by population-scale genome sequencing. *Nature*, *470*(7332), Article 7332. https://doi.org/10.1038/nature09708

Mirjalili Mohanna, S. Z., Djaksigulova, D., Hill, A. M., Wagner, P. K., Simpson, E. M., & Leavitt, B. R. (2022). LNP-mediated delivery of CRISPR RNP for wide-spread in vivo genome editing in mouse cornea. *Journal of Controlled Release: Official Journal of the Controlled Release Society*, *350*, 401–413. https://doi.org/10.1016/j.jconrel.2022.08.042

Mitchell, M. J., Billingsley, M. M., Haley, R. M., Wechsler, M. E., Peppas, N. A., & Langer, R. (2021). Engineering precision nanoparticles for drug delivery. *Nature Reviews Drug Discovery*, *20*(2), Article 2. https://doi.org/10.1038/s41573-020-0090-8

Moghaddam, B., & Javitt, D. (2012). From Revolution to Evolution: The Glutamate Hypothesis of Schizophrenia and its Implication for Treatment. *Neuropsychopharmacology*, *37*(1), 4–15. https://doi.org/10.1038/npp.2011.181

Mohamed, M., Abu Lila, A. S., Shimizu, T., Alaaeldin, E., Hussein, A., Sarhan, H. A., Szebeni, J., & Ishida, T. (2019). PEGylated liposomes: Immunological responses. *Science and Technology of Advanced Materials*, *20*(1), 710–724. https://doi.org/10.1080/14686996.2019.1627174

Mohammadi, A. H., Ghazvinian, Z., Bagheri, F., Harada, M., & Baghaei, K. (2023). Modification of Extracellular Vesicle Surfaces: An Approach for Targeted Drug Delivery. *BioDrugs*, *37*(3), 353–374. https://doi.org/10.1007/s40259-023-00595-5

Mousli, Y., Brachet, M., Chain, J. L., & Ferey, L. (2022). A rapid and quantitative reversed-phase HPLC-DAD/ELSD method for lipids involved in nanoparticle formulations. *Journal of*

Pharmaceutical and Biomedical Analysis, *220*, 115011. https://doi.org/10.1016/j.jpba.2022.115011

Muhuri, M., Maeda, Y., Ma, H., Ram, S., Fitzgerald, K. A., Tai, P. W., & Gao, G. (2021). Overcoming innate immune barriers that impede AAV gene therapy vectors. *The Journal of Clinical Investigation*, *131*(1), e143780, 143780. https://doi.org/10.1172/JCI143780

Mui, B. L., Tam, Y. K., Jayaraman, M., Ansell, S. M., Du, X., Tam, Y. Y. C., Lin, P. J., Chen, S., Narayanannair, J. K., Rajeev, K. G., Manoharan, M., Akinc, A., Maier, M. A., Cullis, P., Madden, T. D., & Hope, M. J. (2013). Influence of Polyethylene Glycol Lipid Desorption Rates on Pharmacokinetics and Pharmacodynamics of siRNA Lipid Nanoparticles. *Molecular Therapy - Nucleic Acids*, *2*. https://doi.org/10.1038/mtna.2013.66

Namiot, E. D., Sokolov, A. V., Chubarev, V. N., Tarasov, V. V., & Schiöth, H. B. (2023). Nanoparticles in Clinical Trials: Analysis of Clinical Trials, FDA Approvals and Use for COVID-19 Vaccines. *International Journal of Molecular Sciences*, *24*(1), 787. https://doi.org/10.3390/ijms24010787

Ndeupen, S., Qin, Z., Jacobsen, S., Bouteau, A., Estanbouli, H., & Igyártó, B. Z. (2021). The mRNA-LNP platform's lipid nanoparticle component used in preclinical vaccine studies is highly inflammatory. *iScience*, *24*(12), 103479. https://doi.org/10.1016/j.isci.2021.103479

Network and Pathway Analysis Subgroup of Psychiatric Genomics Consortium. (2015). Psychiatric genome-wide association study analyses implicate neuronal, immune and histone pathways. *Nature Neuroscience*, *18*(2), 199–209. https://doi.org/10.1038/nn.3922

Niewoehner, J., Bohrmann, B., Collin, L., Urich, E., Sade, H., Maier, P., Rueger, P., Stracke, J. O., Lau, W., Tissot, A. C., Loetscher, H., Ghosh, A., & Freskgård, P.-O. (2014). Increased brain penetration and potency of a therapeutic antibody using a monovalent molecular shuttle. *Neuron*, *81*(1), 49–60. https://doi.org/10.1016/j.neuron.2013.10.061

Noh, J.-E., Oh, S.-H., Park, I.-H., & Song, J. (2020). Intracerebral Transplants of GMP-Grade Human Umbilical Cord-Derived Mesenchymal Stromal Cells Effectively Treat Subacute-Phase Ischemic Stroke in a Rodent Model. *Frontiers in Cellular Neuroscience*, *14*. https://www.frontiersin.org/articles/10.3389/fncel.2020.546659

OBI-NAGATA, K., TEMMA, Y., & HAYASHI-TAKAGI, A. (2019). Synaptic functions and their disruption in schizophrenia: From clinical evidence to synaptic optogenetics in an animal model. *Proceedings of the Japan Academy. Series B, Physical and Biological Sciences*, *95*(5), 179–197. https://doi.org/10.2183/pjab.95.014

Olde Loohuis, N. F. M., Ba, W., Stoerchel, P. H., Kos, A., Jager, A., Schratt, G., Martens, G. J. M., van Bokhoven, H., Nadif Kasri, N., & Aschrafi, A. (2015). MicroRNA-137 Controls AMPA-Receptor-Mediated Transmission and mGluR-Dependent LTD. *Cell Reports*, *11*(12), 1876–1884. https://doi.org/10.1016/j.celrep.2015.05.040

Olfson, M., Gerhard, T., Huang, C., Crystal, S., & Stroup, T. S. (2015). Premature Mortality Among Adults With Schizophrenia in the United States. *JAMA Psychiatry*, *72*(12), 1172–1181. https://doi.org/10.1001/jamapsychiatry.2015.1737

Owen, M. J., Legge, S. E., Rees, E., Walters, J. T. R., & O'Donovan, M. C. (2023). Genomic findings in schizophrenia and their implications. *Molecular Psychiatry*, 1–10. https://doi.org/10.1038/s41380-023-02293-8

Pardridge, W. M. (2023). Brain gene therapy with Trojan horse lipid nanoparticles. *Trends in Molecular Medicine*, S1471491423000369. https://doi.org/10.1016/j.molmed.2023.02.004

Parellada, E., & Gassó, P. (2021). Glutamate and microglia activation as a driver of dendritic apoptosis: A core pathophysiological mechanism to understand schizophrenia. *Translational Psychiatry*, *11*(1), Article 1. https://doi.org/10.1038/s41398-021-01385-9

Patel, K. R., Cherian, J., Gohil, K., & Atkinson, D. (2014a). Schizophrenia: Overview and treatment options. *P & T: A Peer-Reviewed Journal for Formulary Management*, *39*(9), 638–645.

Patel, K. R., Cherian, J., Gohil, K., & Atkinson, D. (2014b). Schizophrenia: Overview and Treatment Options. *Pharmacy and Therapeutics*, *39*(9), 638–645.

Patel, P., Ibrahim, N. M., & Cheng, K. (2021). The Importance of Apparent pKa in the Development of Nanoparticles Encapsulating siRNA and mRNA. *Trends in Pharmacological Sciences*, *42*(6), 448–460. https://doi.org/10.1016/j.tips.2021.03.002

Patel, S., Ryals, R. C., Weller, K. K., Pennesi, M. E., & Sahay, G. (2019). Lipid nanoparticles for delivery of messenger RNA to the back of the eye. *Journal of Controlled Release: Official Journal of the Controlled Release Society*, *303*, 91–100. https://doi.org/10.1016/j.jconrel.2019.04.015

Paunovska, K., Sago, C. D., Monaco, C. M., Hudson, W. H., Castro, M. G., Rudoltz, T. G., Kalathoor, S., Vanover, D. A., Santangelo, P. J., Ahmed, R., Bryksin, A. V., & Dahlman, J. E. (2018). A Direct Comparison of in Vitro and in Vivo Nucleic Acid Delivery Mediated by Hundreds of Nanoparticles Reveals a Weak Correlation. *Nano Letters*, *18*(3), 2148–2157. https://doi.org/10.1021/acs.nanolett.8b00432

Perez-Riverol, Y., Bai, J., Bandla, C., García-Seisdedos, D., Hewapathirana, S., Kamatchinathan, S., Kundu, D. J., Prakash, A., Frericks-Zipper, A., Eisenacher, M., Walzer, M., Wang, S., Brazma, A., & Vizcaíno, J. A. (2022). The PRIDE database resources in 2022: A hub for mass spectrometry-based proteomics evidences. *Nucleic Acids Research*, *50*(D1), D543–D552. https://doi.org/10.1093/nar/gkab1038

Pfrieger, F. W., & Ungerer, N. (2011). Cholesterol metabolism in neurons and astrocytes. *Progress in Lipid Research*, *50*(4), 357–371. https://doi.org/10.1016/j.plipres.2011.06.002

Pinto, D., Delaby, E., Merico, D., Barbosa, M., Merikangas, A., Klei, L., Thiruvahindrapuram, B., Xu, X., Ziman, R., Wang, Z., Vorstman, J. A. S., Thompson, A., Regan, R., Pilorge, M., Pellecchia, G., Pagnamenta, A. T., Oliveira, B., Marshall, C. R., Magalhaes, T. R., … Scherer, S. W. (2014). Convergence of genes and cellular pathways dysregulated in autism spectrum disorders. *American Journal of Human Genetics*, *94*(5), 677–694. https://doi.org/10.1016/j.ajhg.2014.03.018

Preda, A., & Shapiro, B. B. (2020). A safety evaluation of aripiprazole in the treatment of schizophrenia. *Expert Opinion on Drug Safety*, *19*(12), 1529–1538. https://doi.org/10.1080/14740338.2020.1832990

Qian, Y., Li, J., Zhao, S., Matthews, E. A., Adoff, M., Zhong, W., An, X., Yeo, M., Park, C., Yang, X., Wang, B.-S., Southwell, D. G., & Huang, Z. J. (2022). Programmable RNA sensing for cell monitoring and manipulation. *Nature*, *610*(7933), 713–721. https://doi.org/10.1038/s41586-022-05280-1

Qin, Z., Bouteau, A., Herbst, C., & Igyártó, B. Z. (2022). Pre-exposure to mRNA-LNP inhibits adaptive immune responses and alters innate immune fitness in an inheritable fashion. *PLoS Pathogens*, *18*(9), e1010830. https://doi.org/10.1371/journal.ppat.1010830

Raman, S., Mahmood, S., Hilles, A. R., Javed, M. N., Azmana, M., & Al-Japairai, K. A. S. (2020). Polymeric Nanoparticles for Brain Drug Delivery—A Review. *Current Drug Metabolism*, *21*(9), 649–660. https://doi.org/10.2174/1389200221666200508074348

Rasmussen, M. K., Pedersen, J. N., & Marie, R. (2020). Size and surface charge characterization of nanoparticles with a salt gradient. *Nature Communications*, *11*(1), Article 1. https://doi.org/10.1038/s41467-020-15889-3

Rayaprolu, S., Gao, T., Xiao, H., Ramesha, S., Weinstock, L. D., Shah, J., Duong, D. M., Dammer, E. B., Webster, J. A., Lah, J. J., Wood, L. B., Betarbet, R., Levey, A. I., Seyfried, N. T., & Rangaraju, S. (2020). Flow-cytometric microglial sorting coupled with quantitative proteomics identifies moesin as a highly-abundant microglial protein with relevance to Alzheimer's disease. *Molecular Neurodegeneration*, *15*(1), 28. https://doi.org/10.1186/s13024-020-00377-5

Rey, R., Suaud-Chagny, M.-F., Dorey, J.-M., Teyssier, J.-R., & d'Amato, T. (2020). Widespread transcriptional disruption of the microRNA biogenesis machinery in brain and peripheral tissues of individuals with schizophrenia. *Translational Psychiatry*, *10*(1), 376. https://doi.org/10.1038/s41398-020-01052-5

Rhym, L. H., Manan, R. S., Koller, A., Stephanie, G., & Anderson, D. G. (2023). Peptide-encoding mRNA barcodes for the high-throughput in vivo screening of libraries of lipid

nanoparticles for mRNA delivery. *Nature Biomedical Engineering*, *7*(7), Article 7. https://doi.org/10.1038/s41551-023-01030-4

Ripke, S., Neale, B. M., Corvin, A., Walters, J. T. R., Farh, K.-H., Holmans, P. A., Lee, P., Bulik-Sullivan, B., Collier, D. A., Huang, H., Pers, T. H., Agartz, I., Agerbo, E., Albus, M., Alexander, M., Amin, F., Bacanu, S. A., Begemann, M., Belliveau Jr, R. A., … Psychosis Endophenotypes International Consortium. (2014). Biological insights from 108 schizophrenia-associated genetic loci. *Nature*, *511*(7510), Article 7510. https://doi.org/10.1038/nature13595

Ripke, S., O'Dushlaine, C., Chambert, K., Moran, J. L., Kähler, A. K., Akterin, S., Bergen, S. E., Collins, A. L., Crowley, J. J., Fromer, M., Kim, Y., Lee, S. H., Magnusson, P. K. E., Sanchez, N., Stahl, E. A., Williams, S., Wray, N. R., Xia, K., Bettella, F., … Sullivan, P. F. (2013). Genome-wide association analysis identifies 13 new risk loci for schizophrenia. *Nature Genetics*, *45*(10), 1150–1159. https://doi.org/10.1038/ng.2742

Ripke, S., Sanders, A. R., Kendler, K. S., Levinson, D. F., Sklar, P., Holmans, P. A., Lin, D.-Y., Duan, J., Ophoff, R. A., Andreassen, O. A., Scolnick, E., Cichon, S., St. Clair, D., Corvin, A., Gurling, H., Werge, T., Rujescu, D., Blackwood, D. H. R., Pato, C. N., … The Schizophrenia Psychiatric Genome-Wide Association Study (GWAS) Consortium. (2011). Genome-wide association study identifies five new schizophrenia loci. *Nature Genetics*, *43*(10), Article 10. https://doi.org/10.1038/ng.940

Ritchie, M. E., Phipson, B., Wu, D., Hu, Y., Law, C. W., Shi, W., & Smyth, G. K. (2015). Limma powers differential expression analyses for RNA-sequencing and microarray studies. *Nucleic Acids Research*, *43*(7), e47. https://doi.org/10.1093/nar/gkv007

Rizk, M., & Tüzmen, Ş. (2017). Update on the clinical utility of an RNA interference-based treatment: Focus on Patisiran. *Pharmacogenomics and Personalized Medicine*, *10*, 267–278. https://doi.org/10.2147/PGPM.S87945

Robinson, M. D., McCarthy, D. J., & Smyth, G. K. (2010). edgeR: A Bioconductor package for differential expression analysis of digital gene expression data. *Bioinformatics (Oxford, England)*, *26*(1), 139–140. https://doi.org/10.1093/bioinformatics/btp616

Roth, B. L., Sheffler, D. J., & Kroeze, W. K. (2004). Magic shotguns versus magic bullets: Selectively non-selective drugs for mood disorders and schizophrenia. *Nature Reviews Drug Discovery*, *3*(4), Article 4. https://doi.org/10.1038/nrd1346

Rugg-Gunn, F., Miserocchi, A., & McEvoy, A. (2020). Epilepsy surgery. *Practical Neurology*, *20*(1), 4–14. https://doi.org/10.1136/practneurol-2019-002192

Rungta, R. L., Choi, H. B., Lin, P. J., Ko, R. W., Ashby, D., Nair, J., Manoharan, M., Cullis, P. R., & Macvicar, B. A. (2013). Lipid Nanoparticle Delivery of siRNA to Silence Neuronal Gene Expression in the Brain. *Molecular Therapy. Nucleic Acids*, *2*, e136. https://doi.org/10.1038/mtna.2013.65

Saint-Pol, J., Gosselet, F., Duban-Deweer, S., Pottiez, G., & Karamanos, Y. (2020). Targeting and Crossing the Blood-Brain Barrier with Extracellular Vesicles. *Cells*, *9*(4). https://doi.org/10.3390/cells9040851

Sakamoto, K., & Crowley, J. J. (2018). A comprehensive review of the genetic and biological evidence supports a role for MicroRNA-137 in the etiology of schizophrenia. *American Journal of Medical Genetics. Part B, Neuropsychiatric Genetics: The Official Publication of*

the International Society of Psychiatric Genetics, *177*(2), 242–256. https://doi.org/10.1002/ajmg.b.32554

Sakurai, Y., Abe, N., Yoshikawa, K., Oyama, R., Ogasawara, S., Murata, T., Nakai, Y., Tange, K., Tanaka, H., & Akita, H. (2022). Targeted delivery of lipid nanoparticle to lymphatic endothelial cells via anti-podoplanin antibody. *Journal of Controlled Release*, *349*, 379–387. https://doi.org/10.1016/j.jconrel.2022.06.052

Sandau, U. S., Duggan, E., Shi, X., Smith, S. J., Huckans, M., Schutzer, W. E., Loftis, J. M., Janowsky, A., Nolan, J. P., & Saugstad, J. A. (2020). Methamphetamine use alters human plasma extracellular vesicles and their microRNA cargo: An exploratory study. *Journal of Extracellular Vesicles*, *10*(1), e12028. https://doi.org/10.1002/jev2.12028

Santarelli, D. M., Carroll, A. P., Cairns, H. M., Tooney, P. A., & Cairns, M. J. (2020). Schizophrenia-associated MicroRNA-gene Interactions in the Dorsolateral Prefrontal Cortex. *Genomics, Proteomics & Bioinformatics*. https://doi.org/10.1016/j.gpb.2019.10.003

Santos, M. C. T., Tegge, A. N., Correa, B. R., Mahesula, S., Kohnke, L. Q., Qiao, M., Ferreira, M. A. R., Kokovay, E., & Penalva, L. O. F. (2016). miR-124, -128, and -137 Orchestrate Neural Differentiation by Acting on Overlapping Gene Sets Containing a Highly Connected Transcription Factor Network. *Stem Cells*, *34*(1), 220–232. https://doi.org/10.1002/stem.2204

Schoenmaker, L., Witzigmann, D., Kulkarni, J. A., Verbeke, R., Kersten, G., Jiskoot, W., & Crommelin, D. J. A. (2021). mRNA-lipid nanoparticle COVID-19 vaccines: Structure and stability. *International Journal of Pharmaceutics*, *601*, 120586. https://doi.org/10.1016/j.ijpharm.2021.120586

Scholz, C., & Wagner, E. (2012). Therapeutic plasmid DNA versus siRNA delivery: Common and different tasks for synthetic carriers. *Journal of Controlled Release: Official Journal of the Controlled Release Society*, *161*(2), 554–565. https://doi.org/10.1016/j.jconrel.2011.11.014

Schultz, M. L., Fawaz, M. V., Azaria, R. D., Hollon, T. C., Liu, E. A., Kunkel, T. J., Halseth, T. A., Krus, K. L., Ming, R., Morin, E. E., McLoughlin, H. S., Bushart, D. D., Paulson, H. L., Shakkottai, V. G., Orringer, D. A., Schwendeman, A. S., & Lieberman, A. P. (2019). Synthetic high-density lipoprotein nanoparticles for the treatment of Niemann–Pick diseases. *BMC Medicine*, *17*, 200. https://doi.org/10.1186/s12916-019-1423-5

Schulze, H., & Sandhoff, K. (2011). Lysosomal Lipid Storage Diseases. *Cold Spring Harbor Perspectives in Biology*, *3*(6), a004804. https://doi.org/10.1101/cshperspect.a004804

Schumann, C., Chan, S., Millar, J. A., Bortnyak, Y., Carey, K., Fedchyk, A., Wong, L., Korzun, T., Moses, A. S., Lorenz, A., Shea, D., Taratula, O., Khalimonchuk, O., & Taratula, O. (2018). Intraperitoneal nanotherapy for metastatic ovarian cancer based on siRNA-mediated suppression of DJ-1 protein combined with a low dose of cisplatin. *Nanomedicine: Nanotechnology, Biology and Medicine*, *14*(4), 1395–1405. https://doi.org/10.1016/j.nano.2018.03.005

Sekar, A., Bialas, A. R., de Rivera, H., Davis, A., Hammond, T. R., Kamitaki, N., Tooley, K., Presumey, J., Baum, M., Van Doren, V., Genovese, G., Rose, S. A., Handsaker, R. E., Schizophrenia Working Group of the Psychiatric Genomics Consortium, Daly, M. J., Carroll, M. C., Stevens, B., & McCarroll, S. A. (2016). Schizophrenia risk from complex

variation of complement component 4. *Nature*, *530*(7589), 177–183. https://doi.org/10.1038/nature16549

Seki, J., Sonoke, S., Saheki, A., Fukui, H., Sasaki, H., & Mayumi, T. (2004). A nanometer lipid emulsion, lipid nano-sphere (LNS), as a parenteral drug carrier for passive drug targeting. *International Journal of Pharmaceutics*, *273*(1–2), 75–83. https://doi.org/10.1016/j.ijpharm.2003.12.022

Selbach, M., Schwanhäusser, B., Thierfelder, N., Fang, Z., Khanin, R., & Rajewsky, N. (2008). Widespread changes in protein synthesis induced by microRNAs. *Nature*, *455*(7209), 58–63. https://doi.org/10.1038/nature07228

Semple, B. D., Blomgren, K., Gimlin, K., Ferriero, D. M., & Noble-Haeusslein, L. J. (2013). Brain development in rodents and humans: Identifying benchmarks of maturation and vulnerability to injury across species. *Progress in Neurobiology*, *0*, 1–16. https://doi.org/10.1016/j.pneurobio.2013.04.001

Shastry, B. S. (2009). SNPs: Impact on gene function and phenotype. *Methods in Molecular Biology (Clifton, N.J.)*, *578*, 3–22. https://doi.org/10.1007/978-1-60327-411-1_1

Shenton, M. E., Kikinis, R., Jolesz, F. A., Pollak, S. D., LeMay, M., Wible, C. G., Hokama, H., Martin, J., Metcalf, D., & Coleman, M. (1992). Abnormalities of the left temporal lobe and thought disorder in schizophrenia. A quantitative magnetic resonance imaging study. *The New England Journal of Medicine*, *327*(9), 604–612. https://doi.org/10.1056/NEJM199208273270905

Siafis, S., Tzachanis, D., Samara, M., & Papazisis, G. (2018). Antipsychotic Drugs: From Receptor-binding Profiles to Metabolic Side Effects. *Current Neuropharmacology*, *16*(8), 1210–1223. https://doi.org/10.2174/1570159X15666170630163616

Siegert, S., Seo, J., Kwon, E. J., Rudenko, A., Cho, S., Wang, W., Flood, Z., Martorell, A. J., Ericsson, M., Mungenast, A. E., & Tsai, L.-H. (2015). The schizophrenia risk gene product miR-137 alters presynaptic plasticity. *Nature Neuroscience*, *18*(7), 1008–1016. https://doi.org/10.1038/nn.4023

Singh, T., Neale, B. M., Daly, M. J., & Consortium, on behalf of the S. E. M.-A. (SCHEMA). (2020). *Exome sequencing identifies rare coding variants in 10 genes which confer substantial risk for schizophrenia* (p. 2020.09.18.20192815). medRxiv. https://doi.org/10.1101/2020.09.18.20192815

Singh, T., Poterba, T., Curtis, D., Akil, H., Al Eissa, M., Barchas, J. D., Bass, N., Bigdeli, T. B., Breen, G., Bromet, E. J., Buckley, P. F., Bunney, W. E., Bybjerg-Grauholm, J., Byerley, W. F., Chapman, S. B., Chen, W. J., Churchhouse, C., Craddock, N., Cusick, C. M., … Daly, M. J. (2022). Rare coding variants in ten genes confer substantial risk for schizophrenia. *Nature*, *604*(7906), 509–516. https://doi.org/10.1038/s41586-022-04556-w

Smeland, O. B., Frei, O., Dale, A. M., & Andreassen, O. A. (2020). The polygenic architecture of schizophrenia—Rethinking pathogenesis and nosology. *Nature Reviews. Neurology*, *16*(7), 366–379. https://doi.org/10.1038/s41582-020-0364-0

Smucny, J., Dienel, S. J., Lewis, D. A., & Carter, C. S. (2022). Mechanisms underlying dorsolateral prefrontal cortex contributions to cognitive dysfunction in schizophrenia.

Neuropsychopharmacology, *47*(1), 292–308. https://doi.org/10.1038/s41386-021-01089-0

Ståhl, A., Johansson, K., Mossberg, M., Kahn, R., & Karpman, D. (2019). Exosomes and microvesicles in normal physiology, pathophysiology, and renal diseases. *Pediatric Nephrology (Berlin, Germany)*, *34*(1), 11–30. https://doi.org/10.1007/s00467-017-3816-z

Stępnicki, P., Kondej, M., & Kaczor, A. A. (2018). Current Concepts and Treatments of Schizophrenia. *Molecules : A Journal of Synthetic Chemistry and Natural Product Chemistry*, *23*(8), 2087. https://doi.org/10.3390/molecules23082087

Stilo, S. A., & Murray, R. M. (2019). Non-Genetic Factors in Schizophrenia. *Current Psychiatry Reports*, *21*(10), 100. https://doi.org/10.1007/s11920-019-1091-3

Strazisar, M., Cammaerts, S., van der Ven, K., Forero, D. A., Lenaerts, A.-S., Nordin, A., Almeida-Souza, L., Genovese, G., Timmerman, V., Liekens, A., De Rijk, P., Adolfsson, R., Callaerts, P., & Del-Favero, J. (2015). MIR137 variants identified in psychiatric patients affect synaptogenesis and neuronal transmission gene sets. *Molecular Psychiatry*, *20*(4), Article 4. https://doi.org/10.1038/mp.2014.53

Sullivan, C. R., Mielnik, C. A., O'Donovan, S. M., Funk, A. J., Bentea, E., DePasquale, E. A., Alganem, K., Wen, Z., Haroutunian, V., Katsel, P., Ramsey, A. J., Meller, J., & McCullumsmith, R. E. (2019). Connectivity Analyses of Bioenergetic Changes in Schizophrenia: Identification of Novel Treatments. *Molecular Neurobiology*, *56*(6), 4492–4517. https://doi.org/10.1007/s12035-018-1390-4

Sun, G., Ye, P., Murai, K., Lang, M.-F., Li, S., Zhang, H., Li, W., Fu, C., Yin, J., Wang, A., Ma, X., & Shi, Y. (2011). miR-137 forms a regulatory loop with nuclear receptor TLX and LSD1 in

neural stem cells. *Nature Communications*, *2*, 529. https://doi.org/10.1038/ncomms1532

Swayze, E. E., Siwkowski, A. M., Wancewicz, E. V., Migawa, M. T., Wyrzykiewicz, T. K., Hung, G., Monia, B. P., & Bennett, and C. F. (2007). Antisense oligonucleotides containing locked nucleic acid improve potency but cause significant hepatotoxicity in animals. *Nucleic Acids Research*, *35*(2), 687–700. https://doi.org/10.1093/nar/gkl1071

Syama, K., Jakubek, Z. J., Chen, S., Zaifman, J., Tam, Y. Y. C., & Zou, S. (2022). Development of lipid nanoparticles and liposomes reference materials (II): Cytotoxic profiles. *Scientific Reports*, *12*, 18071. https://doi.org/10.1038/s41598-022-23013-2

Szklarczyk, D., Kirsch, R., Koutrouli, M., Nastou, K., Mehryary, F., Hachilif, R., Gable, A. L., Fang, T., Doncheva, N. T., Pyysalo, S., Bork, P., Jensen, L. J., & von Mering, C. (2023). The STRING database in 2023: Protein-protein association networks and functional enrichment analyses for any sequenced genome of interest. *Nucleic Acids Research*, *51*(D1), D638–D646. https://doi.org/10.1093/nar/gkac1000

Tetta, C., Ghigo, E., Silengo, L., Deregibus, M. C., & Camussi, G. (2013). Extracellular vesicles as an emerging mechanism of cell-to-cell communication. *Endocrine*, *44*(1), 11–19. https://doi.org/10.1007/s12020-012-9839-0

Thomas, K. T., Anderson, B. R., Shah, N., Zimmer, S. E., Hawkins, D., Valdez, A. N., Gu, Q., & Bassell, G. J. (2017). Inhibition of the schizophrenia-associated microRNA miR-137 disrupts Nrg1α neurodevelopmental signal transduction. *Cell Reports*, *20*(1), 1–12. https://doi.org/10.1016/j.celrep.2017.06.038

Thomas, K. T., & Zakharenko, S. S. (2021). MicroRNAs in the Onset of Schizophrenia. *Cells*, *10*(10), 2679. https://doi.org/10.3390/cells10102679

Trubetskoy, V., Pardiñas, A. F., Qi, T., Panagiotaropoulou, G., Awasthi, S., Bigdeli, T. B., Bryois, J., Chen, C.-Y., Dennison, C. A., Hall, L. S., Lam, M., Watanabe, K., Frei, O., Ge, T., Harwood, J. C., Koopmans, F., Magnusson, S., Richards, A. L., Sidorenko, J., … Schizophrenia Working Group of the Psychiatric Genomics Consortium. (2022). Mapping genomic loci implicates genes and synaptic biology in schizophrenia. *Nature*, *604*(7906), 502–508. https://doi.org/10.1038/s41586-022-04434-5

Uno, Y., & Coyle, J. T. (2019). Glutamate hypothesis in schizophrenia. *Psychiatry and Clinical Neurosciences*, *73*(5), 204–215. https://doi.org/10.1111/pcn.12823

van Erp, T. G. M., Guella, I., Vawter, M. P., Turner, J., Brown, G. G., McCarthy, G., Greve, D. N., Glover, G. H., Calhoun, V. D., Lim, K. O., Bustillo, J. R., Belger, A., Ford, J. M., Mathalon, D. H., Diaz, M., Preda, A., Nguyen, D., Macciardi, F., & Potkin, S. G. (2014). Schizophrenia miR-137 locus risk genotype is associated with dorsolateral prefrontal cortex hyperactivation. *Biological Psychiatry*, *75*(5), 398–405. https://doi.org/10.1016/j.biopsych.2013.06.016

Verbeke, R., Hogan, M. J., Loré, K., & Pardi, N. (2022). Innate immune mechanisms of mRNA vaccines. *Immunity*, *55*(11), 1993–2005. https://doi.org/10.1016/j.immuni.2022.10.014

Vogel, C., & Marcotte, E. M. (2012). Insights into the regulation of protein abundance from proteomic and transcriptomic analyses. *Nature Reviews. Genetics*, *13*(4), 227–232. https://doi.org/10.1038/nrg3185

Wada, T., & Becskei, A. (2017). Impact of Methods on the Measurement of mRNA Turnover. *International Journal of Molecular Sciences*, *18*(12), 2723. https://doi.org/10.3390/ijms18122723

Wahbeh, M. H., & Avramopoulos, D. (2021). Gene-Environment Interactions in Schizophrenia: A Literature Review. *Genes*, *12*(12), 1850. https://doi.org/10.3390/genes12121850

Walker, S., Busatto, S., Pham, A., Tian, M., Suh, A., Carson, K., Quintero, A., Lafrence, M., Malik, H., Santana, M. X., & Wolfram, J. (2019). Extracellular vesicle-based drug delivery systems for cancer treatment. *Theranostics*, *9*(26), 8001–8017. https://doi.org/10.7150/thno.37097

Wang, H., & Eckel, R. H. (2014). What are Lipoproteins doing in the Brain? *Trends in Endocrinology and Metabolism: TEM*, *25*(1), 8–14. https://doi.org/10.1016/j.tem.2013.10.003

Wang, Y., Chen, R., Zhou, X., Guo, R., Yin, J., Li, Y., & Ma, G. (2020). miR-137: A Novel Therapeutic Target for Human Glioma. *Molecular Therapy. Nucleic Acids*, *21*, 614–622. https://doi.org/10.1016/j.omtn.2020.06.028

Warnica, W., Merico, D., Costain, G., Alfred, S. E., Wei, J., Marshall, C. R., Scherer, S. W., & Bassett, A. S. (2015). Copy number variable microRNAs in schizophrenia and their neurodevelopmental gene targets. *Biological Psychiatry*, *77*(2), 158–166. https://doi.org/10.1016/j.biopsych.2014.05.011

Watanabe, K., Taskesen, E., van Bochoven, A., & Posthuma, D. (2017). Functional mapping and annotation of genetic associations with FUMA. *Nature Communications*, *8*(1), Article 1. https://doi.org/10.1038/s41467-017-01261-5

Weigel, A., Schild, D., & Zeug, A. (2009). Resolution in the ApoTome and the confocal laser scanning microscope: Comparison. *Journal of Biomedical Optics*, *14*(1), 014022. https://doi.org/10.1117/1.3083439

Weiner, D. J., Nadig, A., Jagadeesh, K. A., Dey, K. K., Neale, B. M., Robinson, E. B., Karczewski, K. J., & O'Connor, L. J. (2023). Polygenic architecture of rare coding variation across 394,783 exomes. *Nature*, *614*(7948), 492–499. https://doi.org/10.1038/s41586-022-05684-z

Wiley, D. T., Webster, P., Gale, A., & Davis, M. E. (2013). Transcytosis and brain uptake of transferrin-containing nanoparticles by tuning avidity to transferrin receptor. *Proceedings of the National Academy of Sciences of the United States of America*, *110*(21), 8662–8667. https://doi.org/10.1073/pnas.1307152110

Willemsen, M. H., Vallès, A., Kirkels, L. A. M. H., Mastebroek, M., Olde Loohuis, N., Kos, A., Wissink-Lindhout, W. M., de Brouwer, A. P. M., Nillesen, W. M., Pfundt, R., Holder-Espinasse, M., Vallée, L., Andrieux, J., Coppens-Hofman, M. C., Rensen, H., Hamel, B. C. J., van Bokhoven, H., Aschrafi, A., & Kleefstra, T. (2011). Chromosome 1p21.3 microdeletions comprising DPYD and MIR137 are associated with intellectual disability. *Journal of Medical Genetics*, *48*(12), 810–818. https://doi.org/10.1136/jmedgenet-2011-100294

Wilmarth, P. A., Riviere, M. A., & David, L. L. (2009). Techniques for accurate protein identification in shotgun proteomic studies of human, mouse, bovine, and chicken lenses. *Journal of Ocular Biology, Diseases, and Informatics*, *2*(4), 223–234. https://doi.org/10.1007/s12177-009-9042-6

Wilson, S. C., Baryza, J. L., Reynolds, A. J., Bowman, K., Keegan, M. E., Standley, S. M., Gardner, N. P., Parmar, P., Agir, V. O., Yadav, S., Zunic, A., Vargeese, C., Lee, C. C., & Rajan, S. (2015). Real Time Measurement of PEG Shedding from Lipid Nanoparticles in Serum via NMR Spectroscopy. *Molecular Pharmaceutics*, *12*(2), 386–392. https://doi.org/10.1021/mp500400k

Winter, J. (2015). MicroRNAs of the miR379–410 cluster: New players in embryonic neurogenesis and regulators of neuronal function. *Neurogenesis*, *2*(1), e1004970. https://doi.org/10.1080/23262133.2015.1004970

Wiśniewski, J. R., & Mann, M. (2016). A Proteomics Approach to the Protein Normalization Problem: Selection of Unvarying Proteins for MS-Based Proteomics and Western Blotting. *Journal of Proteome Research*, *15*(7), 2321–2326. https://doi.org/10.1021/acs.jproteome.6b00403

Witwer, K. W., & Wolfram, J. (2021). Extracellular vesicles versus synthetic nanoparticles for drug delivery. *Nature Reviews Materials*, *6*(2), Article 2. https://doi.org/10.1038/s41578-020-00277-6

Wong, E. H. F., Tarazi, F. I., & Shahid, M. (2010). The effectiveness of multi-target agents in schizophrenia and mood disorders: Relevance of receptor signature to clinical action. *Pharmacology & Therapeutics*, *126*(2), 173–185. https://doi.org/10.1016/j.pharmthera.2010.02.001

Woo, J. J., Pouget, J. G., Zai, C. C., & Kennedy, J. L. (2020). The complement system in schizophrenia: Where are we now and what's next? *Molecular Psychiatry*, *25*(1), Article 1. https://doi.org/10.1038/s41380-019-0479-0

Wu, S., Zhang, R., Nie, F., Wang, X., Jiang, C., Liu, M., Valenzuela, R. K., Liu, W., Shi, Y., & Ma, J. (2016). MicroRNA-137 Inhibits EFNB2 Expression Affected by a Genetic Variant and Is Expressed Aberrantly in Peripheral Blood of Schizophrenia Patients. *eBioMedicine*, *12*, 133–142. https://doi.org/10.1016/j.ebiom.2016.09.012

Yang, J. (2019). Patisiran for the treatment of hereditary transthyretin-mediated amyloidosis. *Expert Review of Clinical Pharmacology*, *12*(2), 95–99. https://doi.org/10.1080/17512433.2019.1567326

Yang, X., Koh, C. G., Liu, S., Pan, X., Santhanam, R., Yu, B., Peng, Y., Pang, J., Golan, S., Talmon, Y., Jin, Y., Muthusamy, N., Byrd, J. C., Chan, K. K., Lee, L. J., Marcucci, G., & Lee, R. J. (2009). Transferrin receptor-targeted lipid nanoparticles for delivery of an antisense oligodeoxyribonucleotide against Bcl-2. *Molecular Pharmaceutics*, *6*(1), 221–230. https://doi.org/10.1021/mp800149s

Yilmaz, M., Yalcin, E., Presumey, J., Aw, E., Ma, M., Whelan, C. W., Stevens, B., McCarroll, S. A., & Carroll, M. C. (2021). Overexpression of schizophrenia susceptibility factor human complement C4A promotes excessive synaptic loss and behavioral changes in mice. *Nature Neuroscience*, *24*(2), 214–224. https://doi.org/10.1038/s41593-020-00763-8

Yin, D.-M., Chen, Y.-J., Sathyamurthy, A., Xiong, W.-C., & Mei, L. (2012). Synaptic Dysfunction in Schizophrenia. In M. R. Kreutz & C. Sala (Eds.), *Synaptic Plasticity* (Vol. 970, pp. 493–516). Springer Vienna. https://doi.org/10.1007/978-3-7091-0932-8_22

Yin, J., Lin, J., Luo, X., Chen, Y., Li, Z., Ma, G., & Li, K. (2014). miR-137: A new player in schizophrenia. *International Journal of Molecular Sciences*, *15*(2), 3262–3271. https://doi.org/10.3390/ijms15023262

Yoneda, S., Fukuta, T., Ozono, M., & Kogure, K. (2022). Enhancement of cerebroprotective effects of lipid nanoparticles encapsulating FK506 on cerebral ischemia/reperfusion injury by particle size regulation. *Biochemical and Biophysical Research Communications*, *611*, 53–59. https://doi.org/10.1016/j.bbrc.2022.04.080

Yu, X., Yu, C., Wu, X., Cui, Y., Liu, X., Jin, Y., Li, Y., & Wang, L. (2023). Validation of an HPLC-CAD Method for Determination of Lipid Content in LNP-Encapsulated COVID-19 mRNA Vaccines. *Vaccines*, *11*(5), Article 5. https://doi.org/10.3390/vaccines11050937

Yu, Y. J., Zhang, Y., Kenrick, M., Hoyte, K., Luk, W., Lu, Y., Atwal, J., Elliott, J. M., Prabhu, S., Watts, R. J., & Dennis, M. S. (2011). Boosting Brain Uptake of a Therapeutic Antibody by Reducing Its Affinity for a Transcytosis Target. *Science Translational Medicine*, *3*(84), 84ra44-84ra44. https://doi.org/10.1126/scitranslmed.3002230

Zhang, W., Mehta, A., Tong, Z., Esser, L., & Voelcker, N. H. (2021). Development of Polymeric Nanoparticles for Blood–Brain Barrier Transfer—Strategies and Challenges. *Advanced Science*, *8*(10), 2003937. https://doi.org/10.1002/advs.202003937

Zhang, Z., Qin, Y.-W., Brewer, G., & Jing, Q. (2012). MicroRNA degradation and turnover: Regulating the regulators. *Wiley Interdisciplinary Reviews. RNA*, *3*(4), 593–600. https://doi.org/10.1002/wrna.1114

Zhao, Z., Anselmo, A. C., & Mitragotri, S. (2021). Viral vector-based gene therapies in the clinic. *Bioengineering & Translational Medicine*, *7*(1), e10258. https://doi.org/10.1002/btm2.10258

Zielińska, A., Carreiró, F., Oliveira, A. M., Neves, A., Pires, B., Venkatesh, D. N., Durazzo, A., Lucarini, M., Eder, P., Silva, A. M., Santini, A., & Souto, E. B. (2020). Polymeric

Nanoparticles: Production, Characterization, Toxicology and Ecotoxicology. *Molecules (Basel, Switzerland)*, *25*(16), 3731. https://doi.org/10.3390/molecules25163731

Zolezzi, M., Abouelhassan, R., Eltorki, Y., Haddad, P. M., & Noorizadeh, M. (2021). Long-Acting Injectable Antipsychotics: A Systematic Review of Their Non-Systemic Adverse Effect Profile. *Neuropsychiatric Disease and Treatment*, *17*, 1917–1926. https://doi.org/10.2147/NDT.S309768